1-1-2019

Age estimates for hominin fossils and the onset of the Upper Palaeolithic at Denisova Cave

Katerina Douka
Max Planck Institute for the Science of Human History, University of Oxford, katerina.douka@rlaha.ox.ac.uk

Viviane Slon
Max Planck Institute for Evolutionary Anthropology

Zenobia Jacobs
University of Wollongong, zenobia@uow.edu.au

Christopher Ramsey
Oxford University

Michael Shunkov
Russian Academy of Sciences, Novosibirsk State Tech University, RUSSIA

See next page for additional authors

Publication Details Citation

Douka, K., Slon, V., Jacobs, Z., Ramsey, C., Shunkov, M., Derevianko, A., Mafessoni, F., Kozlikin, M., Li, B., Grün, R., Comeskey, D., Deviese, T., Brown, S., Viola, B., Kinsley, L., Buckley, M., Meyer, M., Roberts, R. G., Paabo, S., Kelso, J., & Higham, T. (2019). Age estimates for hominin fossils and the onset of the Upper Palaeolithic at Denisova Cave. Faculty of Science, Medicine and Health - Papers: Part B. Retrieved from https://ro.uow.edu.au/smhpapers1/546

Age estimates for hominin fossils and the onset of the Upper Palaeolithic at Denisova Cave

Abstract

Denisova Cave in the Siberian Altai (Russia) is a key site for understanding the complex relationships between hominin groups that inhabited Eurasia in the Middle and Late Pleistocene epoch. DNA sequenced from human remains found at this site has revealed the presence of a hitherto unknown hominin group, the Denisovans1,2, and high-coverage genomes from both Neanderthal and Denisovan fossils provide evidence for admixture between these two populations3. Determining the age of these fossils is important if we are to understand the nature of hominin interaction, and aspects of their cultural and subsistence adaptations. Here we present 50 radiocarbon determinations from the late Middle and Upper Palaeolithic layers of the site. We also report three direct dates for hominin fragments and obtain a mitochondrial DNA sequence for one of them. We apply a Bayesian age modelling approach that combines chronometric (radiocarbon, uranium series and optical ages), stratigraphic and genetic data to calculate probabilistically the age of the human fossils at the site. Our modelled estimate for the age of the oldest Denisovan fossil suggests that this group was present at the site as early as 195,000 years ago (at 95.4% probability). All Neanderthal fossils-as well as Denisova 11, the daughter of a Neanderthal and a Denisovan4-date to between 80,000 and 140,000 years ago. The youngest Denisovan dates to 52,000-76,000 years ago. Direct radiocarbon dating of Upper Palaeolithic tooth pendants and bone points yielded the earliest evidence for the production of these artefacts in northern Eurasia, between 43,000 and 49,000 calibrated years before present (taken as ad 1950). On the basis of current archaeological evidence, it may be assumed that these artefacts are associated with the Denisovan population. It is not currently possible to determine whether anatomically modern humans were involved in their production, as modern-human fossil and genetic evidence of such antiquity has not yet been identified in the Altai region.

Publication Details

Douka, K., Slon, V., Jacobs, Z., Ramsey, C. Bronk., Shunkov, M. V., Derevianko, A. P., Mafessoni, F., Kozlikin, M. B., Li, B., Grun, R., Comeskey, D., Deviese, T., Brown, S., Viola, B., Kinsley, L., Buckley, M., Meyer, M., Roberts, R. G., Paabo, S., Kelso, J. & Higham, T. (2019). Age estimates for hominin fossils and the onset of the Upper Palaeolithic at Denisova Cave. Nature, 565 (7741), 640-644.

Authors

Katerina Douka, Viviane Slon, Zenobia Jacobs, Christopher Ramsey, Michael Shunkov, Anatoly Derevianko, Fabrizio Mafessoni, Maxim Kozlikin, Bo Li, Rainer Grün, Daniel Comeskey, Thibaut Deviese, Samantha Brown, Bence Viola, Leslie Kinsley, Michael Buckley, Matthias Meyer, Richard G. Roberts, Svante Paabo, Janet Kelso, and Tom Higham

Age estimates for hominin fossils and the onset of the Upper Palaeolithic at Denisova Cave

Katerina Douka[1,2], Viviane Slon[3], Zenobia Jacobs[4,5], Christopher Bronk Ramsey[2], Michael V. Shunkov[6,7], Anatoly P. Derevianko[6,8], Fabrizio Mafessoni[3], Maxim B. Kozlikin[6], Bo Li[4,5], Rainer Grün[9], Daniel Comeskey[2], Thibaut Devièse[2], Samantha Brown[1,2], Bence Viola[11], Leslie Kinsley[10], Michael Buckley[12], Matthias Meyer[3], Richard G. Roberts[4,5], Svante Pääbo[3], Janet Kelso[3] & Tom Higham[2]

[1] Department of Archaeology, Max Planck Institute for the Science of Human History, D-07743 Jena, Germany

[2] Oxford Radiocarbon Accelerator Unit, Research Laboratory for Archaeology and the History of Art, University of Oxford, Oxford OX1 3TG, United Kingdom

[3] Department of Evolutionary Genetics, Max Planck Institute for Evolutionary Anthropology, D-04103 Leipzig, Germany.

[4] Centre for Archaeological Science, School of Earth, Atmospheric and Life Sciences, University of Wollongong, Wollongong, New South Wales 2522, Australia

[5] Australian Research Council (ARC) Centre of Excellence for Australian Biodiversity and Heritage, University of Wollongong, Wollongong, New South Wales 2522, Australia

[6] Institute of Archaeology and Ethnography, Russian Academy of Sciences, Siberian Branch, Novosibirsk, 630090, Russia.

[7] Novosibirsk State University, Novosibirsk, 630090, Russia.

[8] Altai State University, Barnaul, 656049, Russia.

[9] Australian Research Centre for Human Evolution, Griffith University, Nathan Queensland 4111, Australia.

[10] Research School of Earth Sciences, The Australian National University, Canberra, Australian Capital Territory 2601, Australia.

[11] Department of Anthropology, University of Toronto, Toronto, Ontario M5S 2S2, Canada.

[12] Manchester Institute of Biotechnology, University of Manchester, Manchester M1 7DN, United Kingdom.

Denisova Cave (Siberian Altai, Russia) is a key site in understanding the complex relationships between hominin groups inhabiting Eurasia in the Middle and Late Pleistocene. DNA sequenced from human remains found here has shown the presence of a hitherto unknown hominin, the "Denisovans"[1,2] and high coverage genomes from both Neanderthal and Denisovan fossils provide evidence for admixture between the two groups[3]. Determining the age of these fossils is important if we are to understand the nature of hominin interaction, and aspects of their cultural and subsistence adaptation. Here, we present 50 new radiocarbon determinations from the late Middle and Upper Palaeolithic parts of the site. We also report three newly-discovered directly-dated hominin fossil fragments, and obtain a mitochondrial DNA sequence for one of them. To calculate probabilistically the age of the human fossils at the site, we apply a novel Bayesian age modelling approach that combines chronometric (radiocarbon, uranium-series and optical ages), stratigraphic and genetic data. Our modelled age estimate for the oldest Denisovan fossil suggests that this group was present at the site as early as 195,000 years ago (at 95.4% probability). All Neanderthal fossils, as well as *Denisova 11*, the daughter of a Neanderthal and a Denisovan[4], date between 80,000 and 140,000 years ago. The youngest Denisovan dates up to 51,000 years ago. Direct radiocarbon dating of Upper Palaeolithic tooth pendants and bone points yielded the earliest evidence for the production of such artefacts in northern Eurasia, at *c.* 43,000–49,000 years cal BP. Based on present archaeological evidence, it may be assumed that these artefacts are associated with the Denisovans. Whether anatomically modern humans were involved in their production is not possible to determine at present since their remains have not yet been identified in the Altai region.

Denisova Cave preserves the longest and most notable Palaeolithic sequence in northern Asia. It consists of three chambers: Main, East and South[5] (Supplementary Information 1). Excavations at the site have so far yielded the remains of 12 hominins (Extended Data Fig. 1, Supplementary Information 3), most of which are small and highly fragmentary. Despite this, the preservation of DNA in some of these remains is

very good, and has enabled genome-wide data to be obtained from both Neanderthal and Denisovan human remains, as well as from cave sediments[1-4,6-8].

A key unresolved issue remains the chronology of the site and the age of the recovered human remains. Previous attempts at building a chronology at Denisova Cave have employed radiocarbon dating in the uppermost sections, and thermoluminescence dating of the older layers[9]. More recently, radiocarbon dating from the uppermost Pleistocene layers in the East Chamber revealed some age variations that were ascribed to taphonomic mixing and carnivore bioturbation[2]. A new set of optical ages[10] has been obtained from Pleistocene sedimentary layers in all three chambers.

Here we report 50 new radiocarbon determinations from 40 samples collected from the upper parts of the Pleistocene sequence (layers 9–12) in the Main and East Chambers (Fig. 1 and Extended Data Table 1). A further 23 samples were processed, but did not yield sufficient carbon for dating (Supplementary Information 2). We selected samples of charcoal, humanly-modified bone and artefacts (Supplementary Information 2 and Extended Data Fig. 2) from locations deemed undisturbed during excavation. The samples were prepared using, where possible, robust decontamination protocols, including collagen ultrafiltration and single amino acid extraction of hydroxyproline from bones and teeth, and ABOx-/AOx-SC for charcoal (Supplementary Information 2).

All samples from layers 11.3, 11.4 and 12 in the East Chamber, as well as the directly-dated *Denisova 11*[13], predate the radiocarbon age limit. In layer 11.2, we found two age clusters: three samples, including two humanly-modified bones collected from the same square, sector and year of excavation as the *Denisova 3* phalanx, have infinite ages, and three samples have finite calibrated ages (Extended Data Table 1). A horse tooth from layer 9.2 gave a result of 45,720–50,000 cal BP (OxA-29859). This age is statistically indistinguishable from the group of finite ages (treated with ultrafiltration and ABOx) from layer 11.2.

In the Main Chamber, the new radiocarbon ages reveal a depositional hiatus between layers 12 and 11.4. Samples from layer 12, at the end of the Middle

Palaeolithic, all gave infinite radiocarbon ages compared to samples from layer 11.4, which have ages between ~35,000 and 40,000 cal BP (Fig. 1).

Four pendants made from red deer (*Cervus elaphus*) and elk (*Alces alces*) teeth, often associated with Upper Palaeolithic technocomplexes, provided results of ~32,000, ~40,000 and ~45,000 cal BP (Fig. 1 and Extended Data Fig. 2). The oldest of these ages (OxA-30963) is corroborated by a charcoal date (OxA-31506) from the same stratigraphic location and year of excavation, and is the earliest direct date for an artefact of this type. The younger determinations for some of these artefacts may be considered minimum ages due to small sample sizes and marginal collagen yields (~1% wt. collagen), which prevented the application of robust chemical pretreatment methods. Two bone points were dated to 42,660–48,100 and 41,590–45,700 cal BP (Fig. 1 and Extended Data Fig. 2), also representing the earliest occurrence of such objects in northern Eurasia.

The radiocarbon ages for the oldest Denisova pendants and the bone points overlap with the directly dated modern human femur from Ust'-Ishim in western Siberia[14] (43,200–46,880 cal BP)(Fig. 2). This raises the possibility of a connection between the spread of modern humans and the emergence of innovative behaviours and symbolic artefacts across northern Eurasia at the start of the Initial Upper Palaeolithic, by 43,000–48,000 cal BP.

In an attempt to retrieve further human fossils from the site, we applied collagen peptide mass spectrometry fingerprinting (or ZooMS)[13] to 2,212 non-diagnostic bone fragments and identified three new specimens that contained peptides consistent with the Hominidae (Supplementary Information 8). The bones come from layers 9.3 (*Denisova 14*, DC 3758) and 11.4 (*Denisova* 15, DC 3573) in the East Chamber, and layer 9.1 (*Denisova 16*, DC 4114) in the Main Chamber (Extended Data Fig. 3). *Denisova 14* and *Denisova 15* were directly dated and genetically analysed. The radiocarbon ages are close to, or beyond, the radiocarbon limit (Fig. 1 and Extended Data Table 1). No ancient hominin DNA was retrieved from *Denisova 14*, but *Denisova 15* carries a mitochondrial genome of the Neanderthal type (Supplementary Information 5). *Denisova 16* was too small for radiocarbon dating and aDNA analyses are ongoing.

All directly dated human remains yielded infinite radiocarbon ages and are associated, in most cases, with layers that are beyond the limit of the method. Using optical dating finite ages for layers containing human remains have been obtained[10], but the association between the sediment samples and human fossils is inferred, and the dated sediments do not immediately surround the fossils. Age estimates based on branch shortening of the nuclear genome have been published for *Denisova 3, Denisova 5* and *Denisova 11*[6,3,4], but these are sensitive to sequencing error and the human/chimpanzee divergence date, which is under discussion (Supplementary Information 4). To exploit the different types of information available for Denisova Cave derived from radiocarbon and optical dating, stratigraphy and genetic analyses, we developed a novel Bayesian approach to generate robust age estimates for the human remains and ameliorate the shortcomings of each technique and line of evidence when used individually.

We used OxCal 4.3 software[11] to build a Bayesian model consisting of several types of prior information; the stratigraphic position of all specimens (Fig. 3), the relative genetic ages for seven human remains (*see below*, Extended Fig. 4), the finite radiocarbon age for *Denisova 14*, a *terminus ante quem* boundary for the radiocarbon ages (>50,000 BP), optical ages for layers 22.1 (*n*=2) and 21 (*n*=3) in the Main Chamber and layers 12.3 (*n*=3) and 11.2 (*n*=3) in the East Chamber (Supplementary Information 6) and a minimum uranium-series age of 67,500 ± 2500 years for *Denisova 11* (Supplementary Information 7).

The relative genetic ages of four Denisovans (*2, 3, 4* and *8*) and two Neanderthals (*5* and *15*), as well as *Denisova 11* (who carries a Neanderthal mitochondrial genome), were derived from a multiple sequence alignment of their mitochondrial genome sequences. We achieved this by counting the number of substitutions on the branches leading to each individual since the split from their most recent common ancestor with either the *Sima de los Huesos* individual[14], or with 19 Neanderthals from other archaeological sites and the *Hohlenstein-Stadel* Neanderthal (Extended Data Fig. 4). To convert these differences to time in years, we applied the mitochondrial mutation rate of 2.53×10^{-8}/nucleotide position/year (95% HPD: 1.76-3.23×10^{-8}) inferred for modern humans[15]. We caution that this conversion to time

assumes that the mutation rate in archaic humans is the same as that in modern humans, and that the approach cannot detect back mutations and multiple substitutions occurring at the same position in the mitochondrial genome. The relative ages obtained were then included within the Bayesian model as relative constraints between the hominin remains. The split time estimates in the Denisovan and Neanderthal trees were treated as time differences assuming an Erlang distribution.

We tested four separate Bayesian models (Supplementary Information 9; Extended Data Figs 5-6). When the human remains are placed in their attributed stratigraphic positions (Model 1), low model agreement indices were obtained for *Denisova* 2 and *11*, suggesting that these two fossils must have moved post-depositionally. When we reassigned these to overlying layers (Models 2-4), significantly higher agreement indices were obtained. We tested the results of the models against ages derived using optical and genetic information only (Extended Data Fig. 7*).* The modelled age estimates for the human fossils we report here derived from probability distribution functions using Model 4 (Fig. 4; Extended Data Table 2*;* Supplementary Information 9).

Denisova 2, the oldest Denisovan fossil, yielded a modelled age estimate of 122,700**–**194,400 years. *Denisova 8*, found at the interface between layers 11.4 and 12 of the East Chamber, falls between 105,600–136,400 years. *Denisova 3*, the youngest Denisovan fossil from layer 11.2 in the East Chamber, yielded a modelled age of 51,600**–**76,200 years ago (at 95.4% probability). This is consistent with infinite radiocarbon ages of >48,600 (OxA-29857) and >50,100 BP (OxA-29858) obtained on two humanly-modified bones collected from the same square, sector and year of excavation as *Denisova 3*. The modelled age also overlaps with the age estimated based on branch shortening in the nuclear genome when calculated using transversion polymorphisms only and assuming a human/chimpanzee divergence time of 13 million years (60,000**–**84,000 years)(Supplementary Information 4). *Denisova 4* (layer 11.1, South Chamber) differs by only two mutations in its mtDNA compared to *Denisova 3,* and therefore has a similar age.

The three Neanderthals (*Denisova 5*, *9* and *15*) are derived from similar stratigraphic positions in the East Chamber. *Denisova 5* (layer 11.4) has a modelled age estimate

of 90,900–130,000 years ago, which is consistent with the nuclear genome branch shortening age estimate (110,000–134,800 years)(Supplementary Information 4). *Denisova 15* (layer 11.4) differs by only a single mutation in its mtDNA compared to *Denisova 5*, and therefore yields an overlapping modelled age. No genetic information is available for *Denisova 9* (layer 12.3); its modelled age (119,100–147,300 years) is based on its stratigraphic position and is constrained only by the optical ages from layer 12.3.

Denisova 11, found in layer 12.3 in the East Chamber, pre-dates stratigraphically *Denisova 5*. If this position is maintained (e.g., Model 2), *Denisova 11* has an estimated age of 115,700–140,900 years, compared to the modelled age estimate of 92,800–132,000 years for *Denisova 5.* Genetic information, however, based on the differences in the number of mitochondrial substitutions and the sharing of nuclear substitutions with the high-coverage genome of *Denisova 5*, suggests strongly that *Denisova 11* is younger than *Denisova 5*. To further explore this, we placed *Denisova 11* above *Denisova 5* in Models 3 and 4. Both models yielded much higher agreement indices, supporting the notion that *Denisova 11,* discovered in the assemblage of unidentifiable bones from layer 12, is intrusive to it. This results in a final age estimate of 79,300–118,100 years for this specimen.

The age estimates for *Denisova 11* and all Neanderthal remains from the site largely overlap (Fig. 4). Slon et al.[8] found Neanderthal and Denisovan DNA in underlying sediments in the East Chamber (layers 14 and 15) and Neanderthal DNA in the Main Chamber (layers 14, 17 and 19) (Fig. 3) suggesting that both groups were present in the cave prior to the earliest human fossils currently recorded there. The modelled ages for Neanderthal fossils found in the East Chamber are consistent with optical ages for sediments containing Neanderthal DNA in the Main Chamber. The earliest sediments with Neanderthal DNA (layer 14 in the East Chamber) date to ~190,000 years ago[10]. This also overlaps with the optical age (layer 15, East Chamber)[10] from which Denisovan DNA was extracted[8], as well as with our modelled age for *Denisova 2*. The interstratification and temporal overlap of Denisovan and Neanderthal fossils and sedimentary DNA, as well as the direct genetic evidence[4], suggests that both groups lived in the region, met and, on occasion, interbred over the course of

150,000 years. The integration of all available data from Denisova highlights the very early appearance of Neanderthals in Siberia, as early as 190,000 years ago, during the late part of warm MIS 7, with the majority of the specimens thus far falling into the last Interglacial (MIS 5) (Fig. 4).

Denisovans appear to have survived later than Neanderthals. Our modelled age estimate for the most recent Denisovan fossil (*Denisova 3*: 51,600–76,200 years ago) is earlier than published estimates of the age of Denisovan admixture into modern humans (44,000–54,000[16] and 31,000–50,000 years ago[17]). If these admixture estimates are robust, then the Altai Denisovans may not have been the latest surviving population.

Our results also imply that all known Neanderthal and Denisovan fossils predate the appearance of the Initial Upper Palaeolithic (45,000–48,000 years ago) and the directly-dated personal ornaments and bone points. However, given that previous work on the lithic evidence from Denisova Cave indicated that the Initial Upper Palaeolithic may have developed through a local Middle Palaeolithic substrate[19], it is parsimonious to suggest at present that the makers of these artefacts may have been Denisovans. The presence of anatomically modern humans to the northwest of Denisova Cave as early as 45,000 cal BP at Ust'-Ishim, synchronous with the dated pendants and bone points (Fig. 2), also raises the possibility that modern humans may have been involved in the manufacture of these artefacts. Future discovery of fossils from this site and others, and determination of their ages and genomes, using a combination of methods will shed further light on the relationships between archaic and modern humans and their associated material cultures.

References

1. Krause, J. *et al.* The complete mitochondrial DNA genome of an unknown hominin from southern Siberia. *Nature* **464,** 894–897 (2010).
2. Reich, D. *et al.* Genetic history of an archaic hominin group from Denisova Cave in Siberia. *Nature* **468,** 1053–1060 (2010).
3. Prüfer, K. *et al.* The complete genome sequence of a Neanderthal from the Altai Mountains. *Nature* **505,** 43–49 (2014).

4. Slon, V., *et al*. The genome of the offspring of a Neanderthal mother and a Denisovan father. *Nature* **561**, 113–116 (2018).
5. Derevianko, A. P. The Middle to Upper Palaeolithic transition in the Altai (Mongolia and Siberia) in *The Middle to Upper Palaeolithic transition in Eurasia: Hypotheses and Facts* (ed. Derevianko, A. P.), 183–216 (Institute of Archaeology and Ethnography Press, Novosibirsk) (2005).
6. Sawyer, S. *et al*. Nuclear and mitochondrial DNA sequences from two Denisovan individuals. *Proc. Natl Acad. Sci. USA* **112**, 15696–15700 (2015).
7. Slon, V., *et al*. A fourth Denisovan individual*. Sci. Advances* **3**(7): p. e1700186 (2017).
8. Slon, V. *et al.* Neandertal and Denisovan DNA from Pleistocene sediments. *Science* **356**, 605–608 (2017).
9. Derevianko, A. P., Laukhin, S. A., Kulikov, O. A., Gnibidenko, Z. N. & Shunkov, M. V. First Middle Pleistocene age determinations of the Paleolithic in the Altai Mountains. *Dokl. Akad. Nauk* **326**, 497–501 (1992).
10. Jacobs et al. Timing of archaic hominin occupation of Denisova Cave in southern Siberia. *Nature*, in press.
11. Bronk Ramsey, C. Bayesian analysis of radiocarbon dates. *Radiocarbon* **51**(1), 337–360 (2009).
12. Reimer, P. J. *et al*. IntCal13 and Marine13 Radiocarbon Age Calibration Curves 0–50,000 Years cal BP. *Radiocarbon* **55**(4), 1869–1887 (2013).
13. Brown, S. *et al.* Identification of a new hominin bone from Denisova Cave, Siberia using collagen fingerprinting and mitochondrial DNA analysis. *Sci. Rep.* **6,** 23559 (2016).
14. Meyer, M. *et al.* A mitochondrial genome sequence of a hominin from Sima de los Huesos. *Nature* **505,** 403–406 (2014).
15. Fu, Q. *et al.* Genome sequence of a 45,000-year-old modern human from western Siberia. *Nature* **514,** 445–449 (2014).
16. Sankararaman, S., Mallick, S., Patterson, N. & Reich, D. The Combined Landscape of Denisovan and Neanderthal Ancestry in Present-Day Humans. *Curr. Biol.* **26,** 1241–1247 (2016).

17. Malaspinas, A.-S. *et al.* A genomic history of Aboriginal Australia. *Nature* **538,** 207–214 (2016).
18. Lisiecki, L. E. & Raymo, M. E. A Pliocene-Pleistocene stack of 57 globally distributed benthic $\delta^{18}O$ records. *Paleoceanography* **20**, *PA1003* (2005).
19. Derevianko, A. P. The Upper Paleolithic in Africa and Eurasia and the Origin of Anatomically Modern Humans. Izd-vo Instituta arkheologii i etnografii, Siberian Branch of the Russian Academy of Sciences, Novosibirsk (in Russian) (2011).

Supplementary Information is linked to the online version of the paper at www.nature.com/nature.

Acknowledgements

Funding for this research was received from the European Research Council (ERC) under the European Union's Seventh Framework Program (FP7/2007-2013); grant no. 324139 (PalaeoChron) awarded to T.H.; grant no. 715069 (FINDER) awarded to K.D.; grant no. 694707 (100 Archaic Genomes) awarded to S.P. The Max Planck Society provided support to S.P., V.S., F.M., M.M., J.K., K.D. and S.B. The Australian Research Council funded research fellowships to Z.J. (FT150100138), B.L. (FT14010038) and R.G.R. (FL130100116). The Royal Society funded a University Research Fellowship to M.B. B.V. was supported by the Social Sciences and Humanities Research Council (Canada). The archaeological field studies were funded by the Russian Science Foundation (project no. 14-50-00036 to A.P.D.) and the Russian Foundation for Basic Research (project no. 17-29-04206 to M.V.S. and M.B.K.). K.D., T.H. and T.D. thank Brasenose and Keble Colleges and the John Fell Fund, University of Oxford, for funding and support. Staff at the Oxford Radiocarbon Accelerator Unit (ORAU) and Esther Gillespie and Miriam Higham Jenkins are thanked for their contribution to the radiocarbon dating and ZooMS work. Mark Rubby is thanked for contributing to the marine oxygen isotope curve data used here (https://github.com/markruddy/ois5e-plot). Dana Challinor identified the charcoal prior to radiocarbon dating. Ian Cartwright (University of Oxford) photographed *Denisova*

311 *11, 14, 15* and 16. Yasaman Jafari, Kieran O'Gorman and Terry Lachlan helped with
312 optical dating sample preparation and data analysis. Sarah Nagel, Birgit Nickel,
313 Barbara Schellbach and Antje Weihmann helped with DNA sample preparation; and
314 Alexander Hübner gave input on the BEAST analysis.
315
316 **Contributions:** K.D., V.S., Z.J., B.L., D.C., L.K., T.D., S.B., B.V., and M.B. performed
317 the laboratory work; K.D., T.H., C.B.R., D.C., T.D. obtained and analysed the
318 radiocarbon data. V.S., F.M., J.K., M.M. and S.P. analysed the genetic data; C.B.R.,
319 K.D. and T.H. designed and tested the Bayesian models. S.B. and M.B. analysed the
320 ZooMS samples. B.V. carried out morphological analyses of the fossils. Z.J., B.L. and
321 R.G.R. analysed the optical dating data. L.K. and R.G. obtained and analysed the U-
322 series data. A.P.D., M.V.S. and M.B.K. excavated the site and analysed all
323 archaeological data. K.D., T.H. and Z.J. wrote the manuscript with input from all
324 authors.
325
326 **Author Information:** Reprints and permissions information is available at
327 www.nature.com/reprints. The authors declare no competing interests.
328 Correspondence and requests for materials should be addressed to
329 douka@ssh.mpg.de (K.D.) or thomas.higham@rlaha.ox.ac.uk (T.H.).
330
331 **Methods**
332
333 **Radiocarbon dating and Bayesian modeling**
334 Bones for dating were sampled using an NSK Elector drill with cleaned tungsten
335 carbide drill bits. The routine ORAU chemical pretreatment protocol was applied[20]. A
336 small number of samples were tested using compound-specific methods in which
337 underivatised amino acids were separated from hydrolysed bone collagen samples
338 using preparative High Performance Liquid Chromatography (Prep-HPLC)[21]. Using
339 this procedure, hydroxyproline (Hyp) was isolated and dated. This approach is the
340 most efficient technique to remove contaminants including conservation materials.
341 Samples of charcoal were prepared for dating using ABA (Acid-Base-Acid), ABOx-

SC (Acid-Base-Oxidation/Stepped Combustion)[22] or a modified AOx-SC preparation. OxCal v4.3.2[11] and the IntCal13[12] calibration curve were used to calibrate the radiocarbon data and build Bayesian models incorporating chronometric, stratigraphic and genetic relative dating.

Code availability

CQL codes for Bayesian analyses are included in Supplementary Information, Section 9. These can be imported and used in the OxCal platform[11].

ZooMS collagen fingerprinting analysis for hominin identification

Because ~95% of the bone assemblage from Denisova Cave is unidentifiable to species/genus due to carnivore-derived fragmentation, allied with the fact that ancient DNA is well-preserved, we applied collagen peptide mass fingerprinting (ZooMS) to identify new human remains from the site. We analysed 2,212 non-diagnostic bone fragments using this technique, which we previously used to discover *Denisova 11*[4,13], bringing the total bones analysed from the site so far to 4,527 (Supplementary Information 8). Samples from bone fragments were cut and drilled at the University of Oxford and processed for ZooMS analysis at the University of Manchester, UK. This involved each bone sample being partially decalcified with 0.6 M HCl overnight (~18 h) and then 0.5 mL of solution from each sample being twice ultrafiltered (30 kDa molecular weight cut-off) into 50 mM ammonium bicarbonate. 100 µL was then digested with sequencing grade trypsin at 37^{o}C overnight (~18 h) and 1 µL samples were spotted with 10 mg/mL α-cyano hydroxycinnamic acid matrix on a plate, following Brown *et al.*[13], and allowed to air dry. Using a Brüker Ultraflex II Matrix Assisted Laser Desorption Ionization Time of Flight mass spectrometer, 2,000 laser acquisitions from random walking were acquired for each sample and the resulting spectra were screened for hominin collagen peptide markers published previously[13,23].

DNA sequencing and data processing

Bone powder was removed from the *Denisova 14* and the *Denisova 15* bone

fragments using a disposable dentistry drill. The bone powder samples were treated with 0.5% sodium hypochlorite prior to DNA extraction[24,25]. 20% of each DNA extract (i.e., 10 µl) were converted into single-stranded DNA libraries[26] and indexed with two barcodes[27]. The DNA libraries were enriched for human mtDNA fragments using two rounds of an on-beads hybridization capture protocol[28]. The enriched DNA libraries were pooled with libraries generated as part of other projects and sequenced on a MiSeq platform (Illumina) in 76-cycle paired-end runs[27]. Basecalling was carried out using Bustard (Illumina) and demultiplexing was performed by requiring exact matches to the expected barcode combinations. Overlapping paired-end reads were merged using leeHom[29]. Sequences were mapped to a reference genome using BWA[30] with parameters adapted to ancient DNA. PCR duplicates were collapsed into a single sequence using bam-rmdup (https://github.com/mpieva/biohazard-tools/). Only sequences longer than 35 bases and with a mapping quality higher than 25 were retained.

Methods references

20. Brock, F. et al. Current Pretreatment Methods for AMS Radiocarbon Dating at the Oxford Radiocarbon Accelerator Unit (ORAU). *Radiocarbon* **52**, 103–112 (2010).
21. Devièse, T. et al. New protocol for compound specific radiocarbon analysis of archaeological bones. *Rapid Communications in Mass Spectrometry* **32**, 373–379 (2018).
22. Bird, M. I. *et al.* Radiocarbon Dating of 'Old' Charcoal Using a Wet Oxidation, Stepped-Combustion Procedure. *Radiocarbon* **41**, 127–140 (1999).
23. Buckley, M., Kansa, S.W. Collagen fingerprinting of archaeological bone and teeth remains from Domuztepe, South Eastern Turkey. *Archaeological and Anthropological Sciences* **3**(3), 271–280 (2011).
24. Dabney, J., et al. Complete mitochondrial genome sequence of a Middle Pleistocene cave bear reconstructed from ultrashort DNA fragments. *Proc. Natl. Acad. Sci. USA* **110**(39), 15758–15763 (2013).
25. Korlević, P., et al. Reducing microbial and human contamination in DNA extractions from ancient bones and teeth. *Biotechniques* **59**(2), 87–93 (2015).

404 26. Gansauge, M.T., et al. Single-stranded DNA library preparation from highly
405 degraded DNA using T4 DNA ligase. *Nucleic Acids Res.* **45**(10), e79 (2017).
406 27. Kircher, M., S. Sawyer, and M. Meyer. Double indexing overcomes inaccuracies
407 in multiplex sequencing on the Illumina platform. *Nucleic Acids Res*. **40**(1), p. e3
408 (2012).
409 28. Fu, Q., et al., DNA analysis of an early modern human from Tianyuan Cave,
410 China. *Proc. Natl. Acad. Sci. USA* **110**(6), 2223–2227 (2013).
411 29. Renaud, G., U. Stenzel, and J. Kelso. leeHom: adaptor trimming and merging for
412 Illumina sequencing reads. *Nucleic Acids Res*. **42**(18), p. e141 (2014).
413 30. Li, H. and R. Durbin. Fast and accurate long-read alignment with Burrows-
414 Wheeler transform. *Bioinformatics* **26**(5), 589–595 (2010).

FIGURE LEGENDS

Figure 1 | New radiocarbon age determinations (in calibrated years before present) from the East and Main Chambers at Denisova cave. The radiocarbon determinations (n=40) are calibrated using OxCal 4.3 software[11] and the IntCal13 calibration curve[12] and are plotted in their respective stratigraphic sequences and chambers of origin. The finite probability distributions are in blue with error bars indicating 68.2 and 95.4% highest posterior density ranges. Orange denotes measured ages beyond the radiocarbon limit (50,000 BP). Raw data in Extended Data Table 1. a. East Chamber sequence and associated calibrated dates. b. Main Chamber sequence and associated calibrated dates. Number in stratigraphic columns refers to layer. An asterisk (*) next to the OxA- lab code indicates bone sample and a caret (^) charcoal. Images include the three directly dated human bone fragments (*Denisova 11*, *Denisova 14* and *Denisova 15;* labelled *11*, *14* and *15*, respectively), pendants (P) and bone points (B). Two significantly younger ages for layer 9.3 in the Main Chamber are not shown. *Artefacts and human bones not to scale*.

Figure 2 | Comparison of radiocarbon determinations obtained for the oldest bone points and tooth pendants from Denisova Cave with the two direct ages for the Ust'-Ishim modern human femur[14]. For each measurement, the lab code is indicated and, for the Denisova artefacts, the chamber and stratigraphic context are shown in brackets. Error bars below the probability distributions indicate 68.2 and 95.4% highest posterior density ranges. Marked ages (* and ^) were obtained on the same sample. *Artefacts and human bone not to scale.*

Figure 3 | Stratigraphic sequences for the southeast profiles exposed in the three chambers at Denisova Cave (a) and images of human fossil remains (b). The location of the human remains is denoted by circles and sediment-derived human DNA by a trowel silhouette. Red circle/trowel refers to Denisovans, blue to Neanderthals and grey to *Homo* sp. fossils for which no genetic data exist. Number in circle denotes the fossil number (for example, *Denisova 2*=2). Number in brackets refers to the layer that each of the fossils or human DNA was found. (Further information for each human fossil can be found in Extended Data Fig. 1 and Supplementary Information 3).

Figure 4 | Age estimates for the human fossils from Denisova Cave as determined from Bayesian Model 4, compared against the Marine Oxygen Isotope (MIS) curve from benthic $\delta^{18}O$ records[18] (Extended Data Fig. 6 *and* Supplementary Information 9). The probability distribution for *Denisova 14* is the calibrated radiocarbon age obtained directly for the fossil; it extends beyond the range of the calibration curve hence it is truncated at 50,000 BP. Error bars below the probability distributions indicate 68.2 and 95.4% highest posterior density ranges. Red probabilities: Denisovans; blue: Neanderthals; red-blue: *Denisova 11*, direct offspring of Denisovan and Neanderthal. No genetic data exist for *Denisova 6* and *Denisova 14*, these specimens are attributed only to *Homo* sp. and are shown in grey.

Data availability statement. Raw radiocarbon determinations and associated chemical data, calibrated age ranges, and CQL codes for the Bayesian models are included in Supplementary Information. All MALDI-ToF-MS raw data for the ZooMS analyses are available from the authors upon request. The mtDNA capture data for *Denisova 11*, *Denisova 14* and *Denisova 15* are available in the European Nucleotide Archive under accession PRJEB29061. The mtDNA sequence of *Denisova 15* can be downloaded from GenBank (accession MK033602). All other relevant data are available from the authors or are included in the manuscript (Supplementary Information).

EXTENDED DATA LEGENDS

Extended Data Figure 1 | Human remains from Denisova Cave. Red labels indicate Denisovans, blue Neanderthals, and grey *Homo* sp. bones unassigned to a group. *Denisova 11* is shown in red-blue. *Denisova 13*, mentioned in Supplementary Information 3, is unpublished and is not shown here. a, b: *Denisova 2* in occlusal (a) and lingual (b) views; c: *Denisova 3* in proximal view; d, e: *Denisova 4* in mesial (d) and occlusal (e) views; f, *Denisova 8* in occlusal view; g: *Denisova 9* in palmar view; h, i: µCT based renderings of *Denisova 5* in lateral (h) and plantar (i) views; j, k; *Denisova 15* and *Denisova 11*, l, m: *Denisova 14* and *Denisova 16*, n, o: *Denisova 6* in occlusal (n) and lingual (o) views.

Extended Data Figure 2 | Personal ornaments and bone points from Denisova Cave sampled for radiocarbon dating. N28 was discovered during section

cleaning and is not assigned to a specific layer. N282 failed to produce enough collagen and was not dated. N3856/66 was dated twice. Direct dates are listed in Extended Data Table 1.

Extended Data Figure 3 | Proteomic and genetic data for hominin bones discovered using ZooMS. a-d: Collagen fingerprinting MALDI-ToF-MS spectra for *Denisova 11*, *14*, *15 and 16*; e-g: average coverage of the human mitochondrial reference genome for *Denisova 11*, *14*, and *15*. The average coverage of the mitochondrial genome is 2.0-fold for the sequences from *Denisova 14* and 62.7-fold for *Denisova 15*. Low collagen preservation indicated for *Denisova 14* based on its peptides fingerprint correlates well with poor aDNA recovery for the same specimen.

Extended Data Figure 4 | Inferred number of substitutions occurring on branches leading to the mtDNA genomes of Denisovan and Neanderthal individuals since their split from the common ancestor shared with other archaic individuals. DS and NS refer to Denisovan and Neanderthal split age estimates used in the Bayesian models to enable numerical calculation of the split times of the various points on this tree. Individuals from Denisova Cave are emphasized in bold. a: Denisovan mtDNA genomes; data taken from ref. 7. b; Neanderthal mtDNA genomes. Those used in this analysis are reported in Supplementary Table S6.

Extended Data Figure 5 | Bayesian age models (Models 1–2). Modelling details are given in Supplementary Information 9.

Extended Data Figure 6 | Bayesian age models (Models 3–4). Model 4 contains most prior information and yielded very high agreement index. We use this model to calculate and report the ages of the human fossils (Extended Data Table 2). Modelling details are given in Supplementary Information 9.

Extended Data Figure 7 | Comparison of hominin age estimates based on different types of data. Models 1-4 include stratigraphic information, mitochondrial mutation rates, radiocarbon dates and 11 optical ages, and are described in Supplementary Information 9. The green bars show hominin ages derived from an optical age-only model (not presented here) that included all data reported in ref.10. The red bars show schematic age ranges estimated using both mitochondrial and nuclear data. All ages are at 95.4% probability.

Extended Data Table 1 | New radiocarbon results from Denisova Cave. OxA- is the Oxford radiocarbon lab code, P-code denotes the pretreatment method and dated material (AG is gelatinised bone collagen without ultrafiltration; AF is ultrafiltered bone collagen; HYP is the single amino acid, hydroxyproline; ZR, XR and YR refer to ABA, ABOx-SC or AOx-SC methods, respectively, for charcoal samples). Samples highlighted in grey denote samples that produced more than one radiocarbon determination using different pretreatment methods.

Extended Data Table 2 | Comparison of calibrated age estimates (in thousand years ago) for Bayesian models 1–4. The agreement index for each model is shown in the second row. All age ranges are at 95.4% probability. The ages listed for *Denisova 14* is the direct radiocarbon age and not a modelled estimate.

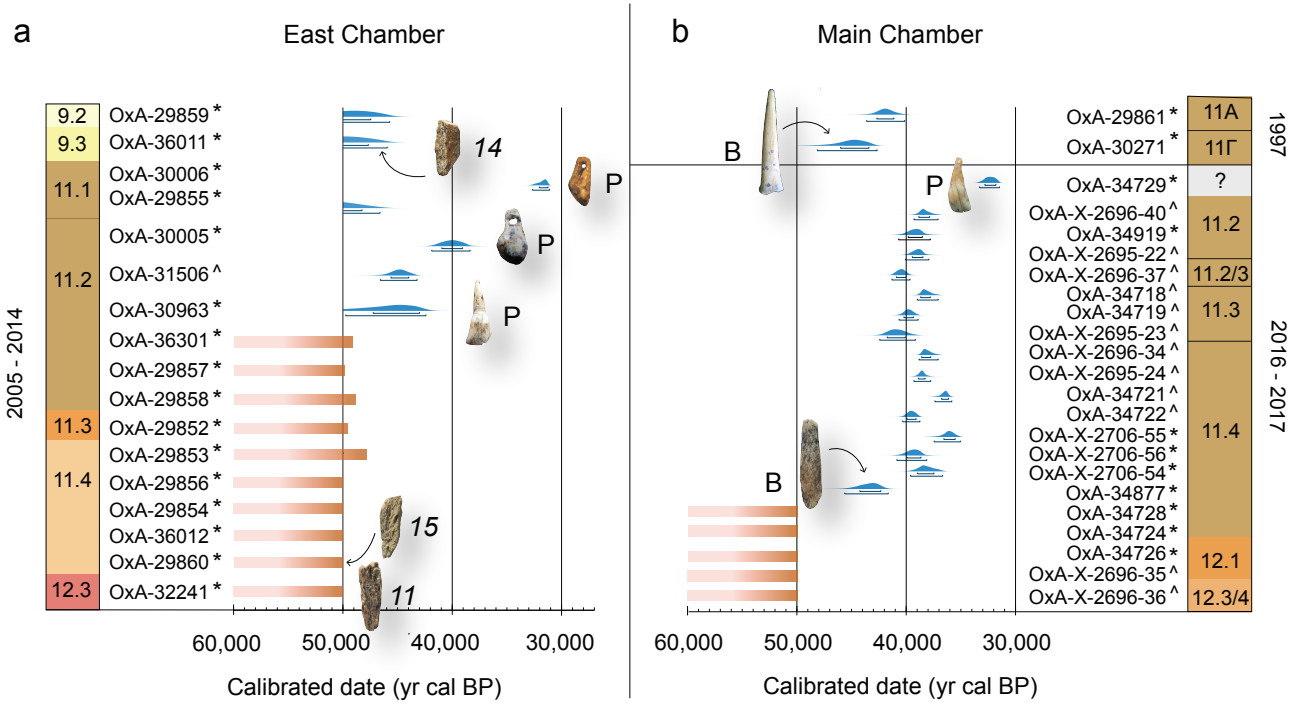
a
East Chamber
b
Main Chamber
2005 - 2014
1997
2016 - 2017
9.2
9.3
11.1
11.2
11.3
11.4
12.3
OxA-29859 *
OxA-36011 *
OxA-30006 *
OxA-29855 *
OxA-30005 *
OxA-31506 ^
OxA-30963 *
OxA-36301 *
OxA-29857 *
OxA-29858 *
OxA-29852 *
OxA-29853 *
OxA-29856 *
OxA-29854 *
OxA-36012 *
OxA-29860 *
OxA-32241 *
14
15
11
P
P
P
B
B
OxA-29861 *
OxA-30271 *
OxA-34729 *
OxA-X-2696-40 ^
OxA-34919 *
OxA-X-2695-22 ^
OxA-X-2696-37 ^
OxA-34718 ^
OxA-34719 ^
OxA-X-2695-23 ^
OxA-X-2696-34 ^
OxA-X-2695-24 ^
OxA-34721 ^
OxA-34722 ^
OxA-X-2706-55 *
OxA-X-2706-56 *
OxA-X-2706-54 *
OxA-34877 *
OxA-34728 *
OxA-34724 *
OxA-34726 *
OxA-X-2696-35 ^
OxA-X-2696-36 ^
11A
11Г
?
11.2
11.2/3
11.3
11.4
12.1
12.3/4
60,000
50,000
40,000
30,000
Calibrated date (yr cal BP)
60,000
50,000
40,000
30,000
Calibrated date (yr cal BP)

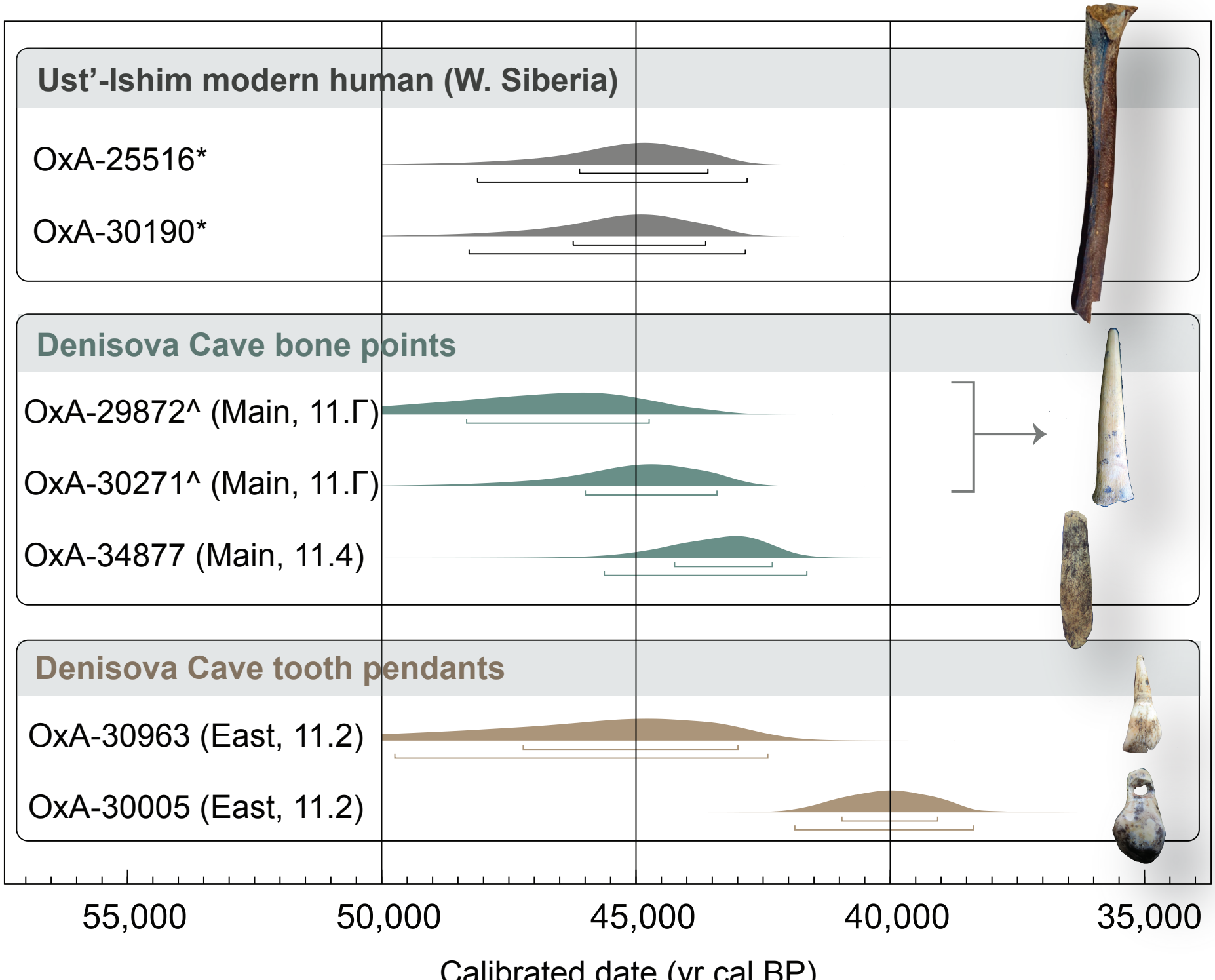
Ust'-Ishim modern human (W. Siberia)
OxA-25516*
OxA-30190*
Denisova Cave bone points
OxA-29872^ (Main, 11.Г)
OxA-30271^ (Main, 11.Г)
OxA-34877 (Main, 11.4)
Denisova Cave tooth pendants
OxA-30963 (East, 11.2)
OxA-30005 (East, 11.2)
55,000
50,000
45,000
40,000
35,000
Calibrated date (yr cal BP)

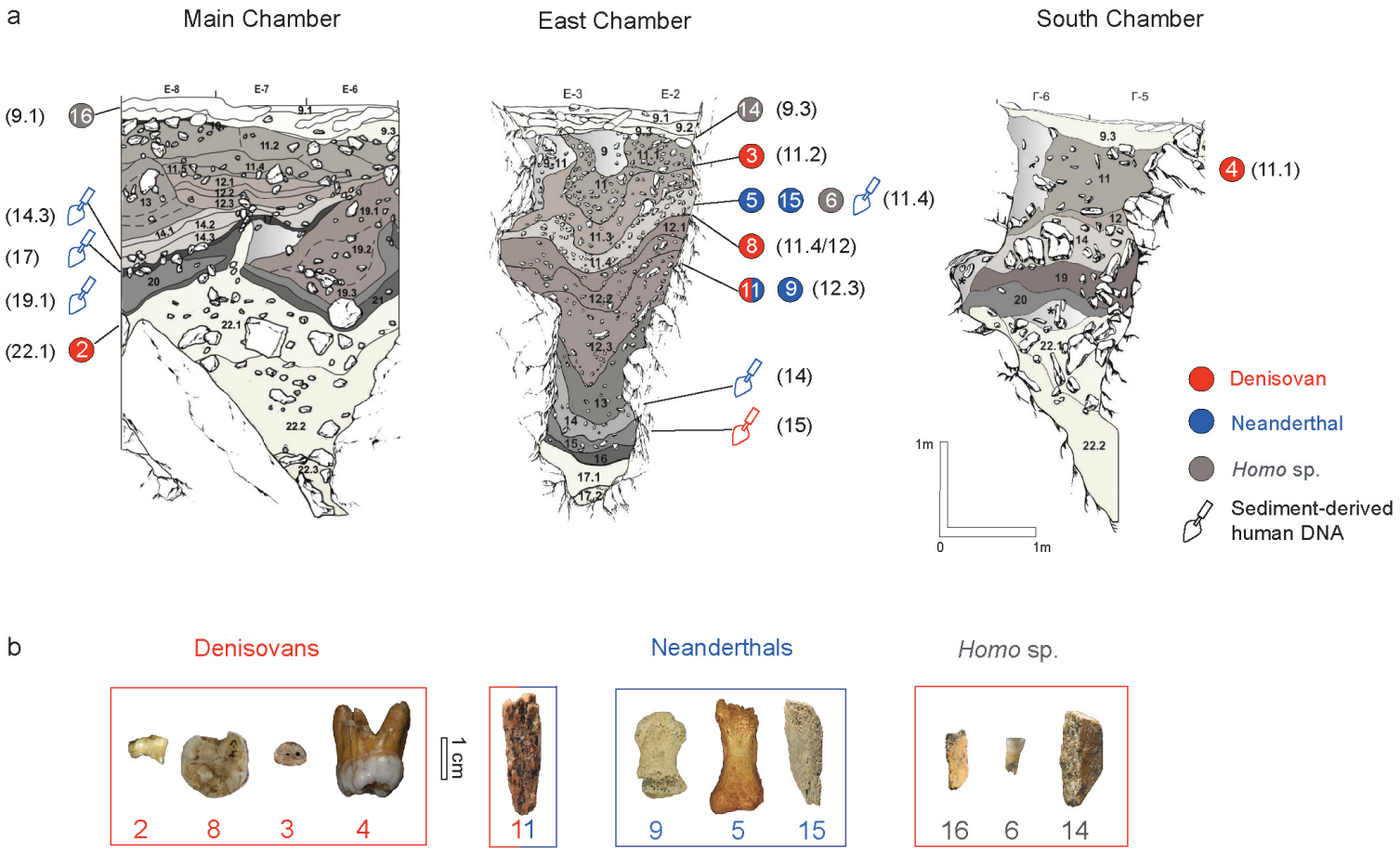
a
Main Chamber
East Chamber
South Chamber
(9.1) 16
(14.3)
(17)
(19.1)
(22.1) 2
E-8
E-7
E-6
E-3
E-2
14 (9.3)
3 (11.2)
5 15 6 (11.4)
8 (11.4/12)
11 9 (12.3)
(14)
(15)
Г-6
Г-5
4 (11.1)
1m
0
1m
Denisovan
Neanderthal
Homo sp.
Sediment-derived human DNA
b
Denisovans
Neanderthals
Homo sp.
1 cm
2
8
3
4
11
9
5
15
16
6
14

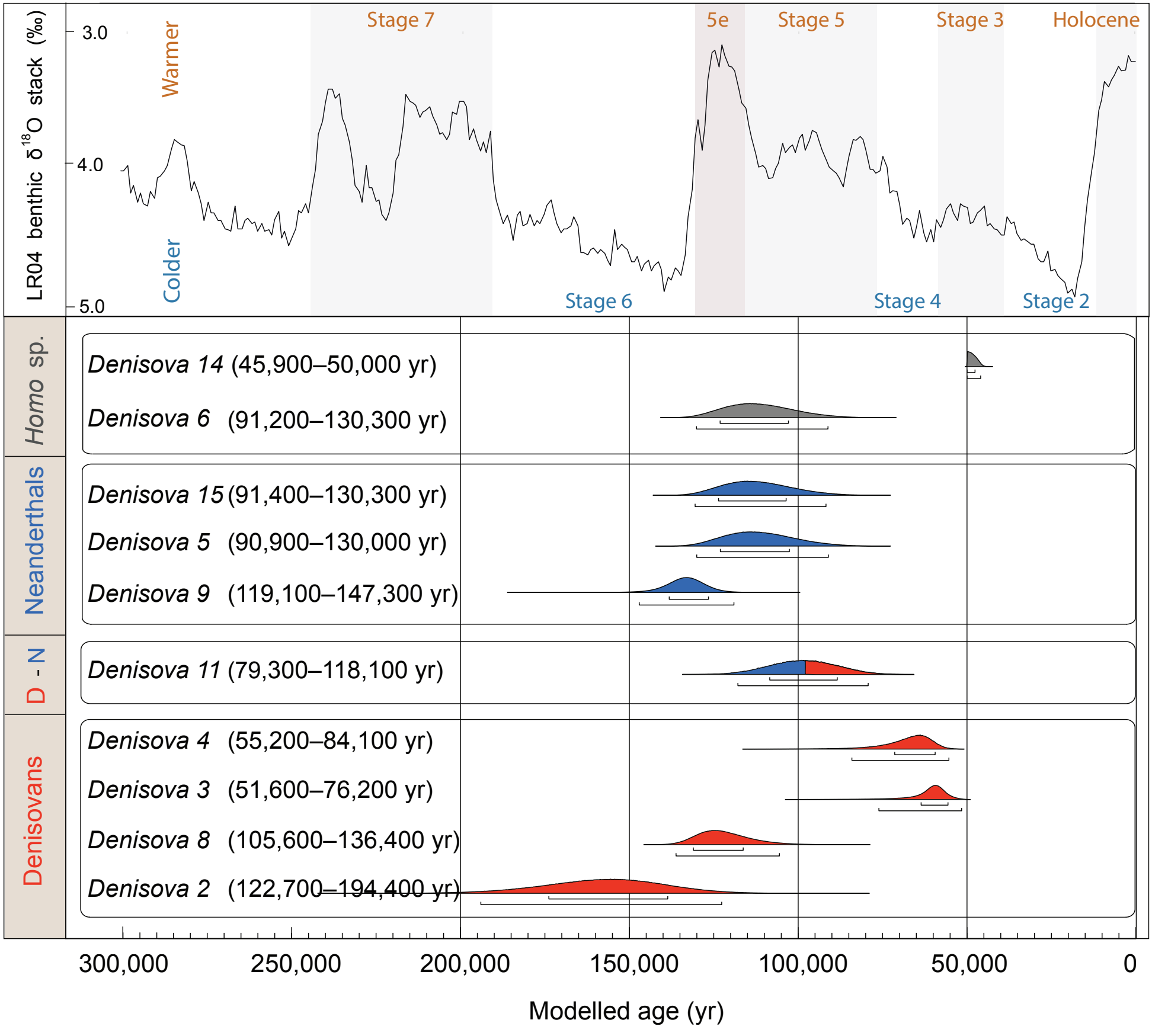
LR04 benthic δ18O stack (‰)
3.0
4.0
5.0
Warmer
Colder
Stage 7
Stage 6
5e
Stage 5
Stage 4
Stage 3
Stage 2
Holocene
Homo sp.
Neanderthals
D - N
Denisovans
Denisova 14 (45,900–50,000 yr)
Denisova 6 (91,200–130,300 yr)
Denisova 15 (91,400–130,300 yr)
Denisova 5 (90,900–130,000 yr)
Denisova 9 (119,100–147,300 yr)
Denisova 11 (79,300–118,100 yr)
Denisova 4 (55,200–84,100 yr)
Denisova 3 (51,600–76,200 yr)
Denisova 8 (105,600–136,400 yr)
Denisova 2 (122,700–194,400 yr)
300,000
250,000
200,000
150,000
100,000
50,000
0
Modelled age (yr)

a b

1 cm

Denisova 2

c

Denisova 3

d e

Denisova 4

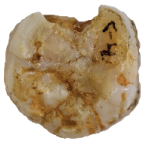

f

Denisova 8

g

Denisova 9

h i

Denisova 5

j

Denisova 15

k

Denisova 11

l

Denisova 14

m

Denisova 16

n o

Denisova 6

Denisovan
Neanderthal
Homo sp.

East Chamber

OxA-30006
(N 133/ 11.1)

OxA-30005
(N 385/ 11.2)

OxA-30963
(N 11/ 11.2)

Failed
(N 282/ 11.2)

Main Chamber

OxA-34729
(N 28/ n/a)

1 cm

OxA-29872 & OxA-30271
(N 3846/66/ 11 Г)

OxA-34877
(N 128/ 11.4.2)

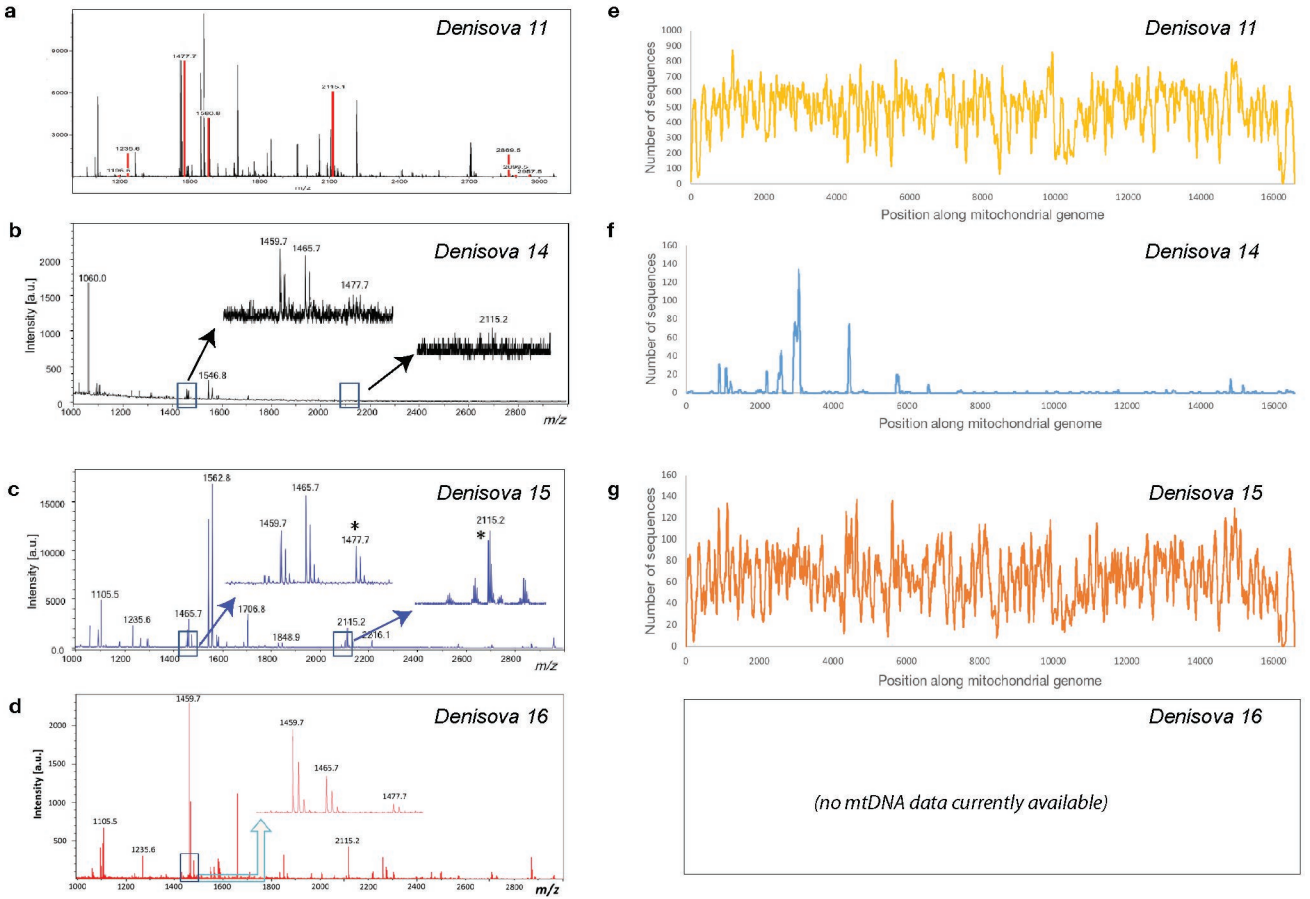
a
Denisova 11
b
Denisova 14
Intensity [a.u.]
m/z
c
Denisova 15
Intensity [a.u.]
m/z
d
Denisova 16
Intensity [a.u.]
m/z
e
Denisova 11
Number of sequences
Position along mitochondrial genome
f
Denisova 14
Number of sequences
Position along mitochondrial genome
g
Denisova 15
Number of sequences
Position along mitochondrial genome
Denisova 16
(no mtDNA data currently available)

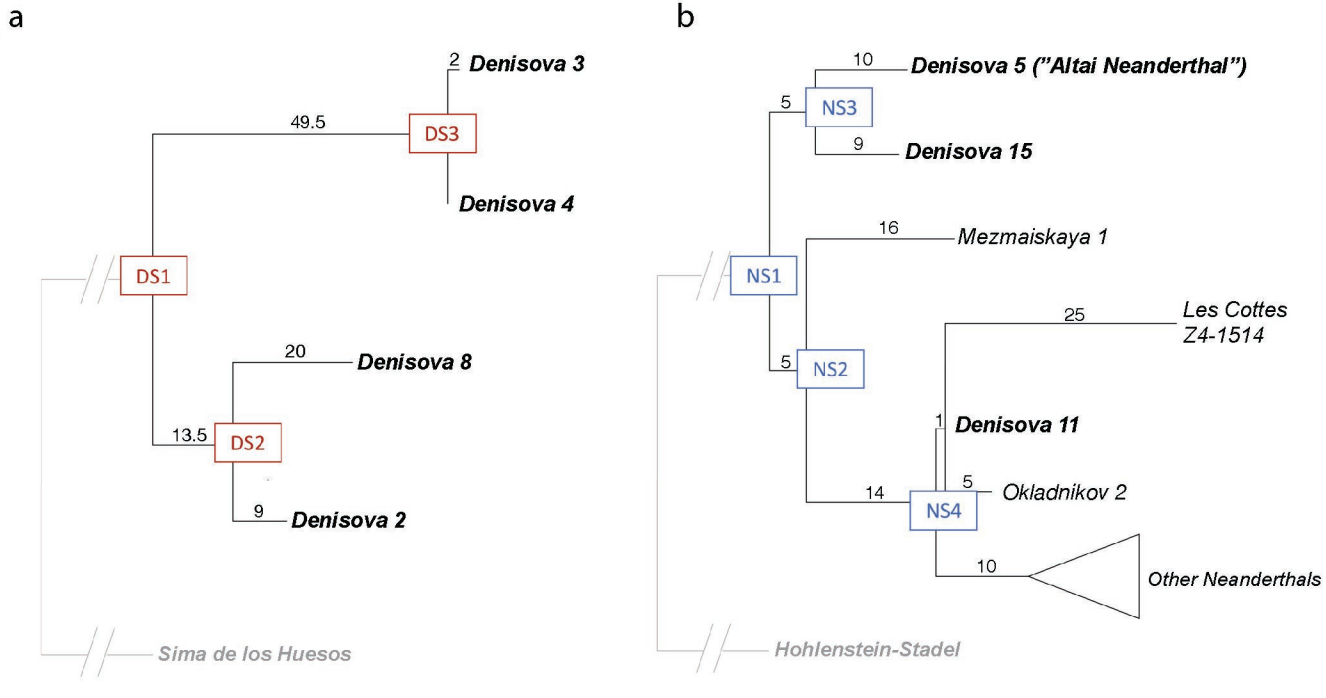
a
2
Denisova 3
49.5
DS3
Denisova 4
DS1
20
Denisova 8
13.5
DS2
9
Denisova 2
Sima de los Huesos
b
10
Denisova 5 ("Altai Neanderthal")
5
NS3
9
Denisova 15
16
Mezmaiskaya 1
NS1
25
Les Cottes
Z4-1514
5
NS2
1
Denisova 11
14
5
Okladnikov 2
NS4
10
Other Neanderthals
Hohlenstein-Stadel

Model 1

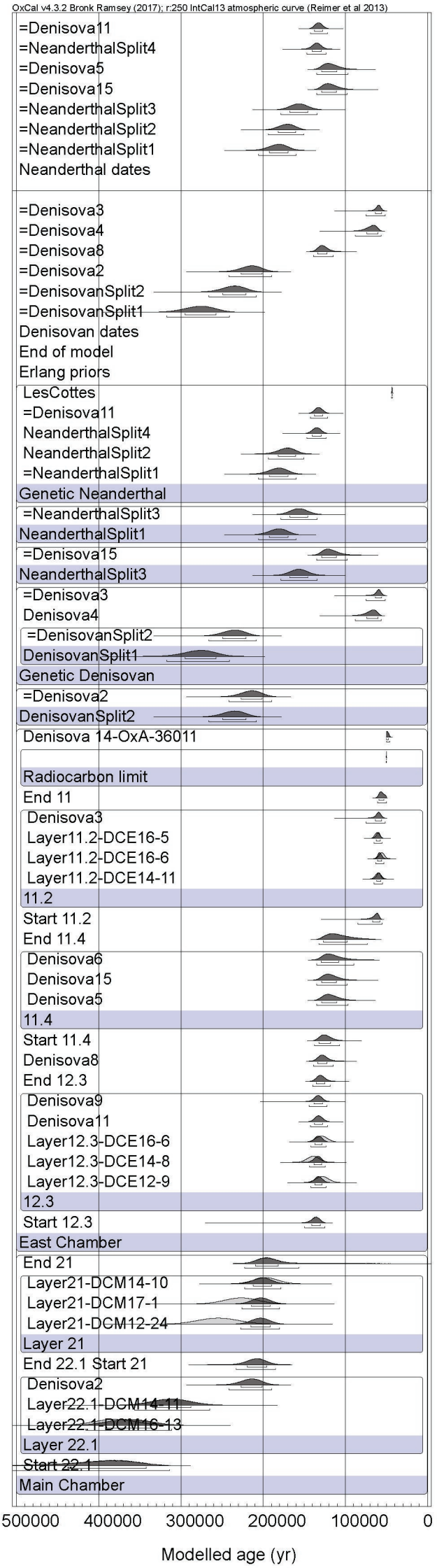

Model 2

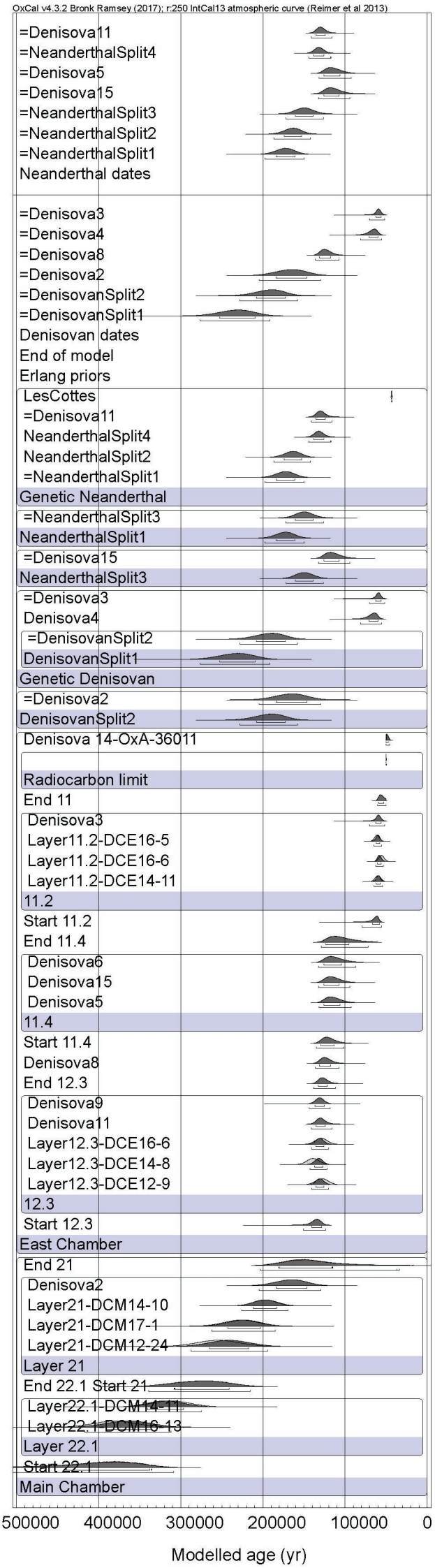

Model 3

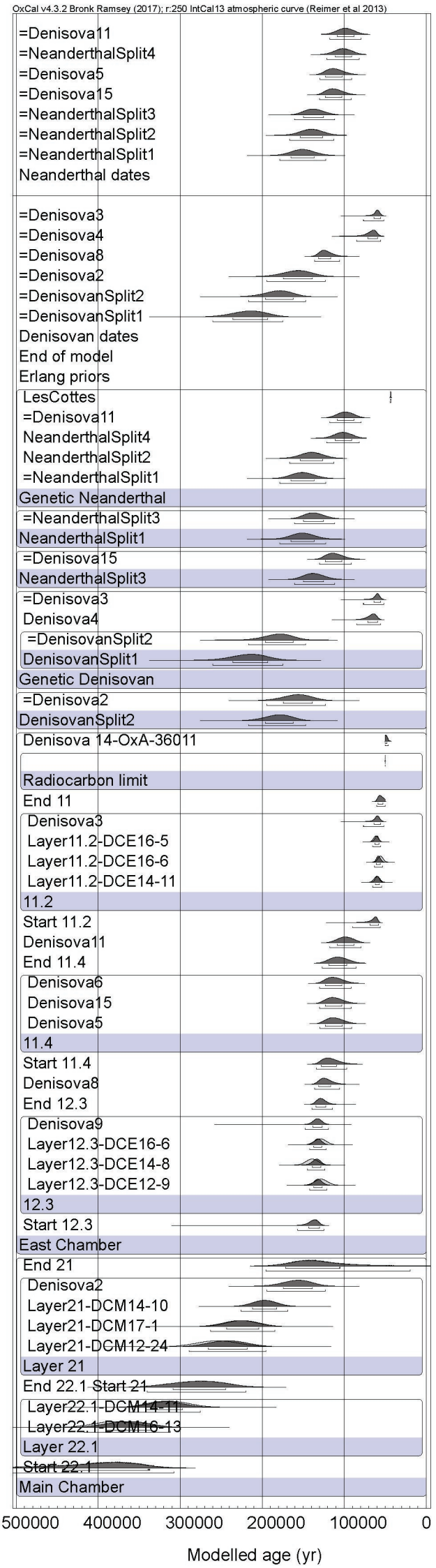

Model 4

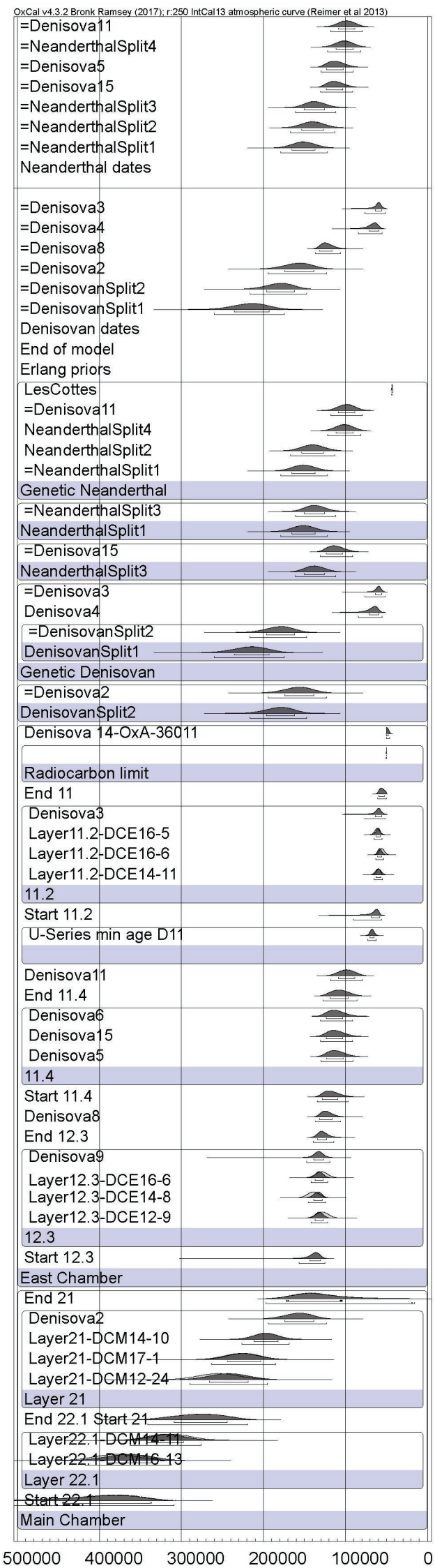

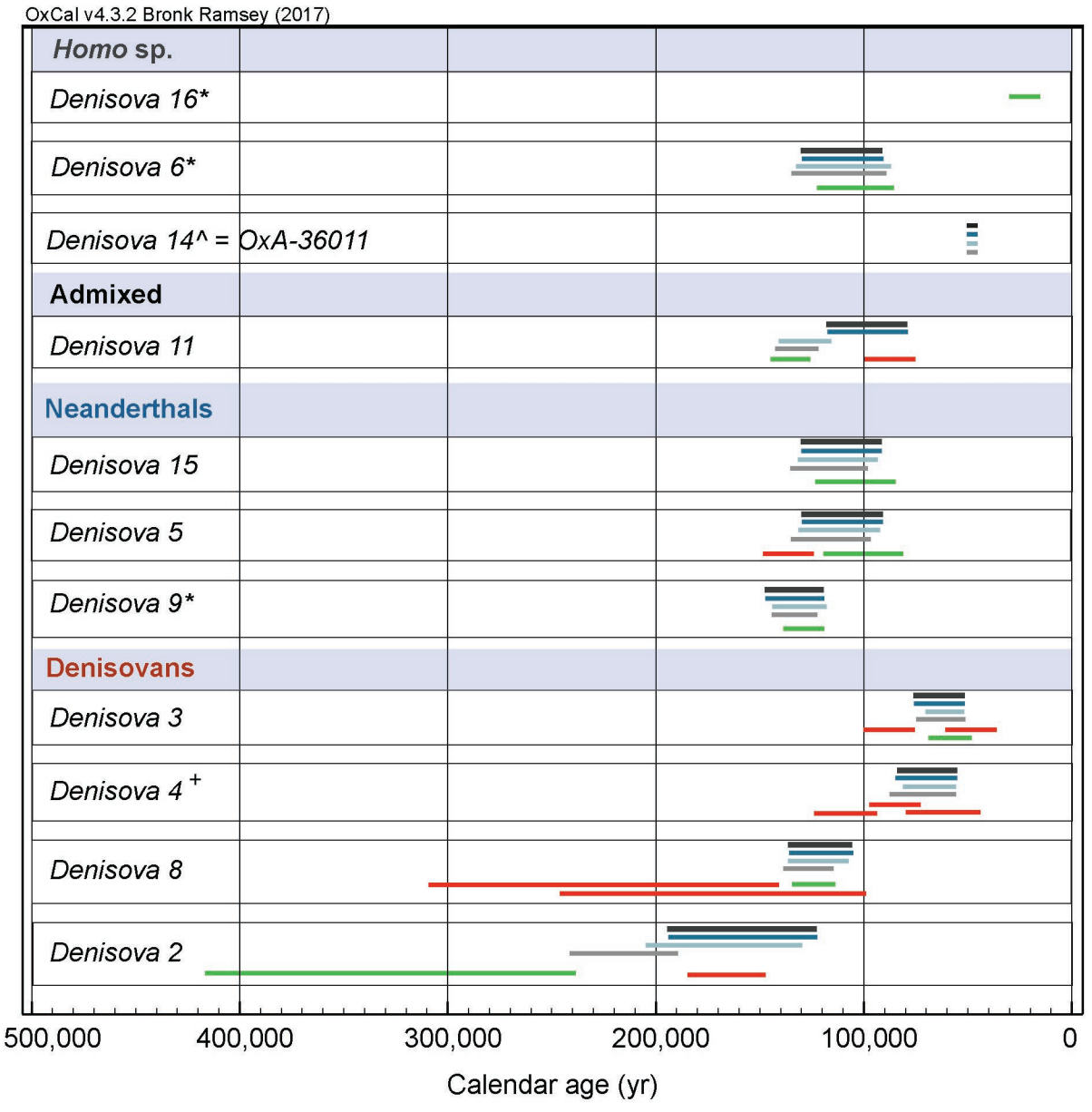

Bayesian model of all optical ages (data from ref. 10)

Genetic age estimates (previously published data in refs 2, 3, 4, 6 and 7)

Bayesian model with a combination of optical, genetic and ^{14}C ages - Model 1

Bayesian model with a combination of optical, genetic and ^{14}C ages - Model 2

Bayesian model with a combination of optical, genetic and ^{14}C ages - Model 3

Bayesian model with a combination of optical, genetic and ^{14}C ages - Model 4

* No ^{14}C or aDNA data, only optical ages available

^ Direct ^{14}C date, same in all models

\+ No ^{14}C or optical dates available

	OxA-	Material	Species ID	Layer	P-code	^{14}C years BP	±	Calibrated years BP			
East Chamber								**68.2%**		**95.4%**	
2005-2014	29859	tooth	*Equus* cf. *hydruntinus*	9.2	AF	45500	2300	>50000	47400	>50000	45720
	36011	human bone	*Homo* sp. *Denisova 14*	9.3	AF	46300	2600	>50000	47680	>50000	45970
	30006	tooth (pendant)	*Cervus* sp.	11.1	AG	27820	340	32020	31230	32660	31100
	29855	bone	*Crocuta crocuta*	11.1	AF	47900	3100	>50000	48630	>50000	49780
	30005	tooth (pendant)	*Cervus* sp.	11.2	AG	35400	900	41000	39120	41900	38400
	33086	charcoal	not id-ed	11.2	ZR	40400	900	44760	43230	45670	42690
	31506				XR	41300	900	45560	44000	46450	43260
	30963	tooth (pendant)	*Alces alces*	11.2	AG	41300	2400	47200	43040	49710	42450
	36301	bone	not id-ed	11.2	AF	>49000					
	29857	bone	*Bison/Bos*	11.2	AF	>50100					
	29858	bone	*Capra sibirica*	11.2	AF	>48600					
	29852	bone	*Equus* cf. *hydruntinus*	11.3	AF	>49400					
	29853	bone	*Cervus elaphus*	11.4	AF	>47900					
	29856	bone	*Bison* sp.	11.4	AF	>49900					
	29854	bone	Equus cf. *hydruntinus*	11.4	AF	>50000					
	36012	human bone	Neanderthal *Denisova 15*	11.4	AF	>50200					
	29860	bone	*Capra sibirica*	11.4	AF	>50000					
	32241	human bone	Neanderthal/Denisovan *Denisova 11*	12	AF	>49900					
Main Chamber											
1997	29861	bone	*Ovis/Capra*	11A	AG	37500	1000	42720	41150	43680	40180
	29872	bone (point)	*Bison* sp.	11Г	AG	42900	2000	48300	44770	>50000	44000
	30271				AF	41200	1400	45980	43410	48100	42660
2016	X-2696-20	charcoal	*Salix/ Populus*	9.2	YR	7255	35	8155	8015	8167	8001
	34713				XR	7209	35	8037	7970	8156	7956
	34729	Tooth (pendant)	*Alces alces*	Section cleaning	AG	28390	330	32800	31800	33280	31480
	X-2696-40	charcoal	*Salix/ Populus*	11.2	YR	33900	380	38850	37870	39290	37100
	34919	bone	*Capra* sp.	11.2	AF	34600	600	39800	38520	40670	37800
	X-2695-22	charcoal	Pinaceae	11.2	YR	34400	450	39440	38450	40070	37860
	X-2696-37	charcoal	Pinaceae	11.2-3	YR	35820	370	40900	40040	41310	39650
	34718	charcoal	*Abies/ Juniperus*	11.3	XR	33790	330	38670	37790	38970	37070
	34719	charcoal	Pinaceae	11.3	XR	35210	360	40220	39340	40660	38910
	X-2695-23	charcoal	Coniferous	11.3	YR	36300	900	41730	40030	42430	39080
	X-2696-34	charcoal	*Abies/ Juniperus*	11.4	YR	33380	260	38240	37260	38460	36780
	34717				XR	33720	300	38590	37780	38830	37100
	34918				ZR	33190	320	37960	36840	38370	36480
	X-2695-24	charcoal	*Abies/ Juniperus*	11.4	YR	33600	550	38580	37130	39150	36440
	34720				XR	34050	290	38890	38270	39290	37760
	34980				ZR	33600	550	38640	37090	39320	36410
	34721	charcoal	Pinaceae	11.4	XR	32530	260	36770	36120	37380	35830
	34722	charcoal	Coniferous	11.4	XR	34990	340	39920	39100	40310	38740
	34725	bone	*Ovis/Capra*	11.4	AF	32150	450	36550	35550	37410	35080
	X-2706-55				HYP	31730	330	36010	35250	36330	34900
	34727	bone	*Ovis/Capra*	11.4	AF	34750	600	39960	38670	40880	38160
	X-2706-56				HYP	33810	360	38750	37720	39140	36950
	34723	bone	*Ovis/Capra*	11.4.1	AF	33850	550	38980	37490	39600	36710
	X-2706-54				HYP	33230	350	38060	36870	38450	36440
	34877	Bone (point)	*Equus* sp.	11.4.2	AG	39300	1200	44260	42290	45700	41590
	34728	bone	*Bison/Bos*	11.4	AF	>50400					
	34724	bone	*Bison/Bos*	11.4	AF	>50300					
	34726	bone	*Bison/Bos*	12.1	AF	>50300					
	X-2696-35	charcoal	Deciduous	12.1	YR	>51600					

	X-2696-36	charcoal	Coniferous	12.3-4	YR	>55600	

	Model 1	**Model 2**	**Model 3**	**Model 4**
Model agreement index %	23.3	82.3	111	111
Denisova 14	45.9–50	45.9–50	45.9–50	45.9–50
Denisova 6	89.5–135.1	87.0–132.3	91.2–130.1	91.2–130.3
Denisova 15	97.9–134.9	94.0–132.1	91.5–130.1	91.4–130.3
Denisova 5	96.4–134.8	92.8–132.0	91.0–129.8	90.9–130.0
Denisova 9	122.3–144.1	117.9–143.7	119.1–147.4	119.1–147.3
Denisova 11	121.8–142.5	115.7–140.9	79.2–117.5	79.3–118.1
Denisova 4	56.2–88.1	55.7–81.2	55.4–84.9	55.2–84.1
Denisova 3	51.7–75.1	51.9–70.3	51.6–76.9	51.6–76.2
Denisova 8	114.5–138.6	107.2–136.4	105.7–136.3	105.6–136.4
Denisova 2	189.9–241.7	129.5–204.5	122.8–194.4	122.7–194.4

SUPPLEMENTARY INFORMATION

1: STRATIGRAPHIC AND ARCHAEOLOGICAL BACKGROUND

M. Shunkov, A. Derevianko, M. Kozlikin

Denisova Cave (51°23'51.3"N, 84°40'34.3"E) is situated in the low and middle mountains of the northwest Altai mountains in the upper Anui Basin. The site is located on the right side of the Anui River (Figure S1). The left side is confined to the slopes of the Karakol Mountain (1315 m) and the right side to the slopes of the Sosnovaya Mountain (1112 m). The valley floor is about 120 m wide (Figure S2) and the river surface is 662 m above sea level.

The cave has formed in a large Silurian marbled coarse-grained limestone block. Its entrance is located in the ledge of a southwest facing sheer rock wall at 28 m above the modern-day river level (Figure S3). The cave consists of a system of short sub-horizontal chambers varying in size, which communicate through the Main Chamber (Figure S4), a vast arched room measuring 11m × 9m and about 10m in height. Two narrow dark chambers, the East Chamber and the South Chamber, stretch southeast deep into the karst massif, where they are completely filled by loose sediments[1].

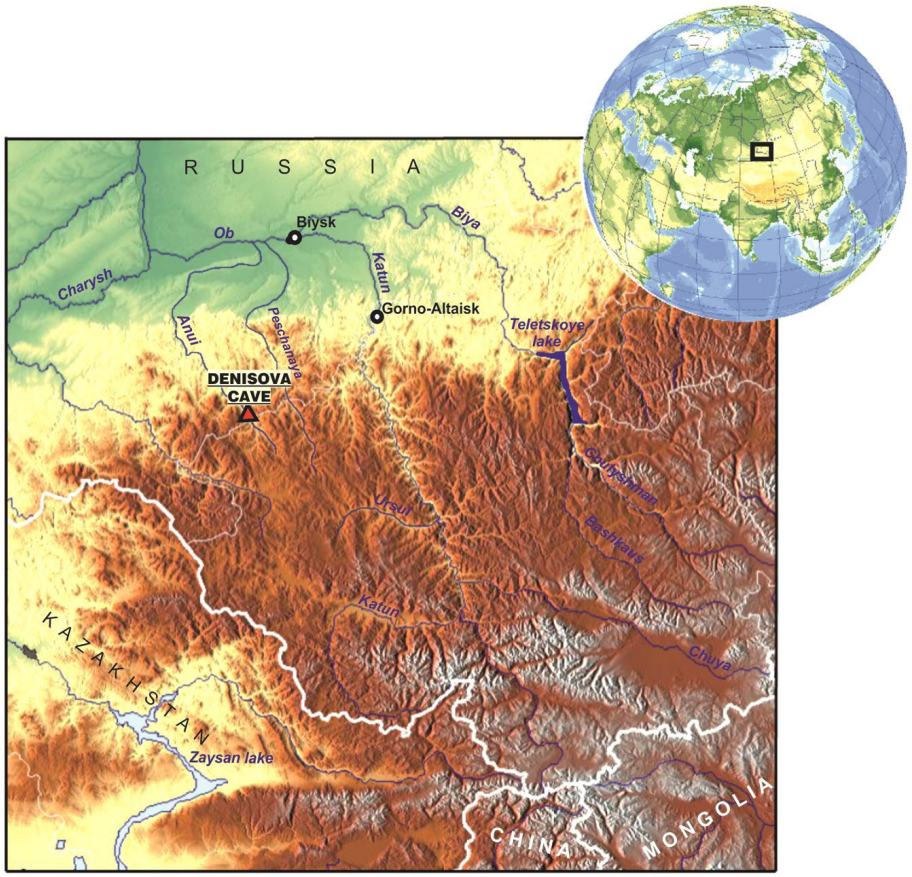

Figure S1. Location of Denisova Cave in the Altai region**.**

Denisova Cave was discovered in 1977 by N.D. Ovodov, a Russian palaeontologist[2]. Systematic investigations began in 1982. In 1982 and 1983, the Holocene deposits from the Main Chamber and the cave entrance were excavated[3]. In 1984, 1993–1995, 1997 and 2016, research focused on the Pleistocene deposits of the Main Chamber. The Pleistocene part of the cave entrance was excavated in 1990, 1991 and 1996 (Figure S4). Between 1999–2003, excavations were undertaken at the mouth of the South Chamber. In the 2004–2016 excavations revealed the Holocene and Pleistocene deposits in the East Chamber.

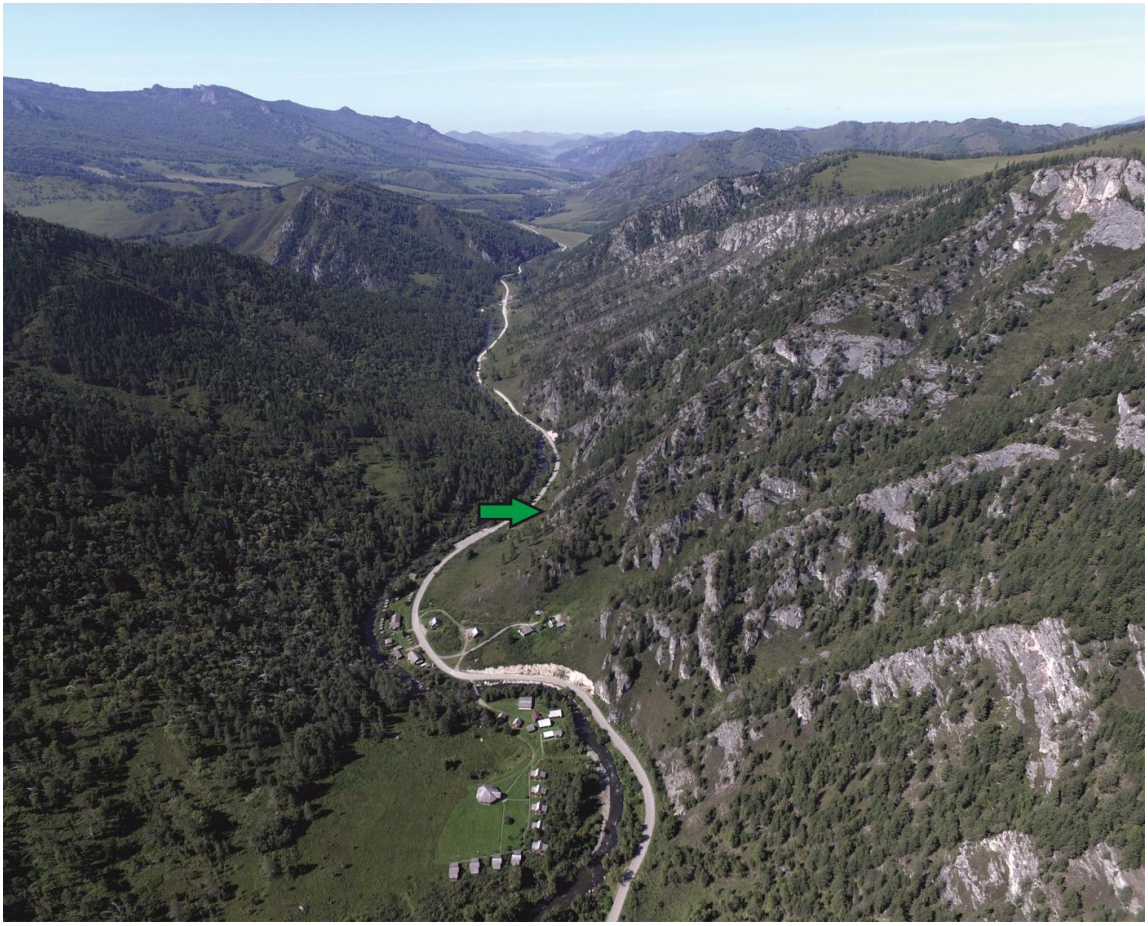

Figure S2. The Anui River valley in the vicinity of Denisova Cave (photograph by A. Postnov). The cave entrance is indicated by the green arrow. View to the north-northwest.

Figure S3. General view of Denisova Cave (photograph by S. Zelensky).

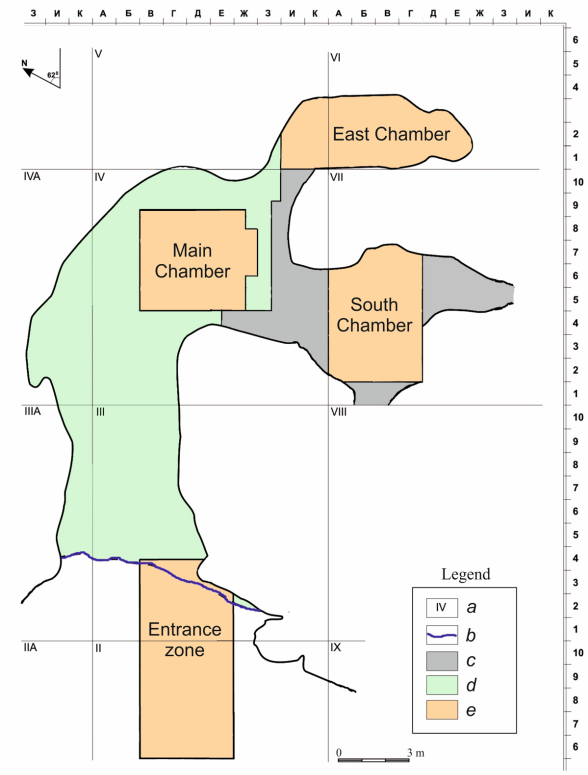

Figure S4. Denisova Cave plan showing excavated areas. Legend: a. sector number; b. cave dripline; c. Holocene surface; d. top of exposed Pleistocene deposits; e. excavation trenches in the Pleistocene deposits.

A. Stratigraphy

Main Chamber

In the Main Chamber, a total of 14 major lithological units (layers 9–22, from top to bottom) were recognised in the Pleistocene deposits of the stratigraphy. Based on a number of texture changes in the sediments, some layers (9, 11–14, 19, 22) were subdivided into additional stratigraphic horizons. Lens-shaped layers 15, 16 and 18 stretched locally in the middle portion of the deposits and were documented only in the sections produced in 1984. The 2016 excavation profile, from which the majority of samples for radiocarbon dating were collected, is shown in Figure S5[4].

The upper part of the Pleistocene deposits (layers 9.2 and 9.3) exposed during the 2016 excavations include light pale yellow loess loams with lenses and occasional inclusions of debris, finely broken stone and the new formations of whitish phosphate. Isolated burrows resulting from the activities of shrews have been identified.

The middle strata (layers 11.2–11.4, 12.1–12.3, 14, 19–21) consist of stratified lens-shaped multi-coloured loams with rubble and debris. The layers vary in thickness and reveal a sinuous shape; they show both well-defined boundaries, and indistinct ones in the form of a zone showing gradual transition.

The lower part (layers 22.1–22.3) of the stratigraphic section comprises heavy, pale ochred-yellow loams with eroded debris of different fractions, including isolated limestone blocks.

East Chamber

The East Chamber is a narrow sub-vertical fissure developed by karst processes formed by a system of steeply dipping fissures that appeared in the limestone massif. The chamber floor consists of alternate transversal rock projections and steeply dipping tunnel-shaped features[5].

Due to major differences in the composition and visual appearance of the sediments, it is not possible to make unambiguous correlation between the stratigraphic sections in the East Chamber and those exposed in the Main Chamber. Therefore, an independent stratigraphic numbering system was introduced for the deposits of the East Chamber. A total of 15 stratigraphic units were recognized in the Pleistocene part of the East Chamber (layers 9-17) (Figure S6)[6]. The deposition of loose sediments in the East Chamber indicates that this location underwent phases similar to those recognised in the Main Chamber. In general, the thick strata of sediments in the East Chamber consist, sedimentologically and lithologically, of three series of layers separated with well-defined depositional gaps.

The upper series (layers 9.1–9.3) comprises light loess loams with lenses and isolated inclusions of debris and finely broken stones. These loams are rich in organic matter resulting in severe chemical alteration of the sediments.

The middle series (layers 11.1–11.4, 12.1–12.3, 13–16) includes stratified lens-shaped rubbly material filled with multi-coloured light loams. Its formation occurred after the karst cavity opened up, in an environment of intense biogenic and anthropogenic impact and against a background of increased local climatic fluctuations.

The lower series (layers 17.1 and 17.2) consists of loamy and heavy loamy deposits of ochre-yellow color, with inclusions of lime-rock particles and leached sinter deposits. It constitutes redeposited material typical of sealed karst cavities. This earliest depositional phase occurred when the cavity was closed to external influences.

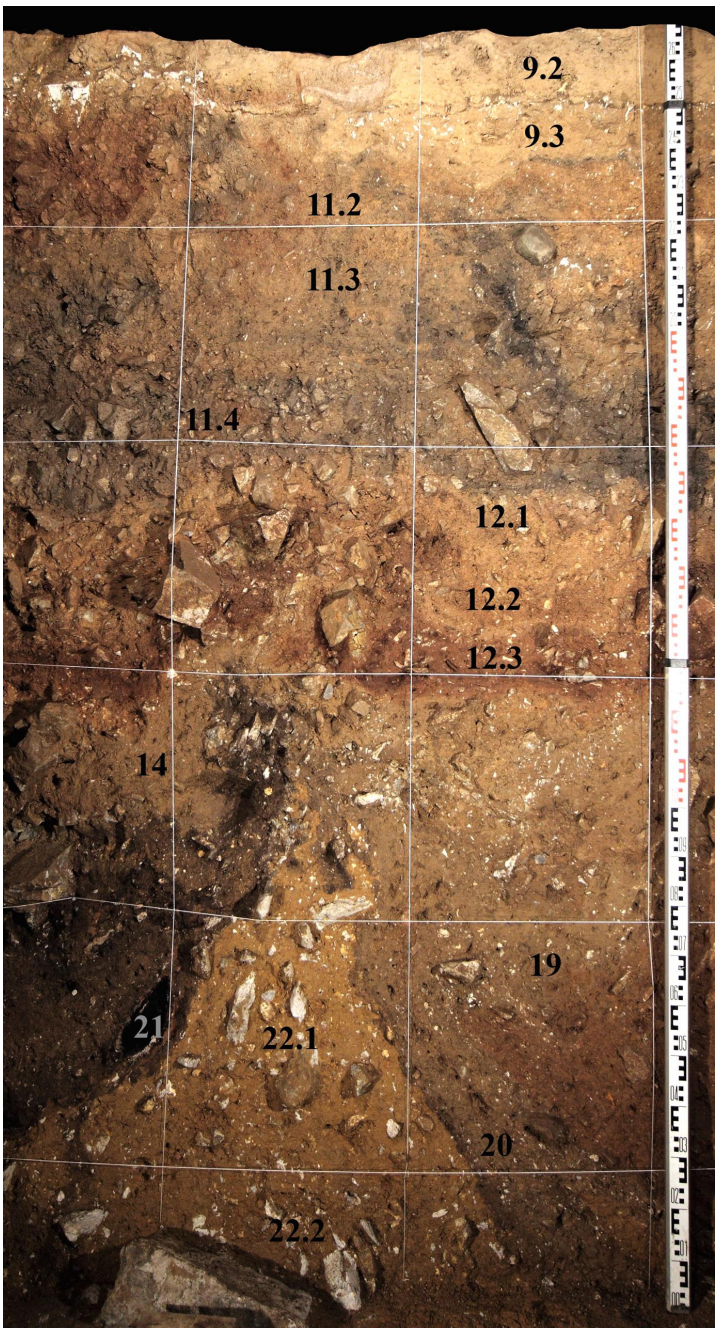

Figure S5. Southeast wall of the 2016 excavation trench in the Main Chamber showing numbers of lithological layers. Most charcoal for radiocarbon dating came from the upper part of this excavation profile.

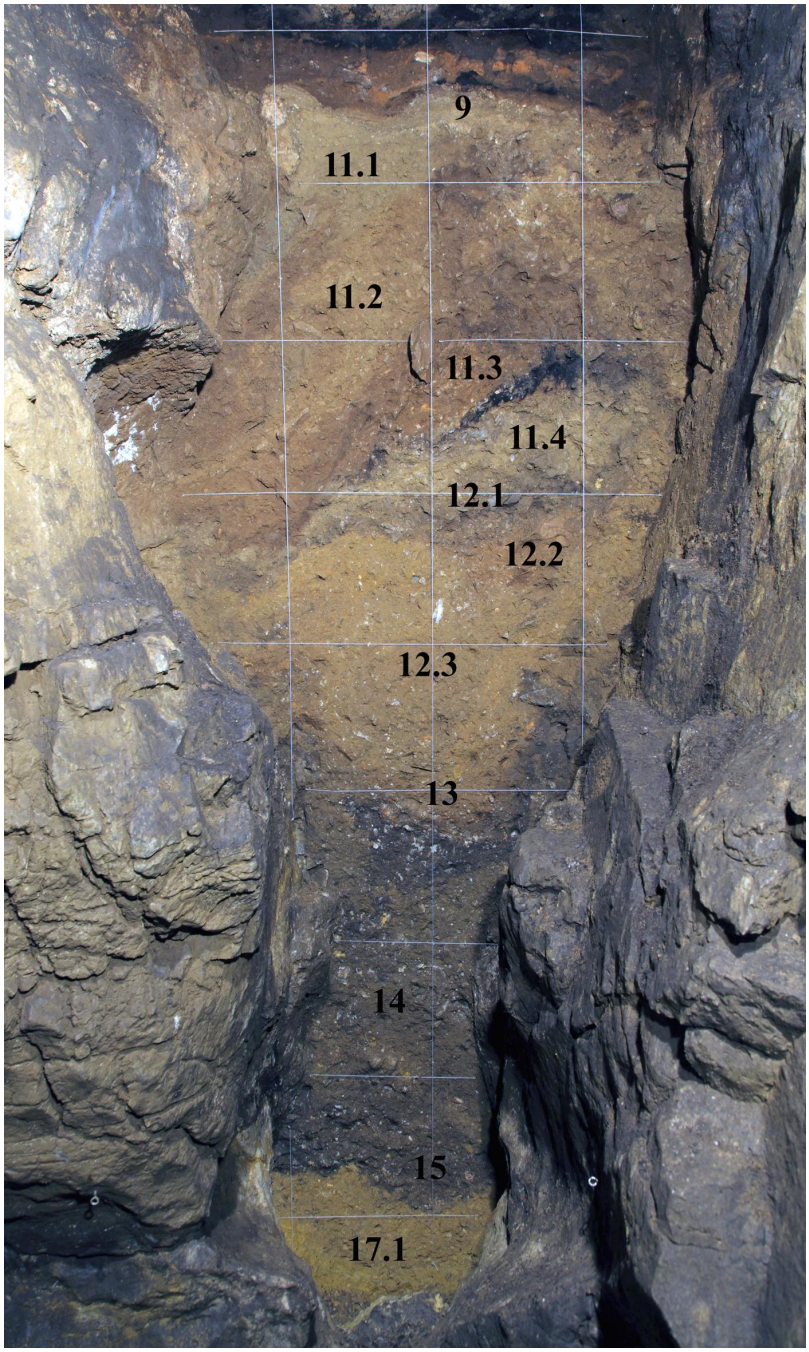

Figure S6. Southeast wall of the 2015 excavation trench in the East Chamber of Denisova Cave with numbers of lithological layers.

B. Archaeology

The upper part of layer 22 in the Main Chamber has yielded the earliest archaeological evidence at Denisova Cave. A small assemblage of lithic artefacts was recovered from this part of the section including a series of cores that indicate the use of parallel, radial and unsystematic flaking. The lithic assemblage is dominated by scrapers, denticulate, notched and spur-like tools. Levallois flakes have been also identified.

The lithic assemblage retrieved from lithological layers 21 and 20 in the Main Chamber and layers 15 and 14 in the East Chamber are attributed to the early Middle Palaeolithic. This is characterized by the use of radial cores and Kombewa-type cores. Levallois cores for the manufacture of flakes were also present. Here, similarly to the assemblage from layer 22, the tools include different types of denticulate, notched, spur-like tools and scrapers.

Archaeological evidence from layers 19–12 in the Main Chamber and from layers 13–11.3 in the East Chamber are attributed to the middle and late Middle Palaeolithic. Flat parallel and radial cores, as well as Kombewa-type cores, are abundant among nucleuses found in the lithic industries recovered from this part of the excavation section. Levallois cores for manufacturing flakes and blades comprise a small sub-set. Isolated sub-prismatic cores are also documented. Here, compared to the preceding early Middle Palaeolithic assemblage, the proportion of elongated flakes in the flake industry increases and regular blades made their appearance. While different types of scrapers dominate the assemblage, a distinct notch-denticulate component remains. Levallois points occur in small numbers. Upper Palaeolithic artefacts, including such types as end-scrapers, burins, chisel-like tools and truncated flakes, appear in the record.

Archaeological materials recovered from layer 11 in the Main Chamber, as well as from layers 11.2 and 11.1 in the East Chamber, are assigned to the "Initial Upper Palaeolithic". The term is used here to denote an early Upper Palaeolithic assemblage with features of Levallois reduction and retouched Upper Palaeolithic components. The lithic assemblage is characterized by the use of cores that were used for both parallel and radial flaking. Volumetric and Levallois flaking was less common. Compared to the Middle Palaeolithic assemblages, the toolkit demonstrates a decrease in the percentage of flake tools resulting from Levallois flaking, and an increase in the proportion of blades. The composition of the Initial Upper Palaeolithic tool assemblage with signs of secondary reduction from the East Chamber and the Main Chamber shows similarities with the preceding Middle Palaeolithic industries. A number of typologically important tools are still based on various types of scrapers, denticulate, notched and spur-like tools. Levallois points are present and Upper Palaeolithic-type pieces constitute no more than 18% of the tools.

Numerous objects linked with symbolic behaviour as well as bone tools were discovered alongside the lithic industry. A wide variety of pendants, tubular beads, beads and rings, were found, made of animal teeth and bones, mammoth ivory, ostrich eggshell, and ornamental stone. These were manufactured using techniques such as cutting, scraping, drilling, grinding and polishing. Local materials were used for the production of some ornaments, but exotic minerals

(serpentine, chloritolite) located 100–250 km from the cave were also used. Ostrich eggshell is likely to have been imported from modern-day Mongolia.

The archaeological record from layer 9 in the Main and East Chambers illustrates further development of the Upper Palaeolithic assemblages. During this time, the role of blade production increased and bladelet technology emerged. Tool assemblages contain very distinctive types of Upper Palaeolithic pieces, although scrapers are still common. Bone tools and ornaments produced from organic materials are also present.

Characteristic tool types from the Main And East Chambers are shown in Figures S7 and S8. According to the excavators, the Palaeolithic assemblages from Denisova Cave reflect a long-term process of progressive evolution in lithic industries, attesting to the continuity of technological traditions among humans inhabiting the site during the Middle and Upper Palaeolithic periods.

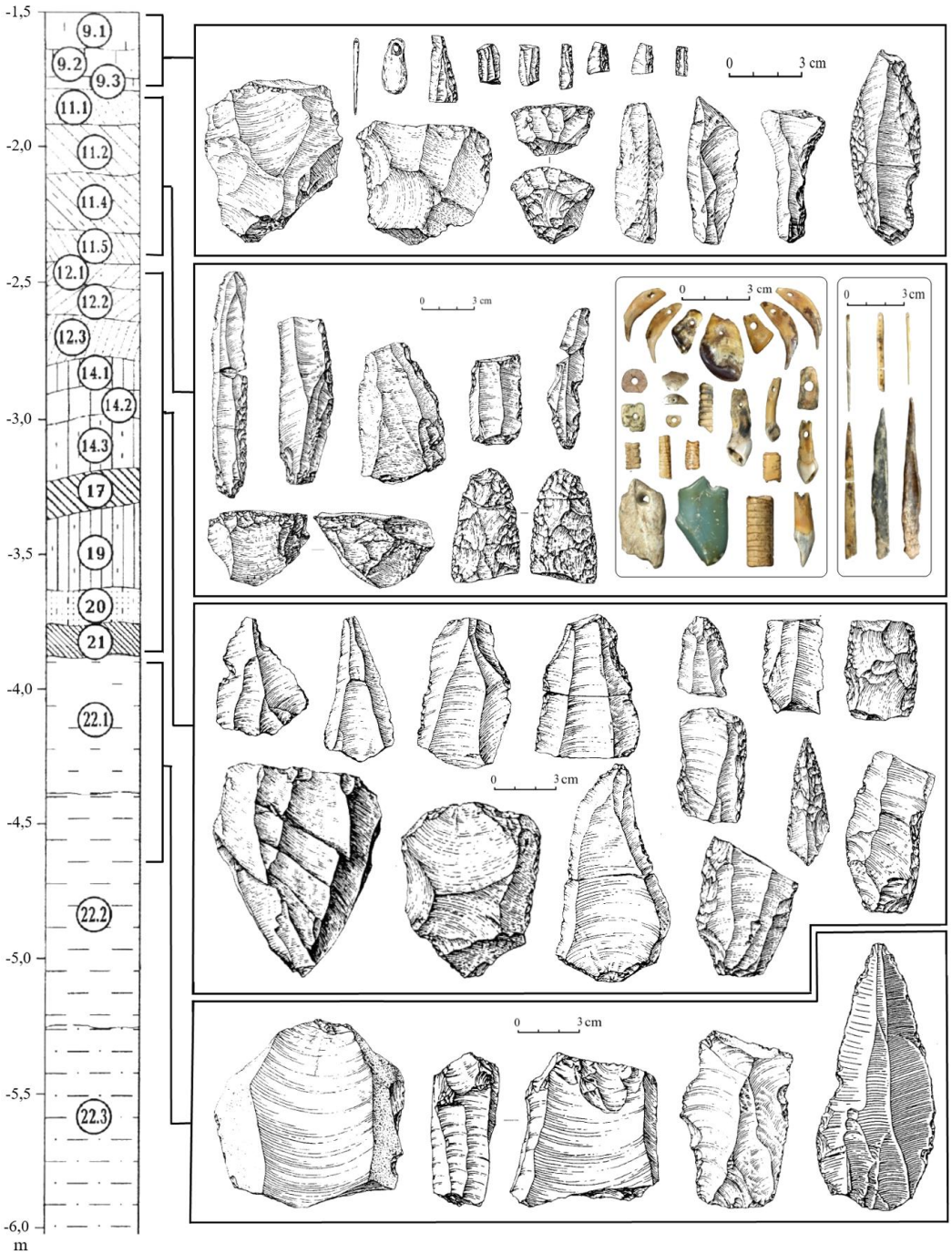

Figure S7. Artefacts from the Main Chamber of Denisova Cave.

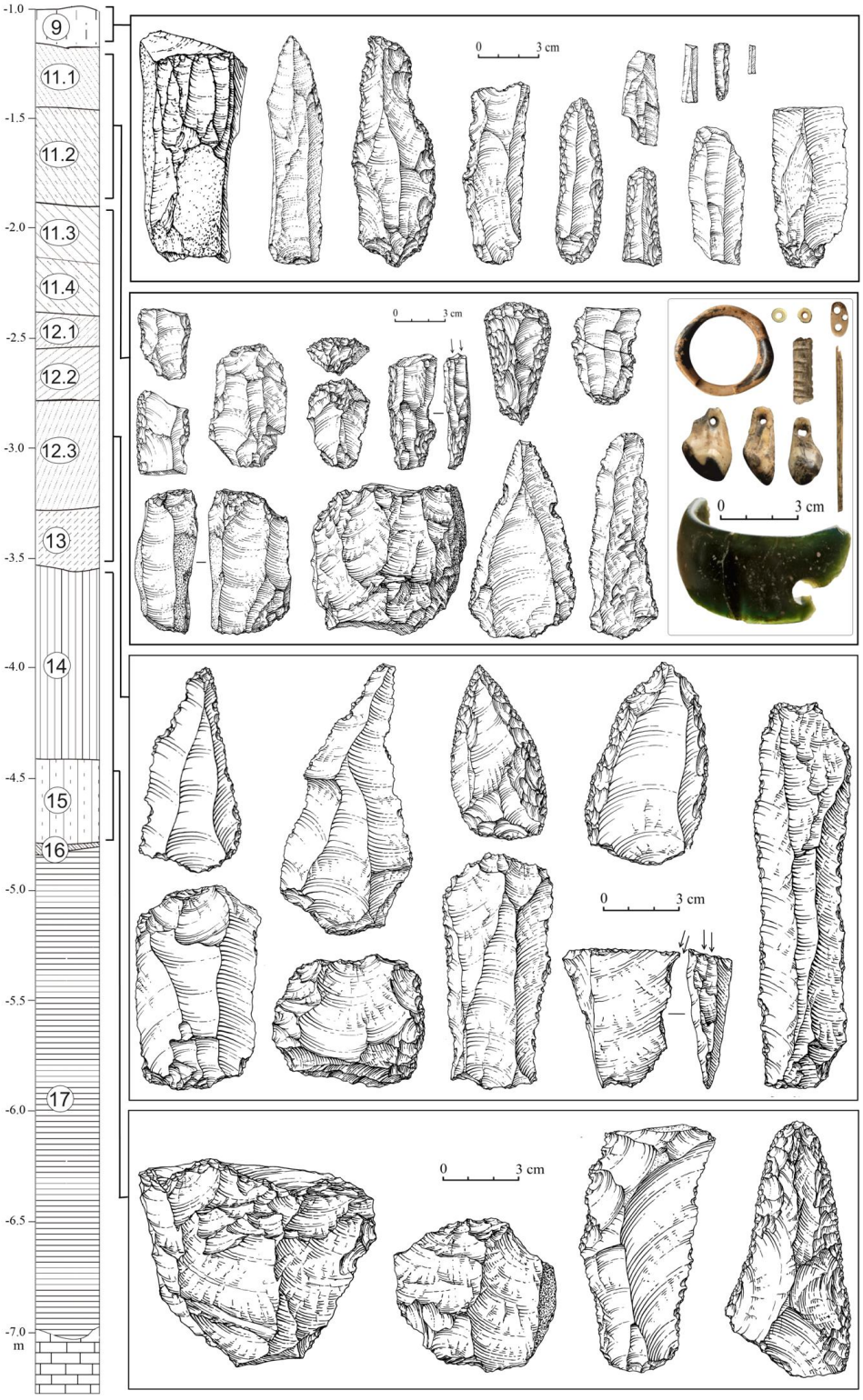

Figure S8. Artefacts from the East Chamber of Denisova Cave.

B. Regional comparisons

In addition to Denisova Cave, eight cave sites and over ten open-air sites, with a total of over 70 occupation layers spanning the Middle and Upper Palaeolithic periods, have been discovered in the Altai Mountains[7,8]. Based on extensive evidence from fieldwork and laboratory studies from these sites, the excavators have argued that there is a uninteruptive evolutionary development of the Middle Palaeolithic industry with no easily discernible effect stemming from the infiltration of populations associated with a different cultural adaptation.

At the final stage of the Middle Palaeolithic (50–60,000 years ago), two variants in the production of lithic industries emerged in the Altai, the Kara-Bom and Karakol variants. These may represent different adaptive strategies by early Upper Palaeolithic hunter-gatherers; both however appear to emerge from a single Middle Palaeolithic tradition.

In areas where the Upper Palaeolithic is linked to the arrival of different human populations, the Middle and Upper Palaeolithic industries demonstrate sharp differences, and discontinuity in both primary and secondary reduction strategies. On the contrary, at sites where Upper Palaeolithic industries developed locally, it is possible to trace the evolutionary development through the Middle Palaeolithic industries. This is the case of Denisova Cave.

The lithic evidence from layer 11 in the Main Chamber and layers 11.2 and 11.1 in the East Chamber of Denisova Cave demonstrates the retention of Middle Palaeolithic elements in primary and secondary reduction, with the emergence of a techno-typological base characteristic of the Upper Palaeolithic.

Based on the lithic and bone industries, numerous non-utilitarian objects, economic strategies, and the presence of seemingly imported materials or finished pieces, the behaviour of populations who inhabited the Altai region is characteristic of that often associated with anatomically modern humans. However, recovery of mitochondrial and nuclear DNA from human fossils found associated with the Upper Palaeolithic layer 11.2 in the East Chamber and layer 11.1 in the South Chamber shows that these hominins were the *Denisovans*[9].

A human population with a distinct Mousterian-type lithic industry, associated with the Neanderthals, also inhabited the Altai region[10]. Evidence in support of this has been found in Okladnikov and Chagyrskaya caves. Materials recovered from these caves share similarities in major technological and typological features, which are not characteristic of other Palaeolithic assemblages in the region. This Mousterian-type industry is characterized by the dominance of radial technology that became the basis for the mass production of angled blanks. The assemblages from both Okladnikov and Chagyrskaya caves demonstrate identical features of secondary reduction. The toolkit includes a broad range of scrapers, points, notch-denticulate tools, retouched flakes and bifaces. A key feature of this industry is the presence of backed scraper knives, as well as various angled pieces including *déjeté* scrapers[11]. Very few and isolated Mousterian-type tools such as the ones discovered at Chagyrskaya and Okladnikov caves have been recognized in the Middle Palaeolithic layers of Denisova Cave, where Neanderthal remains were recovered from layers 11.4 and 12 in the East Chamber and Neanderthal DNA was extracted

from the sediment of layers 11.4 and 14 in the East Chamber and layers 14, 17 and 19 in the Main Chamber[12-13].

One possibility to explain the archaeological evidence is that Denisovans were the producers of the Upper Palaeolithic technocomplexes in the Altai region between 50–35 ka. To date, there is no anthropological or genetic record of anatomically modern humans in the Altai during the late Pleistocene. The presence of the Ust-Ishim modern human in western Siberia at 45,000 cal BP[14], however, raises the possibility that modern humans who were present in the wider region may have also been the makers of the Upper Palaeolithic in the Altai. It is important to consider that our age estimate for *Denisova 3*, the most recent Denisovan fossil at the site pre-dates 50,000 BP and the direct date for Ust-Ishim. More human material is required to answer with more certainty questions regarding the link between hominins and lithic industries and other types of artefacts.

2: RADIOCARBON DATING

K. Douka, T. Higham, T. Devièse, D. Comeskey

A. Dated material

Samples for AMS ^{14}C dating were obtained either at the storage and museum facilities in Novosibirsk (bone and artefacts) or at the cave during, or shortly after, excavation (mainly charcoals). Four series of samples were selected for dating; human bones, cutmarked bones, tooth pendants, bone points and charcoal samples.

Below in brackets are the number of "individual samples"/ "total radiocarbon dates" obtained, per type of material. In some cases indivdual samples were dated more than once, in others they failed to procuded enough C for dating.

1. human bones (n=2/2), plus *Denisova 11* previously published.
2. cut-marked animal bones and teeth (n=23/21) (Figure S9)
3. tooth pendants (ornaments) (n=5/4) (Extended Data Figure 2)
4. bone points (n=2/3) (Extended Data Figure 2)
5. charcoal samples (n=31/20).

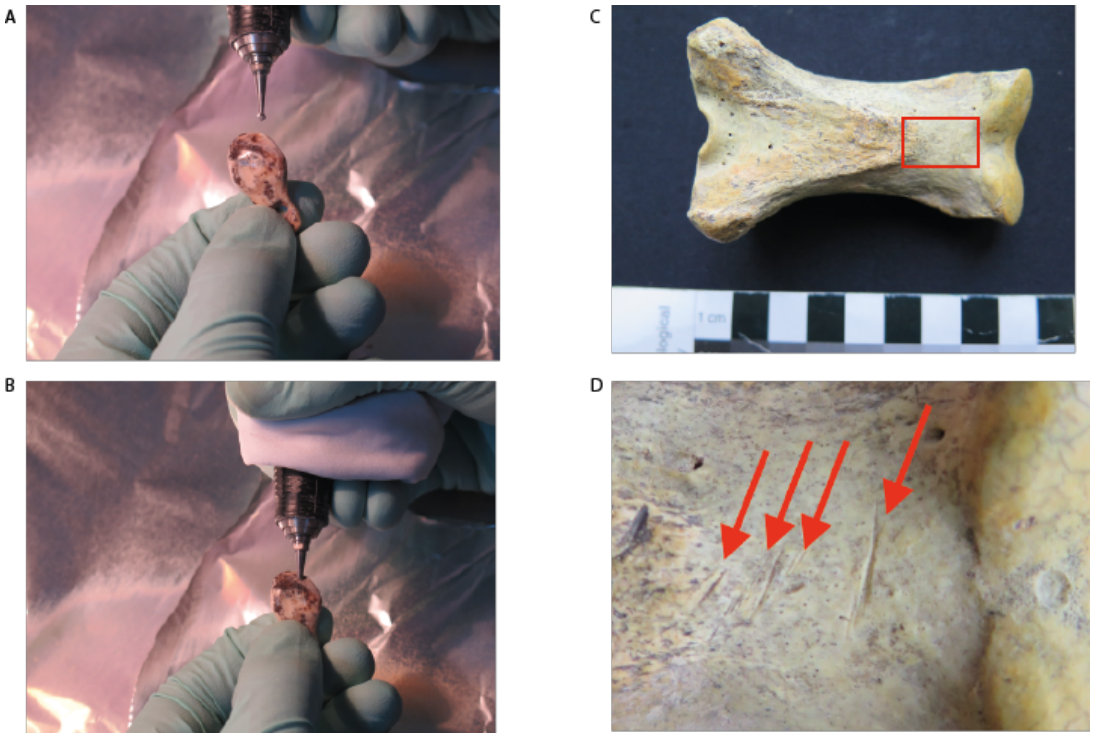

Figure S9: A-B: Tooth pendants from the East and Main Chambers were drilled using the ORAU's keyhole sampling method to minimise sample invasiveness and destruction. C-D: Cut-marked bone was selected for AMS dating; in this example a bone of *Equus cf hydruntinus* from Layer 11.3 (East Chmaber) was dated to >49,400 BP (OxA-29852) (D see inset of photograph C).

B. Charcoal Identification

Charcoal was taxonomically identified prior to radiocarbon dating by Dr Dana Challinor. The fragments were extremely small, with some less than 2mm in transverse section (the standard size required for identification). In all cases, however, it was possible to determine whether coniferous or deciduous wood was present. Identification was also hampered by high levels of vitrification and the inability to fracture without destruction. Standard identification procedures were followed based upon anatomical structure, with reference to modern specimens and reference texts. The material was held in a sand bath for examination.

At least three separate genera were positively distinguished; *Pinus* (pine), *Abies/Juniperus* (fir or juniper) and *Salix/Populus* (willow or poplar). In many cases, it was possible to say, on the basis of resin canal presence, that a member of the Pinaceae was represented, but closer identification was not possible. Only one fragment exhibited the large pitting typical of *Pinus*, but others with smaller pitting could be from a different pine species or from *Picea* (spruce). Notes on the identifications for each fragment are included in Table S1 below, but a couple of other anatomical observations are worth noting: no scalloped tori were visible; bi-seriate bordered pits were absent (which is typical of *Larix*, larch); and no spiral thickenings were observed (which rules out the presence of *Taxus,* yew), although some compression lines (indicating branchwood) were noted.

Table S1: Identifications for the charcoal samples dated from the Main Chamber. *P no*. denotes the Oxford sample reference number.

P no.	Identification	Identification notes
41823	*Abies/Juniperus*	No resin canals, taxadoid-cupressoid pits, single borded pits, uniseriate rays, no spirals. Vitrified.
41824	Pinaceae	Resin canals, single bordered pits, small ray pitting. Vitrified.
41825	Pinaceae	1 resin canal but too small to confirm other characteristics.
41826	Coniferous	Too small to identify further.
41827	Deciduous r-w	Diffuse porous but too small to confirm identify further.
41828	Coniferous	Poss resin canal, but unclear as very distorted.
41833	Pinaceae	Resin canals, single bordered pits so prob *Picea* or *Pinus* – but too small to see pitting
41839	*Abies/Juniperus*	As for <823> but crumbled.
41840	*Pinus* sp.	No resin canals visible, but definite large pitting – pinoid type.
41841	Pinaceae	1 resin canal observed in ray TLS but too small to see other characteristics. Vitrified

41842	Pinaceae	No resin canals but poor confition, vitrified. Taxodoid pits.
41843	*Salix/Populus*	Short radial files, uniseriate rays, distinctive pitting
41844	Deciduous	Diffuse porous but too small to take further.
41845	Coniferous	<1 growth ring. Compression lines
41846	*Abies/Juniperus*	No resin canals, uniseriate rays, single bordered pits, taxadoid to cuppresoid pitting
41847	cf. *Pinus* sp.	Resin canals (not traumatic), horizontal walls pitted, single row bordered pits, ray pitting unclear as small so cf. id. Compression lines
41849	Pinaceae	Possible resin canal, single row bordered pits, uniseriate rays, no spirals
41850	Coniferous	Single row bordered pits, no spirals

C. Radiocarbon dating methods

AMS sample pretreatment and measurment were performed at the Oxford Radiocarbon Accelerator Unit (ORAU), University of Oxford, UK. Bones for dating were sampled as unobtrusively as possible using an NSK micromotor drill with tungsten carbide and diamond drill bits. The samples underwent the routine ORAU chemical pretreatment protocol briefly described below.

Drilled or coarsely ground bone powder was immersed in solutions of 0.5 M HCl (3 washes over 18h at room temperature (RT)), 0.1M NaOH (30 minutes, at RT) and 0.5M HCl (~1 hour; at RT), interspersed with ultra-pure (MilliQ™) water rinses between each reagent. The extracted collagen was gelatinised in a pH 3 solution at 75 °C for 20 hours and filtered through previously-cleaned 9ml polyethylene Ezee-filters™ (Elkay, UK). The filtrate was transferred with glass pipettes into previously-cleaned ultrafilters (Sartorius Vivaspin™ 15–30kD MWCO) and centrifuged at 2500-3000rpm until 0.5–1.0mL of the >30kD gelatin fraction was left (~30-40 mins). The supernatant was collected using glass pipettes, placed into prebaked clean glass tubes, frozen at -18 °C, and freeze-dried for a minimum of 12 hours. Ezee-filters™ and ultrafilter precleaning steps are undertaken as outlined in Brock *et al*. (2010)[15]. For some bones, noted as AG in the pretreatment code column (Table S2), ultrafiltration was not applied due to low amount of recovered collagen.

For three bone samples from the Main Chamber (P 41851, P 41853 and P 41856) we also used the single amino acid radiocarbon dating method developed at the ORAU. This method involves separation of the underivatised amino acids from hydrolysed bone collagen samples using preparative High Performance Liquid Chromatography (Prep-HPLC)[16]. Using this procedure (coded HYP), hydroxyproline (Hyp), which essentially acts as a biomarker of bone collagen, was isolated and dated. This approach is the most efficient technique to remove contaminants including conservation materials.

Samples of charcoal were prepared for dating using three methods: the routine ABA (Acid-Base-Acid) method, the ABOx-SC preparation[17] as applied at Oxford[15] and a modified ABOx-SC preparation which excludes the base step (AOx-SC) (Douka et al. *in preparation*). This latter method has been shown to produce results indistinguishable to those obtained with the ABOx-SC method but without the extensive material loss associated with it. In Table S2, ABA is denoted as ZR, ABOx-SC as XR, AOx-SC as YR.

Gelatin, amino acids, or pre-combusted charcoal samples were analysed using a PDZ-Europa Robo-Prep combustion elemental analyser coupled to a PDZ-Europa 20/20 mass spectrometer operating in continuous flow mode using an He carrier gas. This enables the measurement of $\delta^{15}N$ and $\delta^{13}C$ values and N and C content, and calculation of C:N atomic ratios. VPDB is the standard for $\delta^{13}C$ values, AIR for the $\delta^{15}N$ values. Graphite was produced by reacting the sample CO_2 over an iron catalyst in an excess H_2 atmosphere at 560°C. AMS radiocarbon measurement was undertaken using the ORAU 2.5MV HVEE accelerator.

We used OxCal 4.3.2[18] and the IntCal13 calibration curve[19] to calibrate the radiocarbon data when these were within the working limit of the method, i.e. <50,0000 BP.

D. Radiocarbon dating results

Radiocarbon dates and all analytical data are reported in Table S2. The vast majority of bones were well preserved in terms of collagen, with only one yielding less than 1% wt. collagen (the effective threshold in the ORAU). We did, however, have some bone samples that failed to produce a collagen yield of significance, these failed samples are shown in Table S3. All other analytical parameters we measured, including the C/N atomic ratio, were within accepted ranges. The dates are corrected for routine procedures such as pre-treatment chemistry, combustion and graphitisation. For the HYP dates, the correction also includes the extraneous carbon added during the chromatographic separation[16]. The results obtained for the same sample using AF and HYP protocols are in statistical agreement.

The calibrated radiocarbon data of the finite ages, i.e. those within the limit of the method, are shown in Table S4 and Figure S10 below.

Table S2: New radiocarbon determinations from Denisova Cave. *OxA-* is the Oxford radiocarbon lab code, *P no*. denotes the Oxford sample reference number, *P code* denotes the pretreatment method and dated material used (AG is gelatinised filtered collagen without ultrafiltration for the low collagen bones; AF is ultrafiltered collagen; HYP is the single amino acid, hydroxyproline; ZR, XR and YR refer to ABA, ABOx-SC or AOx-SC methods, respectively, for charcoal samples). Samples highlighted in grey denote samples that produced more than one radiocarbon determination using different pretreatment methods.

	Radiocarbon results										Analytical data						
	OxA-	**P no.**	**Material**	**Species ID**	**Layer**	**Year exc. Square, ID**	**^{14}C yrs BP**	**±**	**F^{14}C**	**±**	**δ^{13}C (‰)**	**N^{15}N (‰)**	**C:N**	**P code**	**Used mg**	**Yield mg (%)**	**%C**
East Chamber																	
Excavations 2005-2014	29859	35677	tooth	*Equus* cf. *hydruntinus*	9.2	2008, n/a	45500	2300	0.00347	0.00099	-19.77	5.01	3.36	AF	790	12.81 (1.6)	40.3
	36011	43830	human bone	*Homo* sp.	9.3	DC 3758 *Denisova 14*	46300	2600	0.00313	0.00101	-18.82	16.49	3.25	AF	290	5.27 (1.8)	42.2
	30006	35672	tooth (pendant)	*Cervus* sp.	11.1	2007, E-4(B), N 133	27820	340	0.03134	0.00133	-19.30	9.72	3.47	AG	230	3.71 (1.6)	35.6
	29855	35673	bone	*Crocuta crocuta*	11.1	2005, B-2, N 382	47900	3100	0.00257	0.00099	-17.71	10.09	3.33	AF	840	97.60 (11.6)	42.7
	30005	35671	tooth (pendant)	*Cervus* sp.	11.2	2006, Г-2, N 385	35400	900	0.01213	0.00137	-18.96	8.91	3.46	AG	290	3.03 (1.0)	38.6
	33086	37599	charcoal	not id-ed	11.2	2014, A-2, N 195	40400	900	0.00655	0.00073	-23.20	0.00	n/a	ZR	52.7	2.73 (5.2)	60.8
	31506						41300	900	0.00586	0.00063	-21.98	0.00	n/a	XR	104	5.74 (5.5)	60.5
	30963	37598	tooth (pendant)	*Alces alces*	11.2	2014, A-2, N 11	41300	2400	0.00582	0.0017	-19.57	6.59	3.11	AG	225	2.22 (1.0)	37.6
	36301	43832	bone	not id-ed	11.2	2013, D, K-2,4	>49000		0.00020	0.00103	-20.5	5.1	3.20	AF	720	6.2 (0.8)	42.9
	29857	35675	bone	*Bison/Bos* sp.	11.2	2008, Δ-3, N 381	>50100		0.0000	0.00098	-19.38	4.66	3.30	AF	970	55.40 (5.7)	42.1
	29858	35676	bone	*Capra sibirica*	11.2	2008, Δ-2	>48600		0.00037	0.00099	-19.20	5.28	3.34	AF	760	32.40 (4.3)	40.2
	29852	35668	bone	*Equus* cf. *hydruntinus*	11.3	2009, Г-3, N 359	>49400		0.00019	0.00097	-20.34	6.72	3.31	AF	700	47.90 (6.8)	42.5
	29853	35669	bone	*Cervus elaphus*	11.4	2009, Г-2, N 615	>47900		0.0006	0.00098	-19.38	6.24	3.31	AF	830	31.70 (3.8)	41.7

	29856	35674	bone	*Bison* sp.	11.4	2011, Г-4, N 23	>49900		0.00002	0.00099	-18.90	12.78	3.34	AF	890	27.30 (3.1)	39.6
	29854	35670	bone	E*quus* cf. *hydruntinus*	11.4	2009, Г-3, N 381	>50000		0.0000	0.00099	-20.09	11.20	3.33	AF	990	37.70 (3.8)	41.8
	36012	43831	human bone	*Neanderthal*	11.4	DC 3573 *Denisova 15*	>50200		0.0000	0.00097	-18.6	12.67	3.17	AF	450	40.84 (9.1)	43.9
	29860	35679	bone	*Capra sibirica*	11.4	2009, Г-2, N 606	>50000		0.0000	0.00098	-19.00	6.05	3.37	AF	1020	45.90 (4.5)	41.3
	32241	39272	human bone	Neanderthal/ Denisovan hybrid	12	2014, A-2, DC 1227, *Denisova 11*	>49900		0.0000	0.001	-17.37	16.35	3.32	AF	290	13.20 (4.6)	43.1
Main Chamber																	
Excavation 1997	29861	35682	bone	*Ovis/Capra*	11A	1997, B-6, N 3846/77	37500	1000	0.00934	0.00117	-18.78	6.37	3.34	AG	240	6.65 (2.8)	41.7
	29872	35681	bone (point)	*Bison* sp.	11Г	1997, A-8, N 3846/66	42900	2000	0.00479	0.00116	-19.90	3.61	3.36	AG	250	24.80 (9.9)	41.3
	30271						41200	1400	0.00593	0.00103	-20.33	3.45	3.34	AF	19	n/a (11.8)	42.7
Excavation 2016	X-2696-20	41575	charcoal	*Salix/Populus*	9.2	2016, E-3	7255	35	0.40529	0.00176	-25.76	0.00	0.00	YR	91	7.16 (7.9)	73.3
	34713						7209	35	0.40763	0.00176	-25.46	0.00	0.00	XR	123	7.43 (6.1)	76.9
	34729	41859	tooth (pendant)	*Alces alces*	n/a	Section cleaning	28390	330	0.02918	0.00119	-18.94	7.36	3.16	AG	360	7.02 (2.0)	38.6
	X-2696-40	41843	charcoal	*Salix/Populus*	11.2	2016, SH-7/cut 12, N 9	33900	380	0.01469	0.00069	-24.70	0.00	n/a	YR	95	3.50 (3.7)	49.1
	34919	41858	bone	*Capra* sp.	11.2	2016, SH-7/cut 12, N 28	34600	600	0.01348	0.001	-18.39	5.47	3.18	AF	710	35.57 (5.0)	43.8
	X-2695-22	41842	charcoal	Pinaceae	11.2	2016, SH-7/cut 12, N 10	34400	450	0.01384	0.00079	-22.41	0.00	n/a	YR	71	11.3 (7.98)	47.8
	X-2696-37	41833	charcoal	Pinaceae	11.2-11.3	2016	35820	370	0.01157	0.00054	-23.38	0.00	n/a	YR	101	7.66 (7.5)	72.9

	34718	41839	charcoal	*Abies/ Juniperus*	11.3	2016, SH-1/cut 22	33790	330	0.01491	0.00061	-22.84	0.00	n/a	XR	87	10.22 (11.8)	71.1
	34719	41841	charcoal	Pinaceae	11.3	2016, SH-7, cut 14, N 13	35210	360	0.01248	0.00056	-22.30	0.00	n/a	XR	74	8.08 (10.9)	72.5
	X-2695-23	41845	charcoal	Coniferous	11.3	2016, SH-7/cut 13, N 12	36300	900	0.01094	0.00126	-21.46	0.00	n/a	YR	62	1.52 (2.5)	56.3
	X-2696-34	41823	charcoal	*Abies/ Juniperus*	11.4	n/a	33380	260	0.01568	0.00052	-22.76	0.00	n/a	YR	100	8.15 (8.2)	75.1
	34717						33720	300	0.01502	0.00055	-22.87	0.00	n/a	XR	136	7.86 (5.8)	76.7
	34918						33190	320	0.01605	0.00065	-23.02	0.00	n/a	ZR	22	7.16 (33.1)	57.2
	X-2695-24	41846	charcoal	*Abies/ Juniperus*	11.4	2016, SH-7/ cut 21, N 15	33600	550	0.01529	0.00101	-22.35	0.00	n/a	YR	84	6.53 (7.7)	41.1
	34720						34050	290	0.01443	0.00052	-23.21	0.00	n/a	XR	100	7.89 (7.9)	71.9
	34980						33600	550	0.01523	0.00109	-24.42	0.00	n/a	ZR	25	4.16 (16.8)	32.7
	34721	41849	charcoal	Pinaceae	11.4	2016, M-7/ cut 13, N 52, hearth	32530	260	0.01743	0.00057	-23.27	0.00	n/a	XR	112	9.03 (8.1)	71.7
	34722	41850	charcoal	Coniferous	11.4	2016, M-8/ cut 21, N 21	34990	340	0.01284	0.00054	-24.60	0.00	n/a	XR	89	3.51 (3.9)	70.0
	34725	41853	bone	*Ovis/Capra*	11.4	2016, M-7/cut 19, N 70	32150	450	0.01824	0.00099	-18.85	5.40	3.15	AF	700	28.21 (4.0)	44.7
	X-2706-55						31730	330	0.01926	0.00083	-23.6	6.7	4.8	HYP	1650	169.0 (10.2)	40.3
	34727	41856	bone	*Ovis/Capra*	11.4	2016, SH7/ cut 23, N 88	34750	600	0.01318	0.00099	-18.25	5.95	3.13	AF	720	27.23 (3.8)	44.0
	X-2706-56						33810	360	0.01486	0.00071	-22.7	7.2	5.0	HYP	1510	129.0 (8.5)	44.5

	34723	41851	bone	*Ovis/Capra*	11.4.1	2016, M-8/ cut 15, N 2143	33850	550	0.01477	0.001	-18.23	5.83	3.12	AF	690	31.73 (4.6)	43.9
	X-2706-54						33230	350	0.01598	0.00074	-22.0	7.1	4.7	HYP	1680	175 (10.4)	41.0
	34877	41860	bone (point)	*Equus* sp.	11.4.2	2016, M-8 (B)/ cut 14, N 128	39300	1200	0.00752	0.00115	-20.85	6.09	3.17	AG	300	10.72 (3.6)	40.8
	34728	41857	bone	*Bison/Bos* sp.	11.4	2016, SH-7/cut 20, N64	>50400		0.0000	0.00094	-20.16	7.02	3.12	AF	750	38.46 (5.1)	45.3
	34724	41852	bone	*Bison/Bos* sp.	11.4	2016, M-7/cut 21, N 70	>50300		0.00001	0.00095	-18.81	5.70	3.13	AF	730	25.06 (3.4)	45.0
	34726	41854	bone	*Bison/Bos* sp.	12.1	2016, SH-7/ cuts 24-25	>50300		0.0000	0.00095	-19.75	6.01	3.12	AF	630	71.16 (11.3)	44.0
	X-2696-35	41827	charcoal	Deciduous	12.1	n/a	>51600		0.00061	0.00051	-26.36	0.00	n/a	YR	63	9.12 (14.4)	65.3
	X-2696-36	41828	charcoal	Coniferous	12.3-12.4	interface of layers	>55600		0.00011	0.00043	-24.99	0.00	n/a	YR	93	10.24 (11)	74.1

Table S3. Samples that failed to produce enough carbon for radiocarbon dating.

	P no.	Material	Species	Layer	Year Excavated, Square, ID no	P. code	Comments
East Chamber							
Excavations 2007-13	35678	bone	Ungulate	9.3	2008, b-2	AF	Failed due to no collagen yield
	34815	charcoal	n/a	11.1	2013, K-4	XR	Failed due to no yield
	34814	bone	Large mammal	11.2	2013, D-4, N 87	AG	Failed due to low collagen yield
	41824	bone	Large mammal	11.2	2013, D-3, N 149	AG	Failed due to low collagen yield
	35667	bone	*Cervus elaphus*	11.2	2009, b-2, N 284	AF	Failed due to no collagen yield
	37206	tooth (pendant)	*Cervus* sp.	11.2	2007, N 282	AF	Failed due to no collagen yield
Main Chamber							
Excavation 2016	41824	charcoal	Pinaceae	11.3	2016	YR	Failed due to no yield
	41825	charcoal	Pinaceae	11.4	2016	YR	Failed due to no yield
	41826	charcoal	Coniferous	11.4	2016	YR	Failed due to no yield
	41829	charcoal	n/a	12.2	2016	n/a	Withdrawn, low starting mass
	41830	charcoal	n/a	11.3	2016	n/a	Withdrawn, low starting mass
	41831	charcoal	n/a	11.2	2016	YR	Failed due to low yield
	41832	charcoal	n/a	11.3	2016	YR	Failed due to no yield
	41834	charcoal	n/a	9.3	2016	YR	Failed due to no yield
	41835	charcoal	n/a	11.3	2016	YR	Failed due to no yield
	41836	charcoal	n/a	11.2	2016	YR	Failed due to no yield
	41837	charcoal	n/a	9.3	2016	YR	Failed due to low yield
	41838	charcoal	n/a	9.3	2016	YR	Failed due to low yield
	41840	charcoal	*Pinus* sp.	12.3	2016, Square 8/cut 30	YR	Failed due to low yield
	41844	charcoal	Deciduous	11.2	2016, Square 7/ cut 12	YR	Failed due to low yield
	41847	charcoal	cf. *Pinus* sp.	11.4	2016, Square 7/ cut 23, N 17	XR	Failed due to no yield
	41848	charcoal	n/a	11.4	2016, Square M-7/ cut 13, N 51, hearth	YR	Failed due to no yield
	41855	bone	n/a	11.2	2016, SH-7/ cut 8	AG	Failed due to no collagen yield

Table S4. Calibrated age ranges BP (68.2% and 95.4% probabilities) for the finite radiocarbon dates we obtained from Denisova Cave. Age ranges are rounded to the nearest 10 years. Samples in grey indicate samples with more than one radiocarbon date.

	Layer	from	to	from	to
East Chamber		**68.2%**		**95.4%**	
OxA-29859	9.2	>50000	47400	>50000	45720
OxA-36011	9.3	>50000	47680	>50000	45970
OxA-30006	11.1	32020	31230	32660	31100
OxA-29855	11.1	>50000	48630	>50000	49780
OxA-30005	11.2	41000	39120	41900	38400
OxA-33086	11.2	44760	43230	45670	42690
OxA-31506		45560	44000	46450	43260
OxA-30963	11.2	47200	43040	49710	42450
Main Chamber					
OxA-29861	11A =11.1?	42720	41150	43680	40180
OxA-29872	11Г = 11.4?	48300	44770	>50000	44000
OxA-30271		45980	43410	48100	42660
X-2696-20	9.2	8155	8015	8167	8001
34713		8037	7970	8156	7956
OxA-34729	n/a	32800	31800	33280	31480
OxA-X-2696-40	11.2	38850	37870	39290	37100
OxA-34919	11.2	39800	38520	40670	37800
OxA-X-2695-22	11.2	39440	38450	40070	37860
OxA-X-2696-37	11.2/11.3	40900	40040	41310	39650
OxA-34718	11.3	38670	37790	38970	37070
OxA-34719	11.3	40220	39340	40660	38910
OxA-X-2695-23	11.3	41730	40030	42430	39080
OxA-X-2696-34	11.4	38240	37260	38460	36780
OxA-34717		38590	37780	38830	37100
OxA-34918		37960	36840	38370	36480
OxA-X-2695-24	11.4	38580	37130	39150	36440
OxA-34720		38890	38270	39290	37760
OxA-34980		38640	37090	39320	36410
OxA-34721	11.4	36770	36120	37380	35830
OxA-34722	11.4	39920	39100	40310	38740
OxA-34725	11.4	36550	35550	37410	35080
OxA-X-2706-55		36010	35250	36330	34900
OxA-34727	11.4	39960	38670	40880	38160
OxA-X-2706-56		38750	37720	39140	36950
OxA-34723	11.4.1	38980	37490	39600	36710
OxA-X-2706-54		38060	36870	38450	36440
OxA-34877	11.4.2	44260	42290	45700	41590

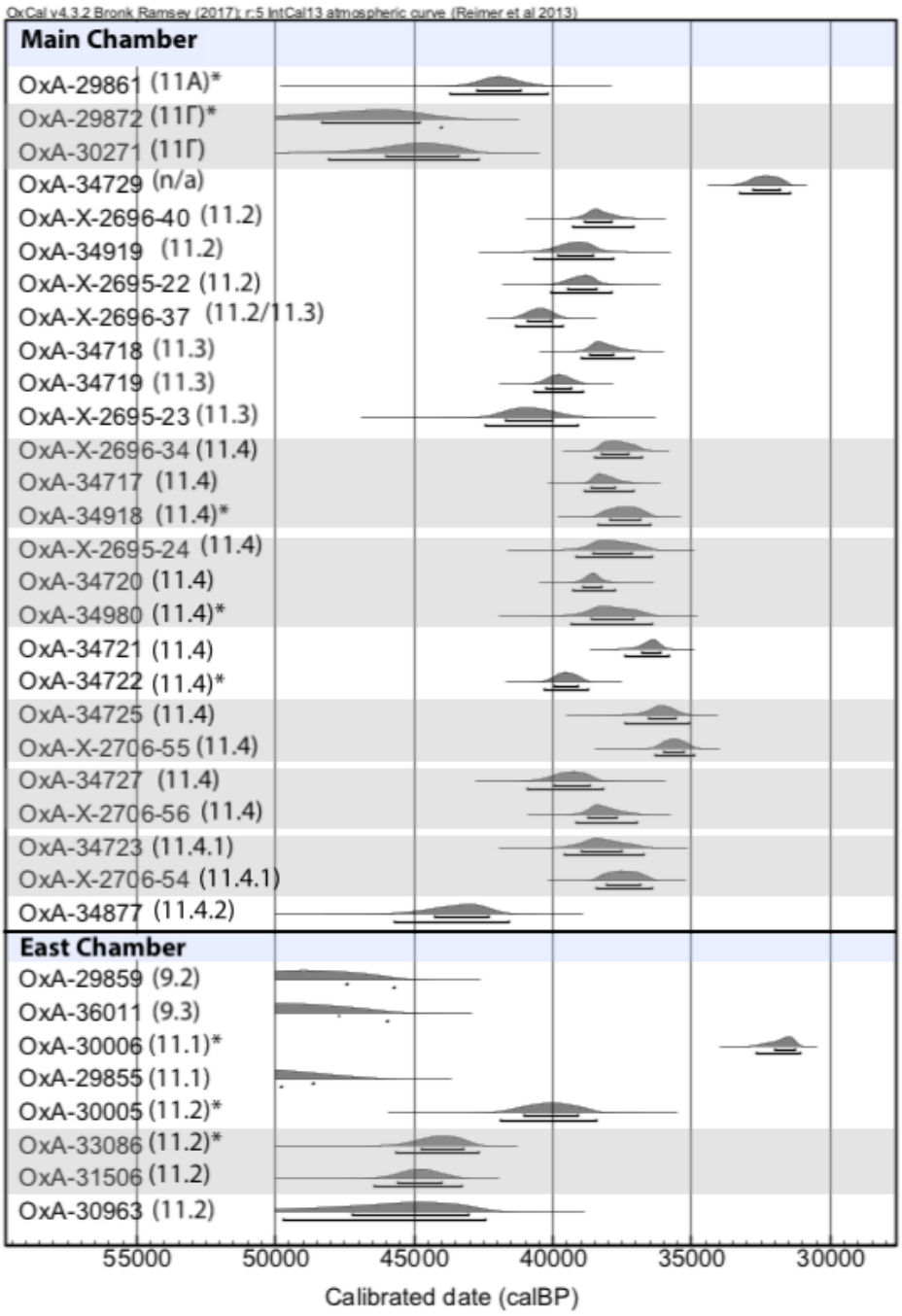

Figure S10. Calibrated dates from Denisova Cave using OxCal 4.3 and the IntCal13 calibration curve. Only the radiocarbon dates falling in the working limit of the method, i.e. <50,0000 BP, are included. The two Holocene dates from layer 9.2 in Main Chamber are not shown here. In grey are dates made on the same sample using different pretreatment protocols. The least reliable protocol (AG, gelatinization but no ultrafiltration for bone collagen; ZR, ABA for charcoals) is marked with an asterisk. In brackets are the layers for each sample. Numerical, raw and calibrated, data can be found in Table S2 and S4, respectively.

3. CATALOGUE OF HOMININ (OR PUTATIVE HOMININ) REMAINS FROM DENISOVA CAVE

B. Viola, K. Douka, T. Higham, M. Shunkov, J. Kelso

Denisova 1, incisor (non-human) (Figure S11 a- d)

1984, Main chamber, Sector 4, Sq. D7, Layer 12

Only the crown of this large incisor is preserved, with the root broken away at the level of the apical margin of the enamel on the labial face. Strong wear removed the crown down to the level of a few small grooves on the lingual margin, probably representing the *tuberculum dentale*.

The specimen was first described[20] as an upper left first incisor. Turner[20] described similarities with the Shanidar 2 upper incisors, but thought that the specimen did not show the typical shovelling seen in the Krapina material. In his opinion, the absence of a flat, or double shoveled labial surface supported European affinities. Later, Shpakova and Derevianko[21] and Shpakova[22] also compared the tooth to Shanidar 2, as well as Asian *Homo erectus*.

The similarities to Shanidar 2 described previously are not convincing. Shanidar 2, just like other Neanderthal upper first incisors[23] has a strongly rounded and convex labial surface, and exhibits both mesial and distal marginal ridges. This strongly contrasts with the morphology of *Denisova 1*, which has an extremely flat labial surface, and only a mesial marginal ridge (if interpreted as an upper left I^1).

The triangular outline in occlusal view and the rather abrupt angle between the mesial and labial surfaces is unlike the morphology usually seen in hominins. The enamel is also quite thin, and the L-shaped cross section of the pulp cavity, as evidenced by the secondary dentine, are all traits that raise questions with regards to the identification of this specimen as hominin. A more likely interpretation is that this is a very worn lower incisor of a large bovid, either *Bison priscus* or *Bos mutus*, both of which have been identified from Layer 12.

Denisova 2, left lower dm_2 (Denisovan) (Figure S11 e, f)

1984, Main chamber, Sector 4, Sq. B8, Layer 22.1

This specimen is a worn left lower second deciduous molar. Originally described by Turner[20] as a right lower dm_1, but the large size and the absence of the *tuberculum molare* make the identification as a dm_2 more plausible. The morphology of the specimen has been described in detail by Slon et al.[12] The morphology of the specimen does not allow assessment of its affinities

in detail, but both its mtDNA and nuclear DNA indicate that it belongs to the Denisovan lineage[12]. Female.

Denisova 3, proximal fragment of distal manual phalanx (Denisovan) (Figure S12 a)

2008, East Chamber, Sector 6, Sq. D-2/91, Layer 11.2

This small (7x5 mm) fragment of a distal hand phalanx does not preserve much morphological information. It derives from a subadult individual between about 7 and 13.5 years[9]. Short descriptions for the specimen were published previously. The mitochondrial DNA was published in 2010[24], the nuclear DNA was reported soon after[25]. Female.

Denisova 4, left upper $M^{2/3}$ (Denisovan) (Figure S11 f)

2000, South Chamber, Sq. G-2/29, Layer 11.1

A mostly complete upper molar, missing the distobuccal root and with slight wear. Morphology and mtDNA for this specimen is reported in 2010[9], 54.6 MB of nuclear DNA was analyzed in 2015[26]. The specimen is both morphologically and genetically distinct from Neanderthals, and a Denisovan. Male.

Denisova 5, proximal pedal phalanx (Neanderthal) (Figure S12 b, d)

2010, East Chamber, Sector 6, Sq. B-3, Subsq. G, Layer 11.4, sublevel (подуровень) 6

A relatively well preserved proximal pedal phalanx, with the trochlea missing and slight damage on the dorsal and medial margins of the proximal end. This specimen has been first published in 2011[27], describing the specimen as very robust and broad compared to Neanderthals. A high coverage nuclear and mitochondrial genome was published in 2014[28], both of which indicate that this specimen was a Neanderthal. Also known as the "Altai Neanderthal". Female.

Denisova 6, left lower second deciduous incisor (hominin indet.) (Figure S11 g, h)

2010, East Chamber, Sector 6, Sq. G-3, Subsq. G, Layer 11.4, sublevel (подуровень) 9

This specimen is a worn lower di_2 with about half of the root resorbed. The specimen has not

been sampled for ancient DNA due to its small size, a detailed description is in preparation.

Denisova 7, parietal fragment (non-human) (Figure S12 g, h)

2008, East Chamber, Sector 6, Sq. D-3, Layer 11.3

This specimen was originally identified as a hominin parietal fragment. Several features, such as the shape of the supposedly coronal suture, the curvature in the coronal plane, the lack of meningeal grooves as well as the marked and sharp edged digital impressions make this identification improbable, and a non-human, probably ursid origin of this specimen more likely. Unpublished ancient DNA analyses by E. Rogaev have found only cave bear DNA in this specimen.

Denisova 8, left upper $M^{2/3}$ (Denisovan) (Figure S11 k)

2010, East Chamber, Sector 6, Sq. G-4, Subsq. V/G, Interface between layer 11.4 and 12.

Recovered in several fragments, slightly above *Denisova 5*, this specimen preserves the almost complete crown of an upper second or more likely third molar. It is similar to Denisova 4 in its large size and complex occlusal morphology. Morphological, mtDNA and nuclear DNA data from this Denisovan individual was published in 2015[26]. Male.

Denisova 9, distal hand phalanx (Neanderthal) (Figure S12 f)

2011, East Chamber, Sector 6, Sq. G-3, Subsq. A, Layer 12.3, sublevel (подуровень) 4.

A relatively complete distal manual phalanx, damaged near the base. The specimen has been described[29] and ancient DNA analyses are in progress. Male.

Denisova 10, immature phalanx fragment (non-human) (Figure S12 c)

2011, East Chamber, Sector 6, Sq. G-2, Subsq. B, Layer 12, sublevel (подуровень) 1.

This specimen was originally identified as a hominin immature pedal phalanx. The specimen is rather well preserved, but is missing the yet unfused proximal epiphysis. In lateral view, this specimen shows a straight and horizontal plantar surface, and a concave dorsal surface. This, together with the very rounded trochlea as well as the strong extensions of the distal articular

surface both medially and laterally on the plantar side are very unlike the toe morphology seen in hominins and fit much better with an identification as a middle pedal phalanx of a sub-adult bear.

Denisova 11, long bone fragment (Neanderthal/Denisovan offspring) (Figure S13 a)

2012, East Chamber, Sector 6, Sq. Д-2, Layer 12.3

This specimen was identified among bulk bone fragment collections using ZooMS (ZooMS ID: DC1227). Mitochondrial[30] and nuclear DNA[34] analyeses have been published, and further results are reported in Section 5. Female.

Denisova 12, molar fragment (non-human) (Figure S11 l)

2015, East Chamber, Sector 6, Sq. М-3, Layer 12, sublevel (подуровень) 9.

Originally identified as a human molar fragment. The thin enamel and the cusp morphology of this specimen make an identification as a lower deciduous molar of a cave bear more likely. Ancient DNA analyses support this conclusion.

Denisova 13, parietal fragment (hominin indet.)

2016, South Chamber, section cleaning, Layer 22?.

Two adjoining fragments of the posterior half of a hominin parietal. They were found during cleaning of the lower part of the stratigraphic section, hence tentatively attributed to Layer 22. Detailed morphological and ancient DNA analyses are in progress.

Denisova 14, long bone fragment (hominin) (Figure S13 b)

2012, East Chamber, Sector 6, Layer 9.3

This specimen was identified among the bulk fragment collection using ZooMS (ZooMS ID: DC3758) and is reported in this paper for the first time. Directly dated by AMS at 46,300 ± 2600 BP. Ancient DNA analyses failed to yield useable DNA (see Section 5 below).

Denisova 15, long bone fragment (Neanderthal) (Figure S13 c).

2012, East Chamber, Sector 6, Layer 11.4

This specimen was identified among the bulk fragment collection using ZooMS (ZooMS ID: DC3573) and is reported in this paper for the first time. Directly dated by AMS at >50,200 BP. MtDNA DNA analyses summarised in Section 5 below indicate this is a Neanderthal.

Denisova 16, bone fragment (hominin) (Figure S13 d).

2016, Central Chamber, Sector 4, Layer 9.1

This specimen was identified among the bulk fragment collection using ZooMS (ZooMS ID: DC4114) and is reported in this paper for the first time. Ancient DNA analyses are currently in progress. Due to small size of the bone radiocarbon dating was not performed.

Figure S11. Dental material from Denisova Cave. a-d: *Denisova 1* in occlusal (a), lingual (b), labial (c) and mesial (d) views. e,f: *Denisova 2* in occlusal (e) and lingual (f) views. g,h: *Denisova 6* in occlusal (g) and lingual (h) views. i,j: *Denisova 4* in mesial (i) and occlusal (j) views. k: *Denisova 8* in occlusal view. l: *Denisova 12* in occlusal view.

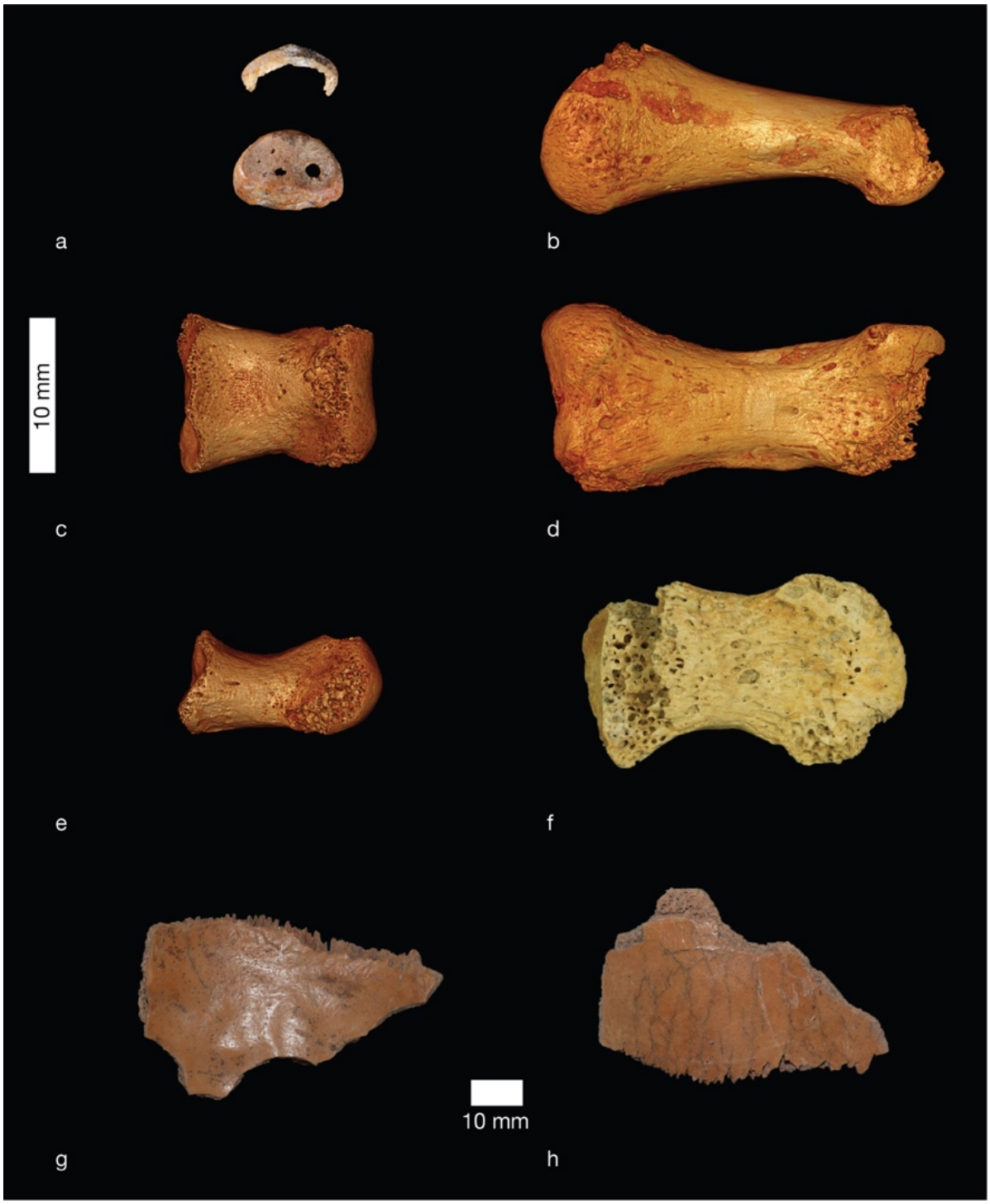

Figure S12. Cranial and postcranial remains from Denisova Cave. a. *Denisova 3* in proximal view. b, d: µCT based renderings of *Denisova 5* in lateral (b) and plantar (d) views. c,e: µCT based renderings of *Denisova 10* in dorsal (c) and lateral (e) views. f: *Denisova 9* in palmar view. g,h: Endocranial (g) and outside (h) views of *Denisova 7*.

Figure S13. Fragments of human remains from Denisova Cave identified using ZooMS. (a) *Denisova 11*[30,34], (b) *Denisova 14*, (c) *Denisova 15*, (d) *Denisova 16*.

4. GENETIC DATA

V. Slon, F. Mafessoni, J. Kelso, M. Meyer, S. Pääbo

A. Age estimates from nuclear DNA

Estimates of ages based on branch shortening have been made for the high-coverage genomes of *Denisova 3* and *Denisova 5* (the "Altai Neanderthal")[25,28,31] (Table S5). We caution that these estimates are sensitive to sequencing error and differ depending on whether all sites or only transversion polymorphisms are used to assess the branch shortening. It is also important to note that the conversion to absolute ages is influenced by whether the divergence from the common ancestor with the chimpanzee is assumed to be 6.5 million or 13 million years ago. In the calculations below we use a divergence of 13 million years, which corresponds to a mutation rate per year of 1.45 x 10-8 mutation per base pair per generation and a generation time of 29 years. This mutation rate is estimated from ancient DNA and from the sequencing of parent-offspring trios[14,32,33]. Although the absolute dates that we obtain using this approach are only approximate due to uncertainties in mutation rates and the generation times, these results indicate that *Denisova 5* is older than *Denisova 3*.

Additionally, the occurrence of admixture between Neanderthals and Denisovans provides an indication about the timing of Denisovan and Neanderthal presence in Denisova cave, and constrains the ages of some of the individuals from Denisova Cave. First, the genome of *Denisova 3* contains segments introgressed from a Neanderthal that is more closely related to *Denisova 5* than to *Vindija 33.19* from Croatia, whose genome has also been sequenced to high-coverage[31]. This admixture must have occurred after *Denisova 5* split from the most recent ancestor shared with *Vindija 33.19* (estimated to have been ~130-145ka) (Table S6), but before *Denisova 3* lived, therefore providing an upper limit on the age of *Denisova 3*. Second, comparisons of the low-coverage genome of *Denisova 11*, the F1-offspring of a Neanderthal mother and a Denisovan father, to the high-coverage Neanderthal and Denisovan genomes allowed us to estimate the times at which the parents of *Denisova 11* split from the lineages leading to *Denisova 3, Denisova 5* and *Vindija 33.19*[34] (Table S6). These provide upper limits on the age of *Denisova 11.* We estimate that *Denisova 11* separated from the lineage leading to *Vindija 33.19* ~40,000 *before Vindija 33.19* lived[31]*.* It was previously estimated that the common ancestor of *Vindija 33.19* and *Denisova 5* lived ~80,000 and ~20,000 after the separation from their common ancestor, respectively, thus we infer that *Denisova 11* lived no earlier than ~40,000 after the *Vindija 33.19-Denisova 5* split (*i.e.,* ~90-105ka)[34], at least 20ky after *Denisova 5*, and likely before *Denisova 3*. Note that the conversion of the split time to absolute ages is sensitive to all the above-mentioned caveats affecting the branch shortening estimates.

Table S5. Branch shortening and estimated ages of *Denisova 3* and *Denisova 5.* Data taken from Refs 28,31.

Specimen	Branch shortening	Estimated age (i)	Estimated age (ii)	Estimated age (iii)
Denisova 3	0.82% (0.74%-0.93%)	48-60 ka	76.6-92.4 ka	60-84 ka
Denisova 5	1.03% (0.96%-1.14)	62-74 ka	116.6-129.4 ka	110-134.8 ka

(i) Calculated on all sites and assuming a divergence time to the common ancestor of humans and chimpanzee of 6.5 million years; (ii) Calculated on all sites and assuming a human-chimpanzee divergence of 13 million years; (iii) Calculated using transversion polymorphisms only and assuming a divergence time to the common ancestor of humans and chimpanzee of 13 million years.

Table S6. Estimates of split times between Neanderthal and Denisovan lineages. Data taken from Refs [31,34].

Lineage 1	Lineage 2	Estimated split time (i)	Estimated split time (ii)
Denisova 5	*Vindija 33.19*	-	130-145 ka
Denisova 11 (Neanderthal parent)	*Denisova 5*	143-159 ka	142-158.5 ka
	Vindija 33.19	87-102 ka	82-97 ka
Denisova 11 (Denisovan parent)	*Denisova 3*	89-93 ka	76.5-80.5 ka

The conversion of split times into absolute dates takes into account the branch shortening estimates for the high-coverage genome, calculated (i) on all sites and assuming a human-chimpanzee divergence of 13 million years; or (ii) using transversion polymorphisms only and assuming a divergence time to the common ancestor of humans and chimpanzee of 13 million years.

B. Age estimates from mitochondrial DNA

(i) Estimating branch shortening by maximum parsimony

From a multiple sequence alignment of the mitochondrial genome sequences of the four Denisovans and the Middle Pleistocene *Sima de los Huesos* individual, we had previously inferred the number of substitutions on each branch since the split from the most recent common ancestor of all Denisovans using maximum parsimony (Figure S14A). We caution that back mutations and multiple substitutions occurring at the same position will not be accounted for, and may affect our inference of the number of substitutions occurring on the various branches. Nonetheless, this analysis suggested that *Denisova 2* is likely the oldest of the four Denisovans, followed by *Denisova 8* and then by the younger and possibly contemporaneous *Denisova 3* and *Denisova 4*[12]. **Error! Bookmark not defined.**

Similarly, we here inferred the number of substitutions on the branches relating the Neanderthal-like mtDNAs of *Denisova 5*, *Denisova 11* and *Denisova 15* with the mtDNA genomes of 19 other Neanderthals from other archaeological sites, using the divergent mtDNA of the *Hohlenstein-Stadel* Neanderthal as outgroup. We infer that since the split from the most recent ancestor shared with *Hohlenstein-Stadel*, a total of 15 and 14 substitutions occurred on the branches leading to *Denisova 5* and *Denisova 15*, respectively, suggesting that these two individuals were roughly contemporaneous; while 19 substitutions occurred on the branch leading to *Denisova 11*, suggesting that the latter individual is younger than *Denisova 5* and *Denisova 15* (Figure S14B).

We converted the differences in the number of inferred substitutions into differences in time by applying the mitochondrial mutation rate inferred for modern humans of 2.53×10^{-8} (95% HPD: $1.76\text{-}3.23 \times 10^{-8}$)[14] (Table S7). Note that this assumes that the mitochondrial mutation rate in archaic humans is the same as that in modern humans.

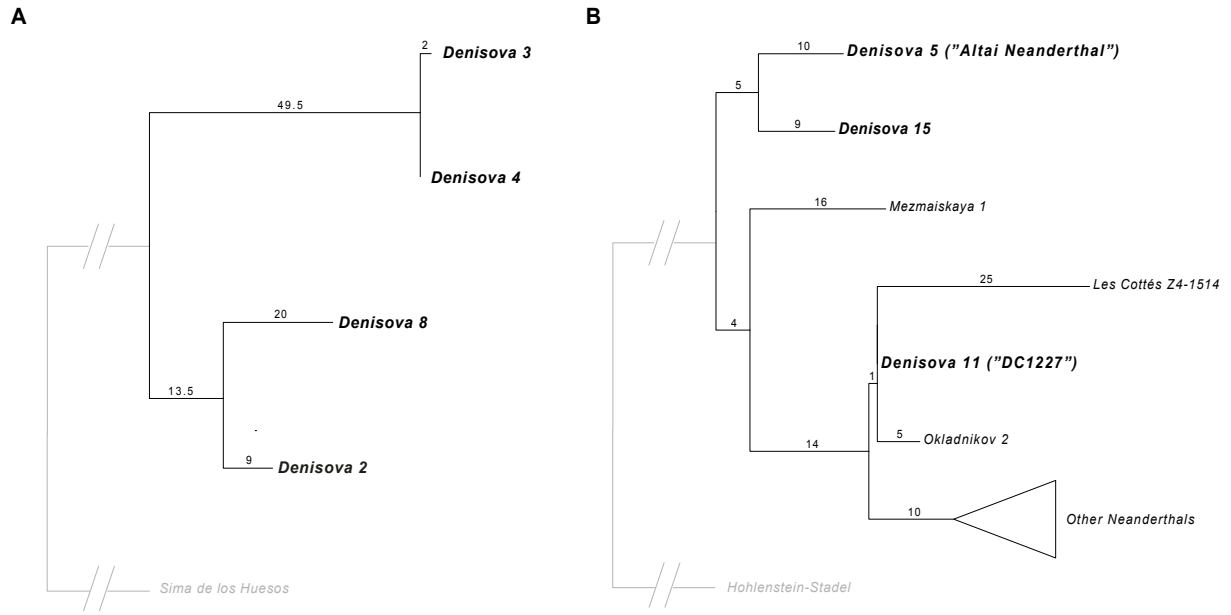

Figure S14. Inferred number of substitutions occurring on branches leading to the mtDNA genomes of individuals from Denisova Cave since their split from the common ancestor shared with other archaic individuals. Individuals from Denisova Cave are emphasized in bold. (A). Denisovan mtDNA genomes; data is taken from Ref. 12. (B) Neanderthal mtDNA genomes. The mtDNA genomes used in this analysis are reported in Table S10.

Table S7. Inferred number of substitutions on the branches leading to each Denisovan or Neanderthal mitochondrial DNA genome and the inferred relative age of each of the individuals.

mtDNA type	**Specimen**	**Substitutions since common ancestor**	**Inferred relative age** (Mutation rate: 2.53×10^{-8} (95% HPD: 1.76-3.23×10^{-8}))
Denisovan mtDNA	*Denisova 2*	22.5	54.2-99.4 ky older than *Denisova 3* 50.5-92.6 ky older than *Denisova 4* 20.6-37.7 ky older than *Denisova 8*
	Denisova 3	51.5	3.7-6.9 ky younger than *Denisova 4* 33.6-61.7 ky younger than *Denisova 8*
	Denisova 4	49.5	29.9-54.9 ky younger than *Denisova 8*
	Denisova 8	33.5	
Neanderthal mtDNA	*Denisova 5*	15	7.5-13.7 ky older than *Denisova 11* 1.9-3.4 ky younger than *Denisova 15*
	Denisova 11	19	9.3-17.1 ky younger than *Denisova 15*
	Denisova 15	14	

(ii) Estimating tip dates in a Bayesian framework

To estimate the tip dates of the Neanderthal mtDNA genomes of individuals from Denisova Cave (*Denisova 5*, *11* and *15*), we used the mtDNA sequences of 11 Neanderthals and 7 ancient modern humans, whose remains have been directly radiocarbon-dated, as calibration points for the rate of the molecular clock in a Bayesian phylogenetic analysis. The inferred ages of the three Neandertal mtDNA genomes are shown in Table S8. Note that this analysis is sensitive to the mutation rate inferred from the analysis (1.45×10^{-8}; 95% HPD: $1.05\text{-}1.88 \times 10^{-8}$). Although the point estimates suggest that *Denisova 5* and *Denisova 15* are nearly contemporaneous and both older than *Denisova 11* (in concordance with the previous analysis), we note that the HPD intervals of all three dates overlap. Note that the lack of directly-dated Denisovan remains that could be used as calibration points hinders attempts to perform a similar analysis to estimate the tip dates of Denisovan mtDNA genomes.

Table S8. Estimated tip dates for the coding region of the mtDNA genomes of three individuals from Denisova Cave.

mtDNA type	**Specimen**	**Inferred age** (mean [95% HPD])
Neanderthal mtDNA	*Denisova 5*	149.3 ka [91.3-214.8 ka]
	Denisova 11	107.8 ka [75.4-144.8 ka)
	Denisova 15	144.1 ka [87.2-209.4 ka]

5. SEQUENCING DATA FROM *DENISOVA 11*, *DENISOVA 14* AND *DENISOVA 15*

V. Slon, F. Mafessoni, J. Kelso, M. Meyer, S. Pääbo

Sample preparation: Following the abrasion of surface material, 19.4 mg and 17.7 mg of bone powder were removed from the *Denisova 14* and the *Denisova 15* bone fragments, respectively, using a disposable dentistry drill. The bone powder was treated with 0.5% sodium hypochlorite prior to DNA extraction[35,36]. 20% of each DNA extract (*i.e.*, 10µl) were converted into single-stranded DNA libraries[37] and indexed with two barcodes[38]. The DNA libraries were enriched for human mtDNA fragments using two rounds of an on-beads hybridization capture protocol[39] (with modifications in Ref. 13), using ~1µg and ~0.5µg DNA as input in the first and second round, respectively. Two DNA libraries prepared from the *Denisova 11* specimen previously[34] using similar methods (except using the single-stranded DNA library preparation protocol described in Ref 37) also underwent enrichment for human mtDNA fragments, in a single round of capture. One extraction blank and one library preparation negative control per setup were carried along (Table S9).

Sequencing and data processing: The enriched DNA libraries were pooled with libraries generated as part of other projects and sequenced on a MiSeq platform (Illumina) in 76-cycle paired-end runs[38]. Basecalling was carried out using Bustard (Illumina) and demultiplexing was performed by requiring exact matches to the expected barcode combinations. Overlapping paired-end reads were merged using leeHom[40]. Sequences were mapped to a reference genome using BWA[41] with parameters adapted to ancient DNA[25]. PCR duplicates were collapsed into a single sequence using bam-rmdup (https://github.com/mpieva/biohazard-tools). Only sequences longer than 35 bases and with a mapping quality higher than 25 were retained.

Table S9. Summary of the DNA extracts and DNA libraries used in the current study. Statistics are based on alignment of sequences to the rCRS. Negative controls are marked in gray.

Specimen	Extract	Bone powder (mg)	Indexed DNA library	Library enriched for human mtDNA	Reads sequenced	Unique mtDNA sequences (L≥35, MQ≥25)	C to T substitutions (%)	
							5'-end	3'-end
Denisova 11	E3652	29.0	R5780	R4290	1,222,917	143,553	38.3	40.7
	E3655	33.5	R5783	R4293	1,026,266	130,496	35.6	37.6
Controls	ENC	-	R5791	R4301	139,517	57	0.0	0.0
	LNC	-	R5792	R4302	146,807	13	0.0	0.0
Denisova 14	E4975	19.4	R6272	D8130	112,770	685	37.7	28.3
Denisova 15	E4976	17.7	R6273	D8131	120,182	18,905	46.9	37.2
Controls	ENC	-	R6277	D8135	12,832	60	20.0	0.0
	LNC	-	R6319	D8175	14,189	0	0.0	0.0

ENC: extraction negative control; LNC: library preparation negative control; L: length; MQ: mapping quality; C: cytosine; T: thymine. The extracts and indexed DNA libraries from *Denisova 11* were prepared elsewhere[34].

Assessing the preservation of ancient hominin mtDNA: Sequences were aligned to the revised Cambridge reference sequence (NC_012920.1) in order to evaluate the frequency of cytosine (C) to thymine (T) substitutions to the reference genome at terminal alignment positions, which are due to damage accumulating at the extremities of DNA fragments over time[42]. The elevated frequencies of terminal C to T substitutions in all four libraries are indicative of the presence of ancient DNA fragments in them (Table S9). For *Denisova 11*, this concurs with previous analyses showing that the preservation of ancient mtDNA of the Neanderthal type in this specimen[30].

To investigate the type of mtDNA fragments present in the data generated from *Denisova 14* and *Denisova 15*, we inspected the sequences that mapped to the human mitochondrial genome. We note that, unlike the sequences from *Denisova 15*, the sequences from *Denisova 14* did not map uniformly along the reference genome but rather tended to cluster in small regions (Figure S15), suggesting that some of the DNA fragments sequenced were not derived from human mtDNA[13].

To verify whether DNA from other mammals were present in the DNA libraries, we compared the DNA fragments to an in-house database of reference mammalian mitochondrial genome using MEGAN[43] with the parameters and thresholds described in Ref. 13. Of the 99 sequences from *Denisova 14* that could be identified at the family level, 59 were inferred to originate from hominins, 32 from hyaenids, and 8 from bovids. In comparison, all of the 15,804 identifiable sequences from *Denisova 15* originate from hominin mtDNA.

To further explore the possible presence of several taxa in the data from *Denisova 14,* we enriched the DNA library for mammalian mtDNA fragments[13,44] and compared them to the reference mammalian mtDNA database as above. We find that 2.1% of identifiable sequences (41 out of 1,937) came from hominin mtDNA fragments. Notably, these do not exhibit C to T substitutions to the rCRS to an extent expected from ancient DNA fragments (*i.e.,* at least 10% on both terminal ends[13,45]). In contrast, sequences attributed to other taxa present damage-derived substitutions typical of ancient DNA at their extremities. These include sequences attributed to bovids, hyaenids, equids and cervids, constituting 50.5%, 28.7%, 6.5% and 3.4% of identifiable fragments in the library, respectively. We conclude that no ancient hominin mtDNA is preserved in the *Denisova 14* specimen, and hypothesize that DNA from other taxa present in the environment contaminated the bone fragment.

To determine the type of ancient hominin mtDNA carried by *Denisova 15*, we evaluated the base presented by its sequences at the "diagnostic" positions for hominin mtDNA defined in Ref. **Error! Bookmark not defined.** following the approach in Ref. 46, *i.e.*, where changes are inferred to have specifically occurred in the mtDNA genomes of Neanderthals, of Denisovans, of modern humans, or of the *Sima de los Huesos* hominin. 95.6% of sequences match the Neanderthal-like state, compared to 1.0%, 2.3% and 1.3% matching the Denisovan, modern human and *Sima de los Huesos* states, respectively. We conclude that *Denisova 15* carries an mtDNA genome of the Neanderthal type.

Figure S15. Average coverage of the human mitochondrial reference genome by sequences from *Denisova 14* (top) and *Denisova 15* (bottom). The average coverage of the mitochondrial genome is 2.0-fold for sequences from *Denisova 14* and 62.7-fold for those from *Denisova 15*.

Estimating contamination by present-day human mtDNA: To estimate the extent of contaminating present-day human DNA in the libraries prepared from *Denisova 11* and *Denisova 15*, we calculated the percentage of sequences carrying the base shared by a panel of 311 present-day human mtDNA genomes at 63 positions in the mitochondrial genome where these differ from Neanderthal mtDNAs[47]. To avoid damage-derived substitutions to affect these estimates, DNA strands incorporated in the library on the forward orientation were ignored where one of the two possible states is a C, and reverse strands were ignored at sites where one of the possible states is a G. For *Denisova 11,* we estimate that 0.3% (95% binomial CI: 0.2-0.5%) of the sequences in the two libraries originate from contamination. For *Denisova 15*, we estimate that contaminating present-day human mtDNA sequences constitute 0.4% (95% binomial CI: 0.1-1.0%) of the data.

Reconstructing the mtDNA genomes of Denisova 11 and *Denisova 15:* Given that the mtDNA genomes of both *Denisova 11* and *Denisova 15* were established to be of the Neanderthal type, and in order to recover sequences that may be difficult to map because of their divergence to the human mtDNA genome, we re-aligned the sequences generated here to the Neanderthal mtDNA reference genome (NC_011137.1). To account for the circularity of the mitochondrial genome, 1000 bases from the start of the reference sequence were copied to its end[46]. Ts on forward strands and As on reverse ones at three terminal positions were converted to Ns to mitigate the effect of DNA damage on the consensus calling.

For *Denisova 11*, the sequences generated from the two DNA libraries were merged[48], yielding a total of 278,379 unique mtDNA sequences and resulting in an average mtDNA genomic coverage of 908.5-fold. The full mtDNA genome sequence of *Denisova 11* was reconstructed by calling bases by a majority vote while requiring each position to be covered by at least 5 sequences, 80% or more of which carry an identical base[46].

Given the lower average mtDNA coverage by sequences from *Denisova 15* (Figure S15), we relaxed the consensus calling criteria and required the presence of only 3 overlapping sequences, of which 67% or more carry the same base, to call a position[46]. We note that of the 55 sequences overlapping position 3829, 54.5% present a G and 45.5% present an A, and that both bases were seen multiple times in both sequence orientation. This suggests that *Denisova 15* had a heteroplasmy[49]. This position was left uncalled (N) in the consensus mtDNA genome sequence.

A maximum-likelihood phylogenetic tree, computed in MEGA 6.0[50], relating the reconstructed mtDNA genomes of *Denisova 11* and *Denisova 15* with those of 25 ancient and present-day modern humans, 26 archaic hominins and a chimpanzee (Table S10) confirms that the mtDNA genomes of *Denisova 11* and *Denisova 15* fall within the known variation of Neanderthal-like mtDNA (Figure S16).

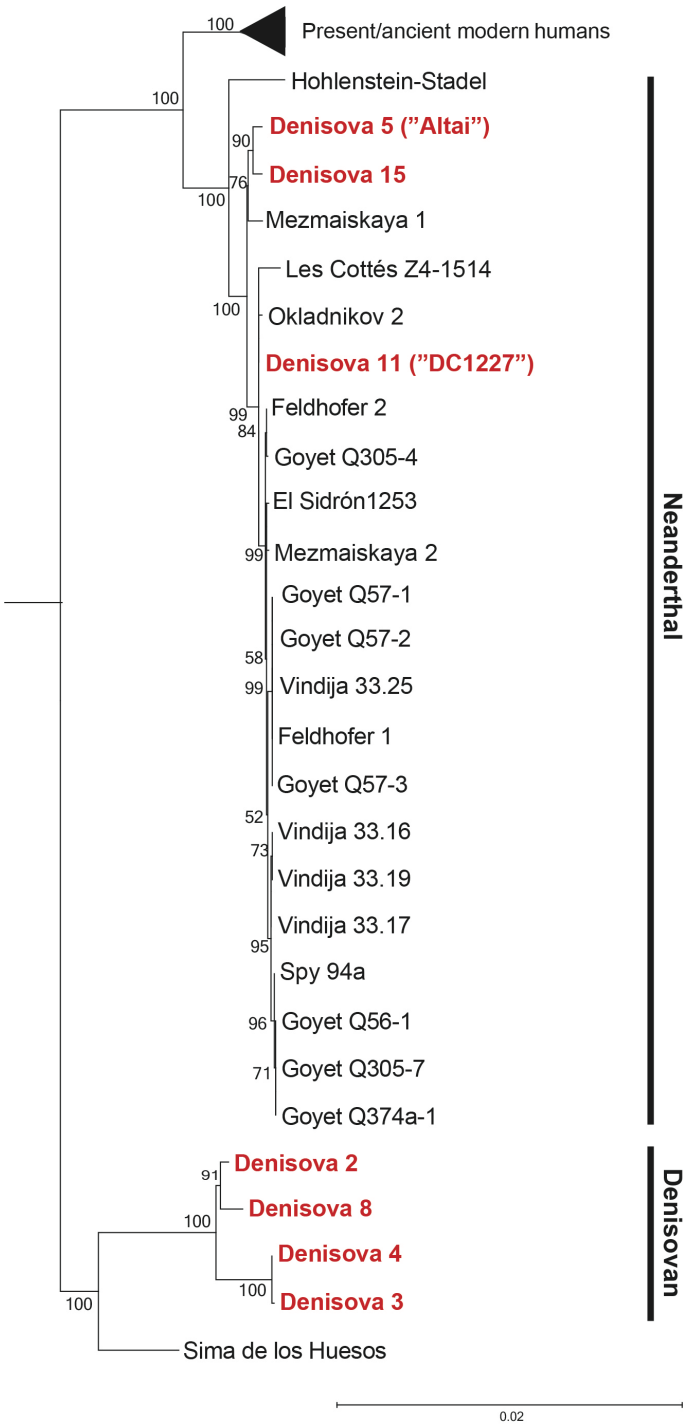

Figure S16. Maximum-likelihood phylogenetic tree relating the mtDNA genomes of individuals from Denisova Cave (in red) to that of other ancient and present-day individuals. The mtDNA types (Neanderthal- or Denisovan-like) are marked on the right. Missing bases and gaps in any of the mtDNA genomes were discarded from the entire dataset, and the mtDNA genome of a chimpanzee was used to root the tree. The Tamura-Nei substitution model with gamma distribution and allowing for invariable sites (TrN+G+I) was used. Branch lengths are scaled based on the number of substitutions per site, and support for each branch is based on 500 bootstrap replications.

Estimating the age of the Neanderthal-like mtDNA genomes from Denisova Cave: To estimate the relative ages of the individuals from Denisova Cave who carried a Neanderthal-like mtDNA, *i.e.*, *Denisova 5* ("*Altai Neanderthal*"), *Denisova 11* and *Denisova 15*, their mtDNA genome sequences were aligned to those of 20 other Neanderthals (Table S10) using MAFFT[51]. The number of base substitutions occurring on each branch leading to these mitochondrial genomes was inferred by parsimony in phangorn[52], with the divergent mtDNA genome of the *Hohlenstein-Stadel* Neanderthal[53] used as outgroup (Figure 14B). The differences in the inferred number of substitutions that occurred on each branch since the split from a common ancestor were converted into relative ages by applying the mitochondrial mutation rate calculated for modern humans of 2.53×10^{-8} (95% HPD: $1.76\text{-}3.23 \times 10^{-8}$)[14] (Table S7).

Additionally, we aimed to estimate the tip dates for these three mtDNA genomes. This was carried out in a Bayesian framework implemented in BEAST v1.8.4[54]. The three Neanderthal-like mtDNA genomes from Denisova Cave were aligned to those of 20 other Neanderthals, 22 ancient and present-day modern humans and one Denisovan to be used as outgroup (Table S10) using MAFFT[51]. Only the coding region of the mtDNA genome (positions 577-16,023 of the rCRS) was retained[55]. The Tamura-Nei substitution model[56] with invariable sites (TrN+I) was determined as the best-suited model using jModelTest v. 2.1.1[57]. The mitochondrial mutation rate of 2.53×10^{-8} was used as an initial prior for the molecular clock, which was allowed to vary between 1.0×10^{-6} and 1.0×10^{-10}. Priors given on the tip dates are shown in Table S10. The four possible combinations of constant population size or Bayesian skyline as tree model, and strict or uncorrelated relaxed lognormal clock, were tested by running 30,000,000 iterations with additional 1,000,000 iterations and sampling every 1,000 steps to compute the log marginal likelihood of each model using stepping-stone sampling. Comparisons were conducted using the difference between the log marginal likelihoods of the two models in each pairwise test (i.e., log10BF=log10(exp(log marginal likelihood for model A - log marginal likelihood for model B))). Using the scale defined in ref 58, the Bayesian skyline model was decisively better supported than the constant population size ($\log_{10}$BF>2.4); and the uncorrelated relaxed lognormal clock strongly supported compared to the strict one ($\log_{10}$BF=1.8). For these parameters, three chains of 75,000,000 iterations were combined after discarding 20% of the iterations as burn-in. The resulting estimated tip dates are shown in Table S8.

Table S10. Dataset of mtDNA genomes used in the genetic analyses. "Accession" refers to the mtDNA genome identifier in the NCBI database; "Date" corresponds to the prior used in the Bayesian analysis (direct radiocarbon-dates of the ancient specimens were calibrated using OxCal 4.3[59] with IntCal13[19], N/A indicates that the mtDNA genome was not used in that analysis); Ref. are references to the publication of the mtDNA genomes and, when relevant, of the radiocarbon date of the ancient individuals.

Individual	Accession	Date	Ref.	Individual	Accession	Date	Ref.
Ancient modern human mtDNA				**Denisovan mtDNA**			
Boshan 11	KC521454	8,234 (8,152-8,316)	[55]	Denisova 2	KX663333	N/A	[12]
Dolní Věstonice 13	KC521459	N/A	[55]	Denisova 3	NC_013993	55,000 (30,000-300,000)	[24]
Dolní Věstonice 14	KC521458	N/A	[55]	Denisova 4	FR695060	N/A	[9]
Iceman	EU810403	5,300 (5,275-5,325)	[60, 61]	Denisova 8	KT780370	N/A	[26]
Kostenki 14	FN600416	37,473 (36,262-38,684)	[62, 63]	**Neanderthal mtDNA**			
Loschbour	KC521455	8,054 (7,948-8,160)	[55, 64]	Denisova 5 (“Altai”)	KC879692	55,000 (30,000-300,000)	[28]
Oberkassel 998	KC521457	N/A	[55]	Denisova 11	XXX	55,000 (50,000-300,000)	[30]
Saqqaq Eskimo	EU725621	4,504 (4,423-4,585)	[65, 66]	Denisova 15	XXX	55,000 (30,000-300,000)	This study
Tianyuan	KC417443	39,008 (37,761-40,254)	[39, 67]	El Sidrón 1253	FM865409	55,000 (30,000-300,000)	[68]
Ust‘-Ishim	-	45,045 (43,212-46,878)	[14]	Feldhofer 1	FM865407	43,707 (42,670-44,744)	[68, 69]
Present-day modern human mtDNA				Feldhofer 2	FM865408	43,268 (42,193-44,342)	[68, 69]
Australian	AF346964	0 (0-100)	[70]	Goyet Q56-1	KX198082	42,515 (42,063-42,967)	[71]
Chinese	AF346973	0 (0-100)	[70]	Goyet Q57-1	KX198082	44,696 (43,834-45,558)	[71]
Filipino	AY289070	0 (0-100)	[72]	Goyet Q57-2	KX198088	41,185 (40,595-41,775)	[71]
Finland	AY195773	0 (0-100)	[73]	Goyet Q57-3	KX198083	42,407 (41,946-42,867)	[71]
Indian	AF382013	0 (0-100)	[74]	Goyet Q305-4	KX198087	44,236 (43,386-45,085)	[71]
Italian	AY882393	0 (0-100)	[75]	Goyet Q305-7	KX198086	55,000 (30,000-300,000)	[71]
Japan	AF346990	0 (0-100)	[70]	Goyet Q374a-1	KX198085	55,000 (30,000-300,000)	[71]
Mandenka	AF346995	0 (0-100)	[70]	Hohlenstein-Stadel	KY751400	55,000 (30,000-300,000)	[53]
Mbuti	AF346998	0 (0-100)	[70]	Les Cottés Z4-1514	MG025536	43,230 (42,720-43,740)	[76]
Native American	AY195748	0 (0-100)	[73]	Mezmaiskaya 1	FM865411	55,000 (30,000-300,000)	[68]
Pakistan	AY882380	0 (0-100)	[75]	Mezmaiskaya 2	MG025537	43,834 (42,038-45,630)	[76, 77]
Papua (Coast)	AY289082	0 (0-100)	[72]	Okladnikov 2	KF982693	55,000 (30,000-300,000)	[78]
Papua (Highlands)	AY289090	0 (0-100)	[72]	Spy 94a	MG025538	40,463 (39,840-41,085)	[76, 79]
San	AF347008	0 (0-100)	[70]	Vindija 33.16	NC_011137	43,707 (39,234-48,179)	[47, 80]
Spain	AY882392	0 (0-100)	[75]	Vindija 33.17	KJ533544	55,000 (30,000-300,000)	[81]
Chimpanzee mtDNA				Vindija 33.19	KJ533545	55,000 (50,000-300,000)	[31, 81]
-	NC_001643	N/A	[82]	Vindija 33.25	FM865410	55,000 (30,000-300,000)	[68]
Sima de los Huesos mtDNA							
Femur VIII	NC_023100	N/A	[46]				

6 . OPTICAL DATING OF SEDIMENT SAMPLES FROM DENISOVA CAVE

Z. Jacobs, B. Li, R. G. Roberts

Optical dating provides an estimate of the time since grains of luminescent minerals, such as quartz and potassium-rich feldspar (K-feldspar), were last exposed to sunlight[83,84,85,86,87,88]. The burial age is estimated by dividing the equivalent dose (D_e, a measure of the radiation energy absorbed by grains during their period of burial) by the environmental dose rate (the rate of supply of ionising radiation to the grains over the same period). The D_e is determined from laboratory measurements of the optically stimulated luminescence (OSL) from quartz or the infrared stimulated luminescence (IRSL) from K-feldspar, and the dose rate is estimated from field and laboratory measurements of environmental radioactivity, plus the small contribution from cosmic rays.

A large optical dating study has been conducted in all three chambers at Denisova Cave since August 2012, with the aim of obtaining a reliable chronology for all major Pleistocene sedimentary layers that contain artefacts (or are culturally sterile) and hominin fossils, as well as the remains of animals and plants. Finite ages for 103 sediment samples are presented in Jacobs *et al*.[89], together with full technical details associated with the measurement and calculation of the D_e values, environmental dose rates and optical ages. Ref. 89 also provides descriptions of the stratigraphic sequences and discussion of post-depositional integrity.

We note that the optical dating study of Jacobs *et al*.[89] and the present study, and their accompanying Bayesian age models, are complementary. One study does not supersede the other; rather, they serve different purposes. The chronological framework based on the optical ages provides a timeline for sediment deposition and, by association, a timeframe for cultural change and occupation of Denisova Cave by different hominin groups. Optical dating of single grains of quartz or K-feldspar enables issues of sediment mixing to be investigated and, hence, stratigraphic integrity examined. This approach may be sufficient to infer general patterns of change in stone-tool assemblages or environmental conditions through time, but it cannot be reliably extended to isolated teeth or bone fragments that may have been displaced since deposition by carnivore bioturbation, for example. A more robust age model for isolated human remains can be constructed by combining the available proxy evidence, including optical ages for sediment deposition, radiocarbon ages obtained for collagen from some of the human fossils, and relative genetic ages estimated for most of the fossils. This combined approach ameliorates the shortcomings specific to each of the methods.

In this study, we focus on the optical ages for four stratigraphic layers: layers 22.1 and 21 in the Main Chamber, to provide a maximum age constraint for hominin occupation of the site and for *Denisova 2* (which was recovered from layer 22.1); layer 12.3 in the East Chamber, to provide a

maximum age constraint for *Denisova 11* (layer 12.3), *Denisova 8* (interface of layers 12 and 11.4) and *Denisova 15* and *Denisova 5* (both from layer 11.4); and layer 11.2 in the East Chamber, from which *Denisova 3* was obtained. We include 11 optical ages from these layers in the Bayesian age models presented in Supplementary Information, Section 8.

Samples were collected at night (using dim red light for illumination), sealed in plastic bags and wrapped in black plastic to prevent light exposure during transport to the University of Wollongong. These sediment samples were used for OSL and/or IRSL measurements, to estimate the field water contents and to make laboratory measurements of the beta dose rate. Measurements of the *in situ* gamma dose rate were made at each sample location using a portable gamma-ray detector. In the laboratory, sand-sized grains of quartz and/or K-feldspar were extracted from the samples under dim red illumination using standard procedures[85]. Each sample was sieved to isolate quartz grains of 180–212 μm diameter and K-feldspar grains of 90–212 μm diameter (Table S11), which were treated with solutions of 10% hydrochloric acid and 30% hydrogen peroxide to remove carbonates and organic matter, respectively. K-feldspar, quartz and heavy-mineral grains were separated from each other using solutions of sodium polytungstate and then etched in either 45% (quartz) or 10% (K-feldspar) hydrofluoric acid for 40 min (to clean the grain surfaces and remove, or greatly reduce in volume, the alpha-irradiated rinds), rinsed in hydrochloric acid (to remove any precipitated fluorides) and, finally, dried and sieved again.

Measurements of the beta dose rate were made on dried, homogenised and powdered portions of each sample using a low-level beta counting system[90] and the data-analysis procedures described in ref. 91. We used a 1-inch diameter NaI(Tl) detector and the 'threshold' technique[92] to estimate the gamma dose rates from the U and Th decay series and ^{40}K, with the detector calibrated using the doped concrete blocks at Oxford[93]. Cosmic-ray dose rates were estimated following ref. 94, taking into account the latitude, longitude and altitude of the site, the thickness and density of sediment overburden and bedrock shielding. The beta dose rates were attenuated for grain size, and the beta, gamma and cosmic-ray dose rates were corrected for long-term water content (Table S11). The total dose rates for K-feldspar grains also include an effective internal dose rate due to the decay of ^{40}K and ^{87}Rb inside the grains. We estimated the K content (12.8 ± 0.5%) from electron microprobe wavelength-dispersive X-ray spectroscopy measurements of 60 individual grains, and assumed a Rb concentration of 400 ± 100 μg/g (ref. 95).

We used a combination of quartz and K-feldspar grains to estimate depositional ages for layer 11.2 in the East Chamber and to test the sensitivity of these estimates to a variety of measurement conditions[89]. The ages for samples from layer 12.3 in the East Chamber and layers 21 and 22.1 in the Main Chamber were determined solely using K-feldspar grains, owing to

saturation of the quartz OSL signal. Single-grain analysis allows for grains with aberrant luminescence properties to be identified and rejected before age determination, and to address any issues of incomplete bleaching before deposition or stratigraphic disturbance after deposition[86,87,88,89,96]. A multiple-aliquot post-infrared IRSL (pIRIR) procedure was used to obtain D_e values for samples from layer 22.1 in the Main Chamber, but single-grain pIRIR measurements were also made for one of the samples (DCM16-13) from layer 22.1 to test the internal consistency of the methods. Samples were measured using automated Risø TL-DA-20 instruments equipped with infrared (870 nm) light emitting diodes for stimulation of multi-grain aliquots, and focussed green (532 nm) and infrared lasers (830 nm) for stimulation of individual quartz and K-feldspar grains, which were loaded on to custom-made discs[97]. The ultraviolet OSL and violet/blue IRSL emissions were detected by Electron Tubes Ltd 9235QA photomultiplier tubes fitted with either U-340 (OSL) or Schott BG-39 and Corning 7-59 (K-feldspar) filters, and beta doses were administered using calibrated $^{90}Sr/^{90}Y$ sources.

For single-grain measurements of quartz, we used a standard single-aliquot regenerative-dose procedure[98,99]. To measure the high-temperature pIRIR signals[100,101] from individual K-feldspar grains, we used a two-step, regenerative-dose pIRIR procedure[102] in which an initial infrared bleach at 200°C is followed by infrared stimulation of the dating signal at 275°C. K-feldspar D_e values were estimated using three methods:

1. Samples from layer 11.2 (East Chamber): projection of the sensitivity-corrected natural signal (L_n/T_n) on to the full dose-response curve regenerated for each grain.
2. Samples from layer 12.3 (East Chamber) and layer 21 (Main Chamber) and one of the samples from layer 22.1 (Main Chamber): projection of the weighted mean re-normalised L_n/T_n ratio for all grains used for D_e determination on to the standardised growth curve (SGC) for K-feldspar grains[103]. Full details and comparisons with other methods are provided in ref. 89.
3. Samples from layer 22.1 (Main Chamber): using a multiple-aliquot regenerative-dose (MAR) procedure[104], six aliquots of both samples were stimulated successively at 50, 100, 150, 200 and 275°C, and the re-normalised L_n/T_n ratios were projected on to a multiple-aliquot SGC to estimate the corresponding D_e values[89].

To determine appropriate D_e values for age determination, we examined each of the single-grain D_e or re-normalised L_n/T_n distributions (Fig. S17) for any patterns in the data, and calculated the extent of overdispersion (OD) for each distribution (i.e., the spread in values remaining after making allowance for measurement uncertainties) using the central age model (CAM)[98,105]. Each distribution was optimally fitted by a single component[105,106], so we used the CAM to estimate the weighted mean D_e values, after rejecting statistical outliers based on the normalised median absolute deviation[107,108].

The re-normalised L_n/T_n distributions for both of the multiple-aliquot samples are shown in Fig. S18. These data were obtained at the highest stimulation temperature (275°C). We have demonstrated that the samples suffer from negligible fading at this temperature[89], so their final ages were estimated from these data.

Optical ages and associated information are provided in Table S11; all uncertainties are reported at 1σ.

Ages for layers 22.1 and 21 in the Main Chamber are included in the Bayesian models (Supplementary Information, Section 8) to stratigraphically constrain *Denisova 2*. This Denisovan tooth was found near the top of layer 22.1 in square B8 during the 1984 excavation season (Fig. S4). This layer is easily recognisable in the Main Chamber as an ochre-coloured cave loam of considerable thickness at the base of the stratigraphic sequence (Fig. S5). Ages of 380 ± 26 kyr (DCM16-13) and 312 ± 24 kyr (DCM14-11) were obtained for layer 22.1. Layer 21 is a dark loam impregnated with organic ashes and fine biological detritus and has ages of 255 ± 25 (DCM12-24), 227 ± 21 (DCM17-1) and 197 ± 15 kyr (DCM14-10). There is a clearly identifiable erosional unconformity between layers 22.1 and 21, with truncation of layer 22 prior to deposition of layer 21 (ref. 89).

Optical ages for layers 12.3 and 11.2 in the East Chamber are included in the Bayesian models (Supplementary Information, Section 8) to chronostratigraphically constrain the human remains recovered from this part of the sequence. Layer 12.3 is well represented throughout the East Chamber as a 50–60 cm-thick grey-brown medium loam. Three optical ages of 128 ± 8 (DCE12-9), 139 ± 7 (DCE14-8) and 129 ± 7 kyr (DCE16-6) were obtained for this layer (Table S11). These ages are also well constrained by the optical ages for samples collected from layers directly above and below[89].

Layer 11.2 is one of the more complex layers at Denisova Cave, with clear evidence in places of bioturbation. It is a 30–50 cm-thick light loam, dark brown in colour with a reddish tint. The layer contains large amounts of angular limestone debris and has uneven and deformed boundaries due to post-depositional subsidence. Five sediment samples were dated from this layer; the D_e values for each sample were measured using both quartz and K-feldspar grains for comparison, and two grain-size fractions of K-feldspar were also measured separately for one sample (DCE16-5). The quartz and K-feldspar ages for three of the samples are in good agreement (Table S11) and their D_e distributions show minimal evidence for large-scale mixing (Fig. S17). The combined quartz and K-feldspar ages for these three samples (Table S11) are 60 ± 3 (DCE14-11), 56 ± 3 (DCE14-14) and 61 ± 3 kyr (DCE16-5). The latter estimates are included in the Bayesian models (Supplementary Information, Section 8), as we have greatest confidence in the stratigraphic

integrity of these samples and their ages. The D_e distributions and optical ages of the other two samples from layer 11.2, one of which shows evidence of mixing, are discussed in ref. 89. Post-depositional disturbance of some parts of layer 11.2 is consistent with the previously published radiocarbon chronology for layer 11.2 (ref. 9) and with the new radiocarbon ages reported in this study (Supplementary Information, Section 2); the latter include samples with infinite ages and others with younger ages, which we presume are intrusive samples.

Table S11. Total dose rate, equivalent dose (D_e) and overdispersion (OD) values and optical ages for quartz (Q) and K-feldspar (KF) samples from layers 22.1 and 12 in the Main Chamber and layers 12.3 and 11.2 in the East Chamber. The age uncertainties represent the total (random plus systematic) uncertainties at 1σ. Ages shown in bold are the weighted mean ages with total (unshared plus shared) uncertainties at 1σ for the combined quartz and K-feldspar age estimates.

Sample	Layer	Mineral	Grain size	Water content (%)	Total dose rate (Gy/kyr)	D_e (Gy)	OD (%)	Optical age (kyr)
DCM16-13	22.1	KF	90-150	30 ± 6	2.66 ± 0.12	1011 ± 46	—	380.3 ± 25.5
DCM14-11	22.1	KF	125-212	30 ± 6	2.70 ± 0.14	842.6 ± 42.8	—	312.0 ± 23.5
DCM12-24	21	KF	180-212	50 ± 10	2.75 ± 0.13	698.9 ± 58.6	15.8 ± 1.91	254.6 ± 25.2
DCM17-1	21	KF	180-212	50 ± 10	2.18 ± 0.11	493.7 ± 36.4	13.1 ± 1.6	226.6 ± 20.5
DCM14-10	21	KF	125-212	60 ± 12	1.99 ± 0.13	391.6 ± 10.6	7.8 ± 1.0	196.9 ± 14.6
DCE12-9	12.3	KF	180-212	30 ± 6	2.50 ± 0.10	320.3 ± 12.7	13.3 ± 1.3	128.2 ± 7.6
DCE14-8	12.3	KF	180-212	30 ± 6	2.19 ± 0.19	304.5 ± 8.5	13.0 ± 0.9	139.0 ± 7.3
DCE16-6	12.3	KF	180-212	30 ± 6	2.33 ± 0.10	300.3 ± 9.2	16.5 ± 1.2	129.0 ± 7.1
DCE14-11	11.2	Q	180-212	20 ± 4	1.10 ± 0.04	65.2 ± 3.4	24.6 ± 4.5	59.5 ± 4.0
		KF			1.91 ± 0.08	113.1 ± 8.3	34.7 ± 5.7	59.1 ± 5.2
							Weighted mean	**59.9 ± 3.4**
DCE14-14	11.2	Q	180-212	20 ± 4	1.04 ± 0.05	62.7 ± 3.9	26.8 ± 5.3	60.3 ± 4.6
		KF	150-180		1.75 ± 0.08	92.7 ± 3.4	25.6 ± 3.1	53.0 ± 3.4
							Weighted mean	**55.7 ± 3.1**
DCE16-5	11.2	Q	180-212	20 ± 4	0.99 ± 0.04	61.7 ± 3.6	31.8 ± 4.8	62.3 ± 4.6
		KF	150-180		1.69 ± 0.07	100.9 ± 4.0	29.3 ± 3.2	59.6 ± 3.7
			125-150		1.55 ± 0.08	91.3 ± 3.9	31.7 ± 3.6	58.9 ± 4.2
							Weighted mean	**61.1 ± 2.9**

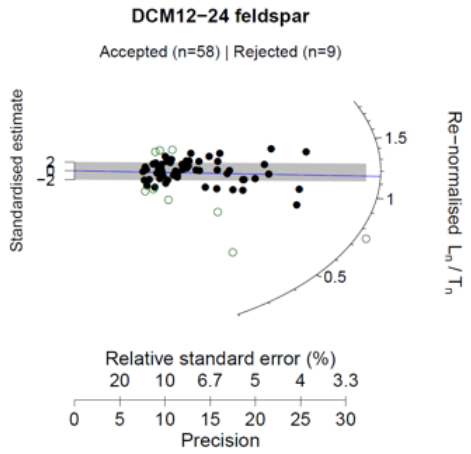
DCM12−24 feldspar
Accepted (n=58) | Rejected (n=9)
Standardised estimate
Re−normalised L_n / T_n
Relative standard error (%)
20 10 6.7 5 4 3.3
0 5 10 15 20 25 30
Precision

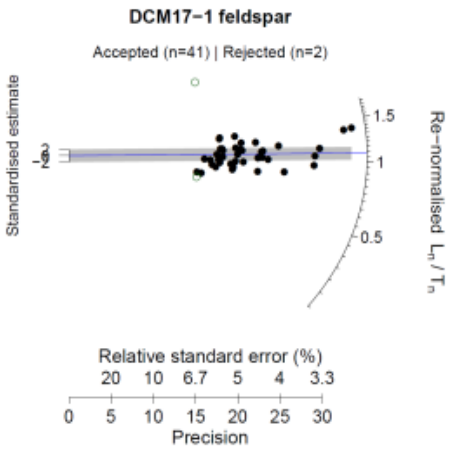
DCM17−1 feldspar
Accepted (n=41) | Rejected (n=2)
Standardised estimate
Re−normalised L_n / T_n
Relative standard error (%)
20 10 6.7 5 4 3.3
0 5 10 15 20 25 30
Precision

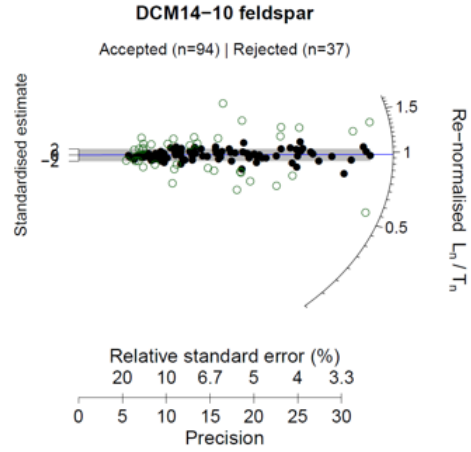
DCM14−10 feldspar
Accepted (n=94) | Rejected (n=37)
Standardised estimate
Re−normalised L_n / T_n
Relative standard error (%)
20 10 6.7 5 4 3.3
0 5 10 15 20 25 30
Precision

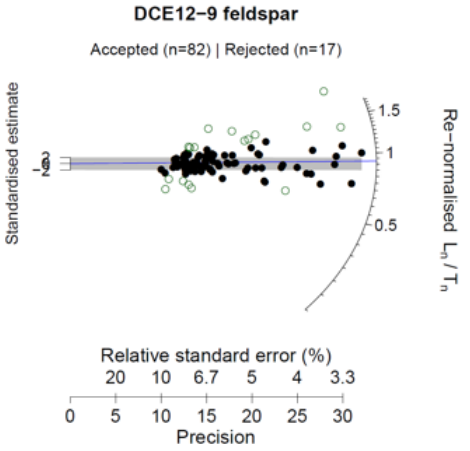
DCE12−9 feldspar
Accepted (n=82) | Rejected (n=17)
Standardised estimate
Re−normalised L_n / T_n
Relative standard error (%)
20 10 6.7 5 4 3.3
0 5 10 15 20 25 30
Precision

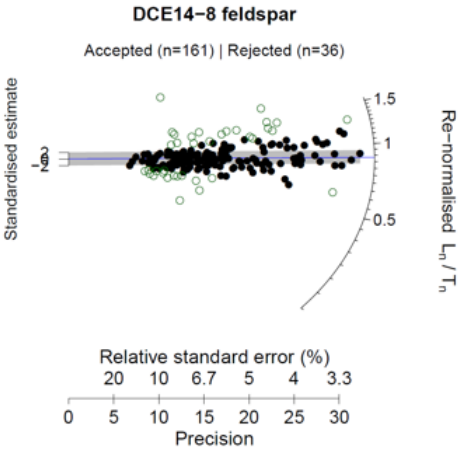
DCE14−8 feldspar
Accepted (n=161) | Rejected (n=36)
Standardised estimate
Re−normalised L_n / T_n
Relative standard error (%)
20 10 6.7 5 4 3.3
0 5 10 15 20 25 30
Precision

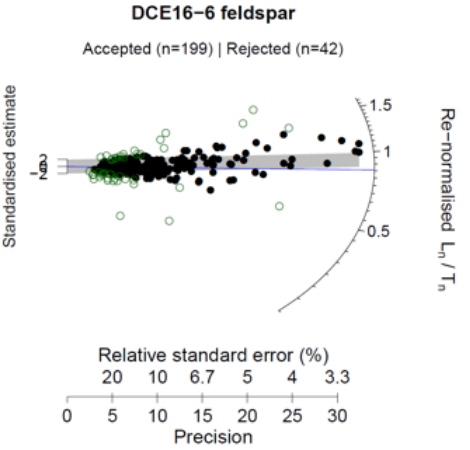
DCE16−6 feldspar
Accepted (n=199) | Rejected (n=42)
Standardised estimate
Re−normalised L_n / T_n
Relative standard error (%)
20 10 6.7 5 4 3.3
0 5 10 15 20 25 30
Precision

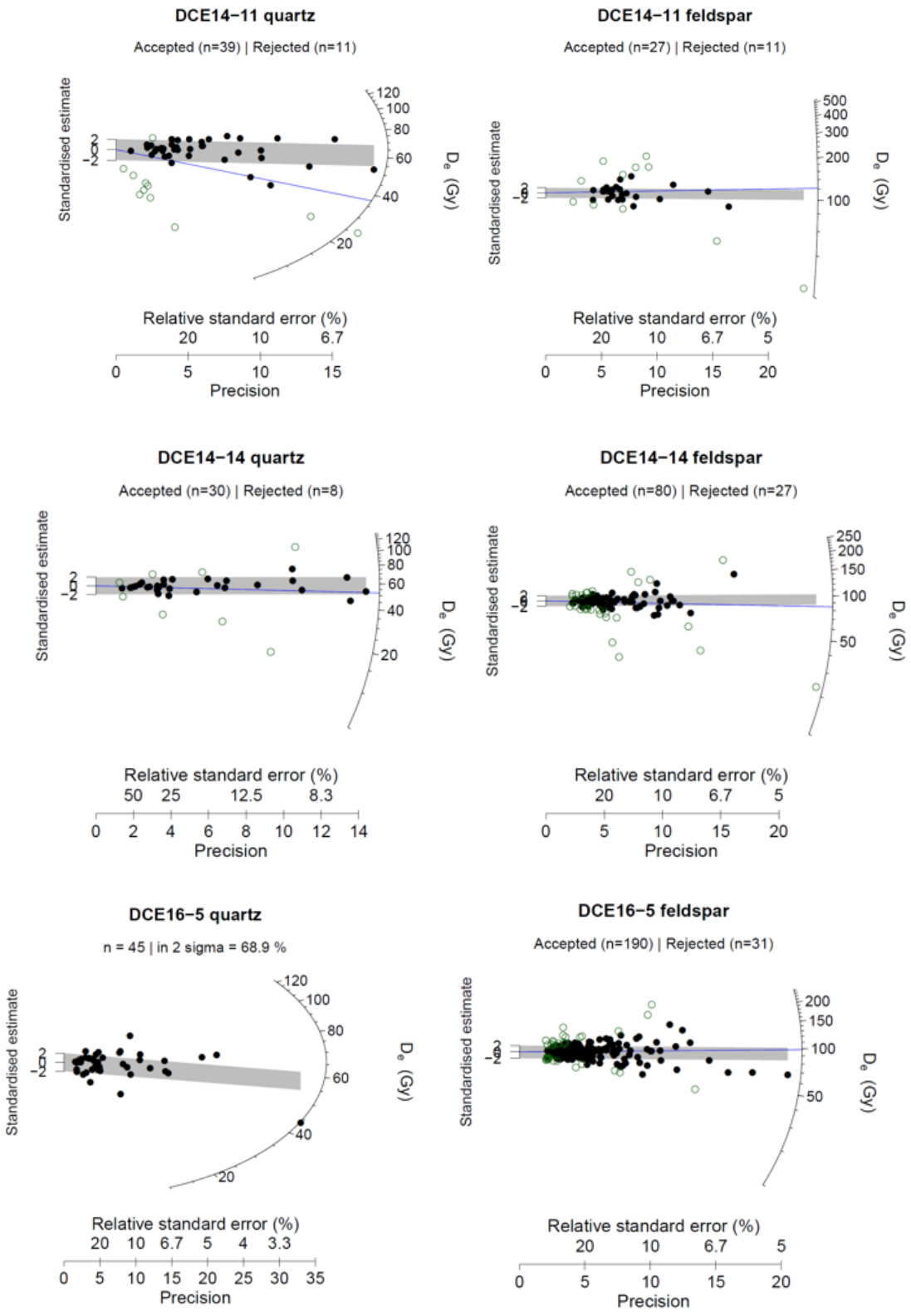

Figure S17. Distributions of D_e values and re-normalised L_n/T_n ratios for individual grains of quartz and K-feldspar from samples collected from layer 21 in the Main Chamber and layers 12.3 and 11.2 in the East Chamber. The grey band in each plot is centred on the weighted mean D_e value or re-normalised L_n/T_n

ratio determined using the CAM, after rejecting outliers (open circles). The blue lines indicate the CAM D_e values or re-normalised L_n/T_n ratios before outlier rejection. N represents the total number of single observations for each sample.

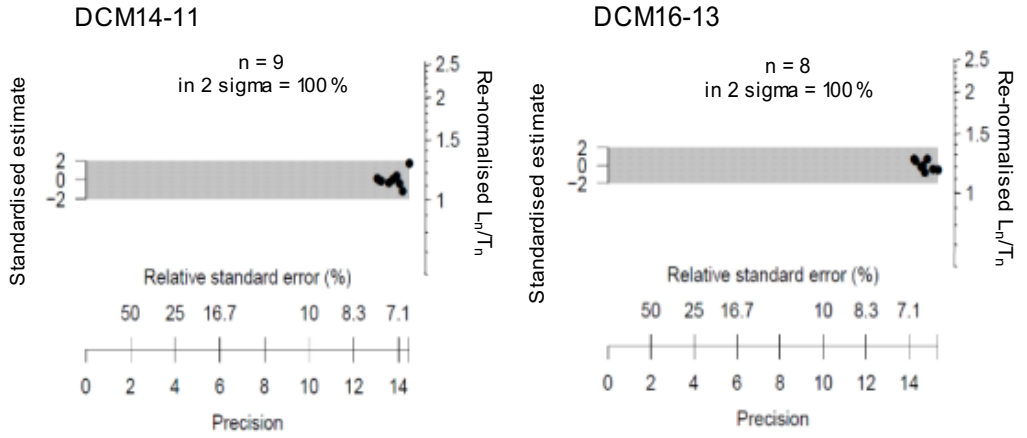

Figure S18. Re-normalised L_n/T_n ratios for two samples from layer 22.1 in the Main Chamber. Data were obtained using the MAR SGC procedure at a stimulation temperature of 275°C. The weighted mean L_n/T_n ratios (centred on the grey bands) were projected on to the MAR SGC to estimate the D_e values for age determination[89]. For DCM14-11, n=9; for DCM16-13, n=8 (where n is the total number of single observations for each sample).

7. URANIUM SERIES DATING OF *DENISOVA 11*

R. Grün, L. Kinsley

A fragment of bone remaining from radiocarbon and genetic analyses was analyses for its U content. We analysed the two cross sections (CC1 and CC2) of the bone as well as three tracks on the outside. The analyses followed the procedures which were described in detail by Grün et al.[109] and were carried out at three separate times. The "A" tracks on CC1 and CC2 were analysed in February 2018, the detailed analysis of CC2 ("B" tracks) and the surface in March 2018 and the detailed analysis of CC2 ("B" tracks) in May 2018. Spot analyses were carried out along 13 tracks on both cross sections of the bone and three tracks on the outer surface. Fig. S19 shows the positions of the analyses on the two cross sections and the three tracks on the outside of the bone and Tables S12 to S14 give all analytical data. The data in the table are shown for the tracks in Figure S19 from the left to the right and start on the outside of the bone. The three tracks on the surface (Fig. S19B) start at the base.

Results

A significant number of analyses show low U/Th ratios, particularly those carried out on the outside of the bone. This clearly demonstrates detrital contamination. To correct for this, U-concentrations were corrected for a Th/U ratio of 4.25, which represents the average value for the Earth's crust[110]. The net result is that the U-concentrations are reduced and assuming secular equilibrium in the detrital component, the $^{230}Th/^{234}U$ ratios decrease and the $^{234}U/^{238}U$ ratios increase, leading overall to younger apparent U-series ages (Fig. S20). For the following data analysis, we only used the corrected data.

Fig. S21 shows the results for the two cross sections, CC1 and CC2. CC1 shows a distinct U-concentration distribution with decreasing U-concentrations towards the outer surface (from around 1.5 ppm towards 0.5 ppm, Fig. S21A). Ages are generally in the range of around 30 to 40 ka, except close to the surface for tracks A1 and B1 to B5 (except B4, Fig. 21B). The older ages are associated with lower $^{234}U/^{238}U$ ratios (Fig. S21C). In contrast, CC2 has generally higher U-concentrations (0.8 to 1.7 ppm, Fig. S21D) without an obvious trend towards the surface of the bone. All ages fall between 25 and 45 ka, without any obvious trend (Figure S21E), the same applies to the $^{234}U/^{238}U$ values, one high data point has to be regarded an outlier (Track A2, 8th data point, Figure S21F), being more than 3-σ different to the surrounding data. The three tracks on the surface show decreasing U-concentrations towards CC2 (Fig. S22A) and increasing ages in tracks 2 and 3 towards CC1 (Fig. S22C).

Discussion

U-series ages are generally regarded as minimum age estimates as the uranium measured in the bones migrated into the skeletal tissue post mortem. Section CC2 shows that there was a major U-accumulation between about 25 and 45 ka, the age differences being due to somewhat delayed U uptake in the different domains of the bone. Cross section CC1 shows some significantly older ages. There is a clear trend between apparent age and U-concentration (Figure S23 top) and the question is whether leaching led to the older apparent ages. On the other hand the older ages are also associated with lower $^{234}U/^{238}U$ values (Fig. S24A). Leaching as such should not change the $^{234}U/^{238}U$ values. When plotting the apparent ages versus the initial $^{234}U/^{238}U$ values (Fig. S24B) any such trend disappears. This means that the source of the uranium in the sample remained with constant initial $^{234}U/^{238}U$ values of around 1.5, and the lower measured $^{234}U/^{238}U$ values in the domains with higher apparent ages are due to the fact that the uranium in these domains had a longer time to disintegrate. This may be due to the fact that these domains became a closed system earlier while the other domains still accumulated more uranium over time. The surface data show increasing apparent ages with increasing U-concentrations (Fig. S23C) and a lower $^{234}U/^{238}U$ values with increasing ages (Figure S24C). However, this trend disappears when the ages are plotted vs the initial $^{234}U/^{238}U$ ratios. Again the data point to the fact that some of the domains closer to the CC1 sections remained a closed system from an earlier time on.

While it is not possible to find an upper age limit for the bone with U-series analyses, its minimum age is in the range of 65 to 70 ka. We include this in the Bayesian modeling section below (Model 4).

Table S12. U-series results on cross section 1.

CC1	U (ppm)	Th (ppb)	U/Th	$^{230}Th/^{238}U$	$^{230}Th/^{238}U$ error	$^{234}U/^{238}U$	$^{234}U/^{238}U$ error	Age (ka)	Age error (ka)	Th-corr Age (ka)	Th-corr Age error (ka)
B1	0.48	182.06	2.6	0.7063	0.0392	1.3368	0.0350	78.8	7.0	71.7	6.1
	0.59	56.29	10.5	0.5859	0.0372	1.3721	0.0276	59.0	5.1	57.3	4.9
	0.98	21.91	44.7	0.4663	0.0240	1.4186	0.0169	42.6	2.7	42.2	2.7
	0.97	49.33	19.7	0.4547	0.0208	1.4104	0.0206	41.6	2.4	40.7	2.3
	1.26	22.12	56.9	0.4234	0.0266	1.4206	0.0190	37.9	2.9	37.6	2.8
	1.54	24.46	62.8	0.3500	0.0165	1.4254	0.0190	30.3	1.7	30.0	1.7
	1.84	11.20	164.5	0.3298	0.0149	1.4434	0.0168	27.9	1.5	27.8	1.5
	1.51	17.62	85.4	0.3603	0.0172	1.4157	0.0170	31.6	1.8	31.4	1.8
B2	0.67	127.36	5.3	0.5793	0.0311	1.3776	0.0275	57.8	4.3	54.4	4.0
	0.56	69.91	8.0	0.5829	0.0443	1.3394	0.0219	60.6	6.2	58.3	5.9
	0.79	35.28	22.4	0.5259	0.0301	1.3874	0.0298	50.7	3.9	49.9	3.8
	0.87	34.70	25.2	0.4957	0.0260	1.3855	0.0301	47.2	3.3	46.5	3.2
	1.28	27.17	47.2	0.4462	0.0224	1.4177	0.0220	40.4	2.5	40.0	2.5

	1.33	28.59	46.6	0.4060	0.0216	1.4133	0.0193	36.3	2.3	35.9	2.3
	1.21	36.52	33.1	0.4180	0.0196	1.4380	0.0322	36.8	2.3	36.3	2.2
	1.56	19.94	78.5	0.3789	0.0181	1.4546	0.0162	32.4	1.8	32.2	1.8
	1.65	19.78	83.5	0.3651	0.0157	1.4184	0.0241	32.0	1.7	31.8	1.7
	1.54	22.94	67.3	0.3475	0.0132	1.4348	0.0237	29.8	1.4	29.6	1.4
A1	0.49	87.38	5.6	0.6134	0.0318	1.3791	0.0269	62.2	4.5	59.0	4.2
	0.54	43.11	12.4	0.5913	0.0302	1.4083	0.0245	57.6	4.0	56.2	3.9
	0.71	35.63	20.0	0.5612	0.0188	1.4174	0.0182	53.5	2.4	52.6	2.4
	0.74	21.12	35.2	0.5306	0.0153	1.3999	0.0219	50.7	2.1	50.2	2.1
	1.32	19.01	69.2	0.4386	0.0131	1.4387	0.0162	38.9	1.5	38.6	1.5
	1.41	13.71	102.9	0.4086	0.0179	1.4496	0.0177	35.5	1.9	35.3	1.9
	1.47	18.79	78.4	0.4080	0.0147	1.4576	0.0196	35.2	1.6	35.0	1.6
	1.39	19.78	70.3	0.4056	0.0128	1.4583	0.0177	34.9	1.4	34.7	1.4
B3	0.87	72.17	12.1	0.4690	0.0260	1.4366	0.0224	42.2	2.9	40.8	2.8
	0.62	51.68	12.0	0.5725	0.0312	1.3796	0.0258	56.9	4.2	55.4	4.1
	0.60	27.58	21.8	0.5229	0.0360	1.3963	0.0346	49.9	4.6	49.1	4.5
	0.65	18.10	35.8	0.5081	0.0274	1.4101	0.0266	47.6	3.3	47.1	3.3
	1.17	15.36	76.4	0.4369	0.0198	1.4181	0.0248	39.4	2.3	39.2	2.3
	1.38	22.89	60.5	0.4243	0.0188	1.4519	0.0236	37.0	2.0	36.7	2.0
	1.20	15.50	77.7	0.4102	0.0211	1.4431	0.0255	35.8	2.3	35.6	2.3
	1.35	15.82	85.1	0.4009	0.0152	1.4270	0.0204	35.3	1.7	35.1	1.7
	1.48	14.89	99.5	0.3713	0.0169	1.4495	0.0232	31.8	1.8	31.6	1.7
	1.50	16.21	92.7	0.3567	0.0151	1.4304	0.0271	30.8	1.6	30.6	1.6
	1.41	24.05	58.5	0.3851	0.0158	1.4546	0.0201	33.0	1.6	32.7	1.6
	1.56	10.40	150.0	0.3468	0.0150	1.4240	0.0192	30.0	1.6	29.9	1.5
B4	0.64	292.17	2.2	0.7008	0.0315	1.3805	0.0195	74.3	4.9	66.0	4.2
	0.63	169.13	3.7	0.7152	0.0403	1.3786	0.0228	76.6	6.3	71.8	5.8
	0.63	27.37	23.1	0.5355	0.0356	1.3916	0.0362	51.7	4.6	50.9	4.6
	1.12	26.88	41.5	0.4909	0.0219	1.4250	0.0251	45.0	2.6	44.6	2.6
	1.31	27.73	47.3	0.4546	0.0187	1.4314	0.0295	40.8	2.3	40.5	2.2
	1.33	11.84	112.3	0.4406	0.0169	1.4474	0.0277	38.8	2.0	38.7	2.0
	1.27	22.74	55.6	0.3928	0.0191	1.4611	0.0175	33.6	1.9	33.3	1.9
	1.42	15.89	89.6	0.3921	0.0166	1.4339	0.0223	34.3	1.8	34.1	1.8
	1.34	17.02	78.5	0.3913	0.0185	1.4399	0.0253	34.0	2.0	33.8	2.0
	1.52	16.79	90.7	0.3793	0.0117	1.4566	0.0288	32.4	1.4	32.2	1.4
	1.35	12.28	109.5	0.3941	0.0192	1.4368	0.0324	34.4	2.1	34.2	2.1
	1.41	21.32	66.3	0.3644	0.0195	1.4409	0.0227	31.3	2.0	31.1	2.0
B5	0.58	113.15	5.1	0.6183	0.0387	1.4227	0.0315	60.2	5.2	56.8	4.8
	0.52	51.52	10.0	0.6423	0.0422	1.3875	0.0276	65.5	6.0	63.8	5.8
	0.72	31.86	22.5	0.5585	0.0304	1.4286	0.0260	52.6	3.8	51.8	3.7
	1.05	23.84	44.0	0.4801	0.0262	1.4173	0.0294	44.1	3.1	43.7	3.1
	1.03	19.71	52.0	0.4699	0.0282	1.4222	0.0259	42.8	3.2	42.5	3.2

	1.26	20.37	61.7	0.4401	0.0200	1.4419	0.0287	38.9	2.3	38.7	2.3
	1.06	16.50	64.4	0.4409	0.0238	1.4152	0.0178	39.9	2.6	39.7	2.6
	0.95	15.25	62.4	0.4130	0.0180	1.4278	0.0199	36.6	2.0	36.3	1.9
	1.49	18.33	81.1	0.3858	0.0210	1.4842	0.0374	32.3	2.2	32.1	2.2
	1.42	16.21	87.6	0.3845	0.0236	1.4433	0.0276	33.2	2.5	33.0	2.5
	1.63	17.44	93.4	0.3775	0.0186	1.4422	0.0232	32.6	1.9	32.4	1.9
	1.53	17.42	87.9	0.3687	0.0185	1.4313	0.0209	32.0	1.9	31.8	1.9
	1.47	20.42	71.9	0.3882	0.0177	1.4609	0.0262	33.1	1.9	32.9	1.9
B6	0.90	57.56	15.7	0.4350	0.0224	1.4555	0.0247	38.0	2.4	36.9	2.3
	0.63	40.20	15.7	0.5808	0.0304	1.4268	0.0278	55.4	3.9	54.3	3.8
	0.59	26.62	22.1	0.6015	0.0330	1.4512	0.0307	56.6	4.3	55.8	4.2
	1.23	40.58	30.3	0.4779	0.0231	1.4274	0.0296	43.5	2.8	42.9	2.7
	1.03	27.57	37.2	0.4586	0.0249	1.4339	0.0276	41.2	2.8	40.7	2.8
	1.37	19.28	71.2	0.4255	0.0206	1.4674	0.0330	36.6	2.3	36.4	2.3
	1.35	20.06	67.4	0.4169	0.0188	1.4549	0.0230	36.2	2.0	35.9	2.0
	1.18	11.30	104.1	0.4107	0.0238	1.4562	0.0233	35.5	2.5	35.3	2.5
	1.37	16.88	81.1	0.4102	0.0182	1.4524	0.0287	35.5	2.0	35.3	2.0
	1.44	21.81	66.2	0.3729	0.0207	1.4355	0.0334	32.3	2.2	32.0	2.2
	1.50	31.56	47.7	0.3969	0.0182	1.4436	0.0250	34.5	2.0	34.1	1.9
	1.44	17.88	80.6	0.3598	0.0176	1.4186	0.0245	31.4	1.9	31.2	1.9
	1.45	21.79	66.4	0.3960	0.0181	1.4521	0.0199	34.1	1.9	33.9	1.9
	1.59	31.14	51.1	0.3940	0.0207	1.4641	0.0258	33.6	2.2	33.3	2.1
A2	0.79	33.92	23.3	0.5061	0.0181	1.4118	0.0245	47.3	2.3	46.5	2.3
	0.93	26.27	35.3	0.5015	0.0164	1.4549	0.0190	45.0	1.9	44.5	1.9
	1.03	14.98	68.4	0.4543	0.0171	1.4622	0.0224	39.7	1.9	39.5	1.9
	0.99	14.13	69.7	0.4328	0.0139	1.4536	0.0149	37.8	1.5	37.6	1.5
	1.21	11.66	103.3	0.4090	0.0139	1.4322	0.0180	36.0	1.5	35.9	1.5
	1.32	11.34	116.4	0.3905	0.0126	1.4540	0.0167	33.5	1.3	33.4	1.3
	1.30	14.93	87.3	0.3859	0.0123	1.4418	0.0164	33.4	1.3	33.2	1.3
	1.30	13.53	96.1	0.3813	0.0107	1.4647	0.0130	32.3	1.1	32.2	1.1
	1.16	16.05	72.5	0.3972	0.0124	1.4616	0.0158	34.0	1.3	33.7	1.3
	1.28	16.85	75.9	0.3823	0.0102	1.4642	0.0135	32.5	1.1	32.2	1.0
B7	0.70	27.36	25.5	0.4841	0.0269	1.4580	0.0242	43.0	3.0	42.4	2.9
	0.81	19.17	42.3	0.5241	0.0229	1.4399	0.0284	48.1	2.9	47.7	2.8
	0.91	14.97	61.0	0.4665	0.0222	1.4489	0.0266	41.5	2.5	41.2	2.5
	1.27	13.35	95.3	0.4533	0.0209	1.4865	0.0361	38.8	2.4	38.7	2.4
	1.15	14.76	77.8	0.4343	0.0202	1.4450	0.0270	38.2	2.3	38.0	2.2
	1.19	16.04	74.2	0.4046	0.0181	1.4374	0.0272	35.4	2.0	35.2	2.0
	1.23	14.82	82.9	0.4060	0.0213	1.4571	0.0396	35.0	2.4	34.8	2.4
	1.22	14.46	84.6	0.4124	0.0183	1.4584	0.0372	35.6	2.1	35.4	2.1
	1.39	27.63	50.1	0.4064	0.0166	1.4512	0.0266	35.2	1.8	34.9	1.8
	1.38	12.49	110.7	0.4015	0.0151	1.4507	0.0170	34.7	1.6	34.6	1.6
	1.12	22.69	49.5	0.3826	0.0181	1.4555	0.0237	32.7	1.9	32.4	1.9
	1.38	14.65	94.1	0.3848	0.0176	1.4484	0.0223	33.1	1.8	32.9	1.8
	1.46	13.01	111.9	0.3804	0.0176	1.4489	0.0223	32.7	1.8	32.5	1.8

	1.45	10.24	142.0	0.3675	0.0125	1.4616	0.0285	31.1	1.4	31.0	1.4
B8	0.82	30.72	26.5	0.5251	0.0273	1.4397	0.0279	48.3	3.3	47.6	3.3
	1.01	19.31	52.4	0.4735	0.0239	1.4431	0.0246	42.4	2.7	42.1	2.7
	1.07	20.85	51.5	0.4830	0.0179	1.4544	0.0205	43.0	2.1	42.7	2.0
	1.10	16.09	68.1	0.4474	0.0197	1.4334	0.0204	40.0	2.2	39.7	2.2
	1.23	28.36	43.5	0.4357	0.0189	1.4443	0.0289	38.4	2.2	38.0	2.1
	1.30	13.88	93.4	0.4174	0.0201	1.4419	0.0290	36.6	2.2	36.4	2.2
	1.28	11.38	112.2	0.4188	0.0232	1.4515	0.0289	36.4	2.5	36.3	2.5
	1.39	12.95	107.1	0.3781	0.0165	1.4167	0.0191	33.3	1.8	33.2	1.7
	1.33	28.53	46.7	0.4033	0.0194	1.4605	0.0221	34.6	2.0	34.3	2.0
	1.36	11.80	115.3	0.3879	0.0169	1.4617	0.0226	33.1	1.8	32.9	1.8
	1.35	32.44	41.6	0.4049	0.0175	1.4424	0.0212	35.3	1.9	34.9	1.9
	1.32	19.96	66.1	0.4167	0.0211	1.4610	0.0233	35.9	2.2	35.7	2.2
	1.40	16.81	83.1	0.3827	0.0148	1.4483	0.0194	32.9	1.6	32.7	1.5
	1.47	33.85	43.3	0.3924	0.0158	1.4440	0.0273	34.0	1.8	33.6	1.7
B9	0.74	27.18	27.4	0.5304	0.0283	1.4607	0.0256	47.9	3.3	47.3	3.3
	0.83	26.60	31.2	0.5041	0.0255	1.4546	0.0288	45.3	3.0	44.8	3.0
	1.06	18.86	56.3	0.4581	0.0207	1.4170	0.0227	41.7	2.4	41.4	2.4
	1.16	16.37	70.7	0.4432	0.0198	1.4556	0.0212	38.8	2.2	38.6	2.1
	1.19	16.64	71.8	0.4236	0.0209	1.4357	0.0328	37.4	2.4	37.2	2.4
	1.26	22.64	55.5	0.4289	0.0188	1.4545	0.0191	37.4	2.0	37.1	2.0
	1.10	21.21	51.6	0.4196	0.0183	1.4460	0.0220	36.7	2.0	36.4	2.0
	1.20	13.47	88.8	0.4013	0.0135	1.4446	0.0315	34.9	1.6	34.7	1.6
	1.44	14.44	99.9	0.3926	0.0177	1.4166	0.0249	34.8	2.0	34.6	1.9
	1.31	23.26	56.4	0.4161	0.0171	1.4527	0.0271	36.1	1.9	35.8	1.9
	1.33	14.92	89.0	0.4112	0.0162	1.4528	0.0302	35.6	1.9	35.4	1.8
	1.51	24.25	62.3	0.4109	0.0158	1.4555	0.0174	35.5	1.7	35.3	1.7
	1.60	23.65	67.8	0.4002	0.0180	1.4546	0.0193	34.5	1.9	34.2	1.9
B10	0.94	25.86	36.4	0.4850	0.0265	1.4493	0.0232	43.4	3.0	43.0	2.9
	1.11	25.83	42.8	0.4938	0.0206	1.4356	0.0208	44.9	2.4	44.5	2.4
	0.98	28.78	33.9	0.4714	0.0238	1.4335	0.0259	42.6	2.7	42.1	2.7
	0.93	21.41	43.5	0.4738	0.0271	1.4746	0.0468	41.3	3.3	41.0	3.2
	1.29	19.25	67.0	0.4144	0.0219	1.4267	0.0299	36.8	2.5	36.5	2.4
	1.30	17.13	76.1	0.4306	0.0222	1.4224	0.0307	38.6	2.6	38.4	2.5
	1.41	19.00	74.3	0.4068	0.0215	1.4635	0.0233	34.9	2.2	34.7	2.2
	1.39	10.81	128.1	0.4193	0.0173	1.4561	0.0201	36.4	1.8	36.2	1.8
	1.39	12.39	112.5	0.4053	0.0156	1.4533	0.0195	35.0	1.7	34.9	1.6
	1.53	20.37	74.9	0.4138	0.0156	1.4358	0.0244	36.4	1.8	36.2	1.8
	1.37	15.64	87.7	0.4073	0.0158	1.4573	0.0208	35.1	1.7	34.9	1.7
	1.50	18.31	82.0	0.3881	0.0195	1.4765	0.0292	32.7	2.0	32.5	2.0
B11	0.96	48.86	19.7	0.4839	0.0255	1.4524	0.0303	43.2	3.0	42.3	2.9
	0.91	30.87	29.5	0.5199	0.0244	1.4313	0.0308	48.0	3.1	47.4	3.0
	0.92	20.85	44.2	0.4913	0.0258	1.4568	0.0229	43.8	2.9	43.4	2.9
	1.19	23.61	50.5	0.4515	0.0218	1.4521	0.0198	39.8	2.4	39.5	2.3
	1.39	26.38	52.7	0.4343	0.0202	1.4444	0.0268	38.3	2.3	37.9	2.2

	1.47	25.29	58.0	0.4176	0.0212	1.4287	0.0341	37.0	2.4	36.7	2.4
	1.53	21.57	70.9	0.4272	0.0187	1.4445	0.0191	37.5	2.0	37.3	2.0
	1.30	19.86	65.6	0.4245	0.0207	1.4469	0.0225	37.2	2.2	36.9	2.2

Table S13. U-series results on cross section 2

CC2	U (ppm)	Th (ppb)	U/Th	$^{230}Th/^{238}U$	$^{230}Th/^{238}U$ error	$^{234}U/^{238}U$	$^{234}U/^{238}U$ error	Age (ka)	Age error (ka)	Th-corr Age (ka)	Th-corr Age error (ka)
B1	1.77	119.22	80	0.3251	0.0114	1.4374	0.0224	27.6	1.2	26.4	1.1
	1.65	128.07	70	0.3482	0.0112	1.4517	0.0273	29.5	1.3	28.1	1.2
	1.70	94.36	90	0.3380	0.0157	1.4438	0.0174	28.7	1.6	27.7	1.5
	1.72	103.46	90	0.3639	0.0146	1.4437	0.0151	31.2	1.5	30.1	1.4
	1.67	109.26	80	0.3740	0.0140	1.4334	0.0158	32.5	1.5	31.3	1.4
	1.50	96.68	80	0.3860	0.0162	1.4371	0.0156	33.5	1.7	32.4	1.6
	1.58	62.84	130	0.3914	0.0118	1.4475	0.0150	33.8	1.2	33.1	1.2
	1.06	74.63	70	0.4214	0.0203	1.4371	0.0185	37.2	2.2	35.9	2.1
	0.80	69.23	60	0.4351	0.0177	1.4360	0.0255	38.6	2.0	37.1	1.9
	1.06	78.93	70	0.4255	0.0184	1.4079	0.0176	38.5	2.0	37.2	2.0
	1.14	92.17	60	0.4620	0.0183	1.4292	0.0193	41.7	2.1	40.3	2.0
	0.94	129.69	30	0.4979	0.0197	1.4104	0.0266	46.4	2.5	44.0	2.3
	0.94	201.68	20	0.5185	0.0212	1.4056	0.0217	49.0	2.7	45.2	2.4
	0.84	286.19	10	0.5049	0.0225	1.4330	0.0225	46.3	2.7	40.2	2.3
	0.84	396.91	10	0.4718	0.0226	1.4400	0.0205	42.4	2.5	33.9	2.0
B2	1.39	70.26	100	0.3601	0.0151	1.4332	0.0144	31.1	1.5	30.2	1.5
	1.57	73.28	110	0.3479	0.0141	1.4359	0.0176	29.8	1.4	29.0	1.4
	1.65	74.05	120	0.3335	0.0134	1.4399	0.0136	28.3	1.3	27.6	1.3
	1.57	129.32	60	0.3573	0.0147	1.4325	0.0186	30.8	1.5	29.4	1.4
	1.69	124.40	70	0.3668	0.0125	1.4495	0.0113	31.3	1.3	30.1	1.2
	1.62	80.44	100	0.3588	0.0128	1.4361	0.0159	30.9	1.3	30.0	1.3
	1.63	98.60	80	0.3677	0.0103	1.4270	0.0171	32.0	1.1	30.9	1.1
	1.31	136.37	50	0.4237	0.0145	1.4396	0.0200	37.3	1.6	35.5	1.5
	1.32	107.56	60	0.4052	0.0120	1.4295	0.0185	35.7	1.3	34.3	1.3
	1.38	117.16	60	0.4023	0.0145	1.4410	0.0204	35.1	1.6	33.6	1.5
	1.31	102.23	60	0.4443	0.0165	1.4144	0.0209	40.3	1.9	38.9	1.8
	1.18	127.78	50	0.4590	0.0234	1.4144	0.0257	41.9	2.7	40.0	2.6
	0.96	228.42	20	0.5023	0.0211	1.4092	0.0267	47.0	2.7	42.7	2.4
	1.07	434.22	10	0.4725	0.0200	1.4252	0.0151	43.0	2.3	35.7	1.8
	1.04	503.93	10	0.4867	0.0150	1.4513	0.0162	43.5	1.7	34.9	1.3
B3	1.45	190.70	40	0.4276	0.0313	1.3891	0.0324	39.4	3.6	37.0	3.3
	1.54	160.18	50	0.3637	0.0132	1.4435	0.0223	31.2	1.4	29.4	1.3
	1.64	54.09	160	0.3492	0.0146	1.4427	0.0157	29.8	1.5	29.2	1.4
	1.61	75.61	110	0.3506	0.0123	1.4537	0.0163	29.7	1.2	28.8	1.2
	1.49	99.10	80	0.3670	0.0132	1.4378	0.0147	31.7	1.4	30.5	1.3

	1.43	93.47	80	0.3823	0.0154	1.4496	0.0169	32.8	1.6	31.7	1.5
	1.35	89.86	80	0.3822	0.0141	1.4479	0.0185	32.9	1.5	31.7	1.4
	1.12	66.10	90	0.4067	0.0162	1.4132	0.0189	36.4	1.8	35.3	1.7
	1.11	54.34	110	0.4103	0.0173	1.4241	0.0184	36.4	1.9	35.6	1.8
	1.15	88.80	70	0.4306	0.0177	1.4544	0.0173	37.6	1.9	36.2	1.8
	1.08	122.60	40	0.4513	0.0199	1.4341	0.0276	40.4	2.3	38.4	2.2
	1.03	118.61	40	0.4535	0.0184	1.4312	0.0206	40.7	2.1	38.7	2.0
	0.87	123.49	30	0.5027	0.0215	1.4309	0.0211	46.1	2.5	43.6	2.4
	0.85	232.92	10	0.5147	0.0248	1.4361	0.0261	47.2	3.0	42.4	2.6
	0.98	220.26	20	0.3783	0.0140	1.4474	0.0215	32.5	1.5	28.6	1.3
A1	1.10	26.48	40	0.3438	0.0206	1.3837	0.0384	30.7	2.3	30.3	2.3
	1.21	25.00	40	0.3776	0.0182	1.4146	0.0175	33.3	1.9	33.0	1.9
	1.33	26.72	40	0.3653	0.0161	1.3957	0.0221	32.6	1.8	32.2	1.7
	1.56	18.25	80	0.3647	0.0153	1.4042	0.0170	32.3	1.6	32.1	1.6
	1.55	19.19	80	0.3570	0.0167	1.4298	0.0216	30.9	1.7	30.7	1.7
	1.56	16.61	90	0.3293	0.0153	1.4100	0.0226	28.6	1.6	28.4	1.6
	1.65	17.69	90	0.3486	0.0168	1.4317	0.0462	30.0	2.0	29.8	2.0
	1.64	14.85	110	0.3069	0.0145	1.4013	0.0224	26.6	1.5	26.5	1.5
	1.63	21.32	70	0.3214	0.0151	1.4261	0.0198	27.5	1.5	27.3	1.5
	1.72	15.19	110	0.3158	0.0159	1.4175	0.0171	27.1	1.6	27.0	1.6
	1.96	12.87	150	0.3075	0.0140	1.4184	0.0171	26.3	1.4	26.2	1.4
	1.74	15.15	110	0.3164	0.0172	1.4210	0.0185	27.1	1.7	27.0	1.7
	1.89	24.47	70	0.3641	0.0137	1.4232	0.0190	31.7	1.5	31.5	1.4
B4	1.54	87.84	90	0.3501	0.0125	1.4573	0.0176	29.5	1.3	28.5	1.2
	1.55	77.99	100	0.3454	0.0160	1.4427	0.0173	29.4	1.6	28.5	1.5
	1.57	105.66	80	0.3430	0.0148	1.4301	0.0253	29.5	1.6	28.3	1.5
	1.44	80.91	90	0.3460	0.0129	1.4427	0.0220	29.5	1.4	28.5	1.3
	1.52	77.44	100	0.3681	0.0122	1.4460	0.0204	31.5	1.3	30.7	1.3
	1.44	113.07	60	0.3667	0.0140	1.4385	0.0158	31.6	1.4	30.2	1.4
	1.35	85.01	80	0.3803	0.0126	1.4381	0.0196	33.0	1.4	31.9	1.3
	1.36	113.74	60	0.4123	0.0124	1.4468	0.0223	35.9	1.4	34.5	1.4
	1.46	93.78	80	0.4157	0.0178	1.4235	0.0156	37.0	1.9	35.9	1.8
	1.30	102.63	60	0.4201	0.0178	1.4387	0.0141	37.0	1.9	35.6	1.8
	1.39	76.14	90	0.4177	0.0162	1.4360	0.0173	36.8	1.8	35.9	1.7
	1.16	133.80	40	0.4615	0.0200	1.4441	0.0249	41.1	2.3	39.1	2.2
	0.88	119.39	40	0.4831	0.0163	1.4427	0.0235	43.5	2.0	41.1	1.9
	0.84	114.27	40	0.4652	0.0222	1.4365	0.0228	41.8	2.5	39.4	2.4
	1.06	226.63	20	0.3965	0.0164	1.4562	0.0181	34.1	1.7	30.4	1.5
B5	1.57	73.17	110	0.3505	0.0139	1.4647	0.0212	29.4	1.4	28.6	1.4
	1.54	93.17	90	0.3513	0.0146	1.4328	0.0263	30.2	1.6	29.2	1.5
	1.48	79.62	100	0.3547	0.0131	1.4176	0.0182	30.9	1.4	30.0	1.3
	1.56	89.83	90	0.3579	0.0120	1.4426	0.0226	30.6	1.3	29.6	1.2
	1.35	127.75	50	0.3843	0.0159	1.4679	0.0247	32.5	1.7	30.9	1.6
	1.39	94.68	80	0.3868	0.0132	1.4403	0.0148	33.5	1.4	32.4	1.3
	1.36	65.59	110	0.3690	0.0132	1.4316	0.0199	32.0	1.4	31.2	1.4

	1.41	102.85	70	0.3795	0.0144	1.4385	0.0282	32.9	1.6	31.6	1.6
	1.42	89.73	80	0.3979	0.0120	1.4394	0.0238	34.7	1.4	33.6	1.3
	1.39	147.67	50	0.4278	0.0155	1.4435	0.0227	37.6	1.7	35.8	1.6
	1.27	91.85	70	0.4250	0.0172	1.4298	0.0188	37.8	1.9	36.5	1.8
	1.27	140.59	40	0.4306	0.0170	1.4341	0.0228	38.2	1.9	36.3	1.8
	1.06	173.82	30	0.4655	0.0218	1.4388	0.0231	41.7	2.5	38.9	2.3
	1.20	230.15	20	0.4387	0.0147	1.4532	0.0213	38.4	1.7	35.1	1.5
	1.28	307.00	20	0.3789	0.0137	1.4280	0.0170	33.1	1.5	28.8	1.2
B6	1.46	100.55	70	0.3574	0.0196	1.4608	0.0286	30.1	2.0	29.0	1.9
	1.48	66.75	120	0.3712	0.0110	1.4499	0.0187	31.7	1.2	31.0	1.1
	1.34	89.59	80	0.3597	0.0120	1.4392	0.0175	30.9	1.3	29.7	1.2
	1.44	72.09	100	0.3603	0.0115	1.4414	0.0269	30.9	1.3	30.0	1.3
	1.43	85.10	90	0.3633	0.0179	1.4542	0.0237	30.9	1.8	29.8	1.8
	1.37	93.64	70	0.3817	0.0148	1.4358	0.0155	33.2	1.5	32.0	1.5
	1.36	71.03	100	0.3859	0.0182	1.4316	0.0185	33.7	1.9	32.8	1.8
	1.52	147.33	50	0.3864	0.0132	1.4365	0.0168	33.6	1.4	31.9	1.3
	1.40	134.75	50	0.4060	0.0171	1.4423	0.0257	35.4	1.9	33.7	1.8
	1.26	88.74	70	0.4109	0.0147	1.4324	0.0258	36.2	1.7	35.0	1.6
	1.15	101.79	60	0.4373	0.0166	1.4407	0.0181	38.7	1.8	37.1	1.7
	1.25	186.95	30	0.4379	0.0164	1.4422	0.0211	38.7	1.8	36.1	1.7
	1.25	302.71	20	0.4301	0.0173	1.4527	0.0225	37.6	1.9	33.3	1.7
	1.40	314.74	20	0.4111	0.0184	1.4449	0.0179	35.9	1.9	31.9	1.7
	1.28	458.80	10	0.4076	0.0162	1.4733	0.0245	34.7	1.7	28.4	1.4
B7	1.48	19.21	70	0.3905	0.0162	1.4261	0.0185	34.3	1.7	34.1	1.7
	1.50	13.47	110	0.3769	0.0151	1.4362	0.0232	32.7	1.6	32.5	1.6
	1.43	15.65	90	0.3895	0.0175	1.4379	0.0252	33.9	1.9	33.7	1.9
	1.48	13.99	100	0.3695	0.0148	1.4302	0.0137	32.1	1.5	31.9	1.5
	1.47	14.70	100	0.3655	0.0142	1.4165	0.0182	32.1	1.5	31.9	1.5
	1.34	13.65	90	0.3996	0.0162	1.4272	0.0156	35.2	1.7	35.0	1.7
	1.59	15.24	100	0.4087	0.0159	1.4485	0.0177	35.5	1.7	35.4	1.7
	1.40	15.00	90	0.4198	0.0170	1.4387	0.0243	36.9	1.9	36.7	1.9
	1.52	19.64	70	0.4397	0.0142	1.4155	0.0180	39.8	1.6	39.6	1.6
	1.45	21.00	60	0.4899	0.0207	1.4048	0.0302	45.7	2.7	45.5	2.6
	1.49	29.31	50	0.4722	0.0136	1.4092	0.0134	43.6	1.6	43.2	1.6
	1.36	86.64	10	0.4671	0.0130	1.4226	0.0198	42.5	1.6	41.4	1.6
B8	1.51	21.56	70	0.3665	0.0143	1.4471	0.0159	31.4	1.5	31.1	1.4
	1.45	23.01	60	0.3834	0.0142	1.4329	0.0214	33.4	1.5	33.1	1.5
	1.22	19.90	60	0.3833	0.0143	1.4494	0.0166	33.0	1.5	32.7	1.5
	1.48	14.72	100	0.3782	0.0159	1.4495	0.0196	32.4	1.7	32.3	1.6
	1.51	13.63	110	0.3887	0.0156	1.4491	0.0270	33.5	1.7	33.3	1.7
	1.39	17.28	80	0.3923	0.0134	1.4501	0.0225	33.8	1.5	33.6	1.5
	1.28	14.82	80	0.4008	0.0174	1.4297	0.0240	35.3	1.9	35.1	1.9
	1.36	21.11	60	0.4048	0.0163	1.4548	0.0192	34.9	1.7	34.7	1.7
	1.19	17.40	60	0.4368	0.0152	1.4427	0.0467	38.6	2.2	38.3	2.2
	1.44	36.23	30	0.4206	0.0158	1.4310	0.0175	37.3	1.7	36.8	1.7

B9	1.52	19.56	70	0.3862	0.0411	1.4505	0.0351	33.2	4.2	33.0	4.1
	1.49	17.64	80	0.3764	0.0145	1.4403	0.0190	32.5	1.5	32.3	1.5
	1.27	19.64	60	0.3663	0.0157	1.4462	0.0148	31.4	1.6	31.1	1.6
	1.50	19.44	70	0.3658	0.0128	1.4331	0.0188	31.7	1.4	31.4	1.3
	1.50	17.75	80	0.3949	0.0148	1.4403	0.0233	34.4	1.6	34.2	1.6
	1.48	15.11	90	0.3944	0.0153	1.4315	0.0200	34.6	1.7	34.4	1.6
	1.56	15.99	90	0.4029	0.0137	1.4310	0.0184	35.4	1.5	35.3	1.5
	1.42	27.29	50	0.4231	0.0176	1.4240	0.0198	37.7	2.0	37.4	1.9
	1.20	26.72	40	0.4438	0.0168	1.4237	0.0175	39.9	1.9	39.6	1.9
A2	1.48	29.99	40	0.3664	0.0177	1.4101	0.0197	32.3	1.9	32.0	1.8
	1.46	21.97	60	0.3402	0.0151	1.4134	0.0260	29.6	1.6	29.4	1.6
	1.80	15.21	110	0.3247	0.0166	1.4086	0.0293	28.2	1.8	28.1	1.7
	1.70	22.24	70	0.3295	0.0155	1.4013	0.0171	28.9	1.6	28.6	1.6
	1.79	15.53	110	0.3007	0.0120	1.4234	0.0276	25.6	1.3	25.4	1.3
	1.85	20.84	80	0.3154	0.0145	1.4461	0.0315	26.5	1.5	26.3	1.5
	1.69	20.98	80	0.3352	0.0128	1.4108	0.0175	29.2	1.3	29.0	1.3
	1.75	19.54	80	0.3445	0.0150	1.5351	0.0232	27.3	1.4	27.1	1.4
B10	1.63	16.81	90	0.3897	0.0118	1.4484	0.0220	33.6	1.3	33.4	1.3
	1.55	20.04	70	0.4098	0.0149	1.4382	0.0197	35.9	1.6	35.7	1.6
	1.72	16.64	100	0.3858	0.0177	1.4363	0.0252	33.6	1.9	33.4	1.9
	1.48	19.66	70	0.3822	0.0148	1.4343	0.0130	33.2	1.5	33.0	1.5
	1.59	18.73	80	0.4066	0.0147	1.4545	0.0221	35.1	1.6	34.9	1.6
	1.56	39.29	30	0.4302	0.0156	1.4403	0.0141	38.0	1.7	37.5	1.7
B11	1.50	18.33	80	0.3811	0.0137	1.4269	0.0184	33.3	1.5	33.1	1.5
	1.64	21.51	70	0.3812	0.0135	1.4393	0.0157	33.0	1.4	32.8	1.4
	1.45	20.01	70	0.3891	0.0169	1.4370	0.0215	33.9	1.8	33.6	1.8
	1.50	23.54	60	0.3842	0.0118	1.4483	0.0214	33.1	1.3	32.8	1.3
	1.40	26.90	50	0.4227	0.0149	1.4304	0.0212	37.5	1.7	37.2	1.7
	1.61	15.27	100	0.3693	0.0118	1.4526	0.0233	31.5	1.3	31.3	1.3

Table S14. U-series results on side tracks

Side	U (ppm)	Th (ppb)	U/Th	$^{230}Th/^{238}U$	$^{230}Th/^{238}U$ error	$^{234}U/^{238}U$	$^{234}U/^{238}U$ error	Age (ka)	Age error (ka)	Th-corr Age (ka)	Th-corr Age error (ka)
B1	0.73	416.30	1.76	0.5620	0.0259	1.3743	0.0185	55.8	3.4	45.1	2.6
	0.84	456.29	1.85	0.5809	0.0255	1.3826	0.0189	57.8	3.4	47.7	2.7
	0.81	338.49	2.39	0.6011	0.0252	1.3961	0.0329	59.6	3.8	52.0	3.2
	0.85	152.35	5.55	0.5649	0.0241	1.4134	0.0212	54.1	3.1	51.0	2.9
	0.86	123.33	6.95	0.5419	0.0247	1.4228	0.0201	50.9	3.0	48.4	2.8
	0.91	117.10	7.77	0.5278	0.0180	1.4095	0.0244	49.9	2.4	47.6	2.3
	0.93	130.06	7.18	0.5630	0.0238	1.4207	0.0201	53.5	3.0	51.1	2.9
	0.99	158.48	6.22	0.5788	0.0206	1.4115	0.0279	55.9	2.9	53.1	2.7
	1.10	139.48	7.87	0.5099	0.0224	1.3398	0.0247	51.1	3.1	48.7	2.9

	1.13	413.78	2.73	0.6300	0.0293	1.3897	0.0216	63.7	4.1	57.1	3.6
	1.28	467.09	2.74	0.6901	0.0300	1.4010	0.0152	71.2	4.4	64.7	3.8
	1.15	378.36	3.03	0.6541	0.0225	1.4151	0.0182	65.3	3.2	59.5	2.8
	1.07	423.02	2.53	0.6878	0.0340	1.4457	0.0230	67.8	4.7	60.9	4.1
	1.04	435.75	2.39	0.6780	0.0286	1.4301	0.0191	67.5	4.0	60.2	3.5
	1.18	612.17	1.92	0.7569	0.0461	1.4266	0.0175	78.8	6.9	69.7	5.8
B2	0.69	34.15	20.17	0.4056	0.0457	1.4214	0.0348	36.0	4.9	35.1	4.7
	0.80	50.53	15.88	0.4060	0.0227	1.4297	0.0273	35.8	2.5	34.7	2.4
	0.75	44.51	16.79	0.4211	0.0221	1.4241	0.0249	37.5	2.4	36.5	2.4
	0.68	54.73	12.46	0.4651	0.0231	1.4216	0.0306	42.3	2.8	40.9	2.7
	0.76	145.46	5.24	0.5135	0.0205	1.4161	0.0251	47.9	2.6	44.6	2.4
	0.87	74.37	11.65	0.5426	0.0257	1.4054	0.0225	51.8	3.3	50.3	3.1
	0.90	52.82	17.08	0.5697	0.0204	1.3937	0.0157	55.7	2.7	54.7	2.6
	1.00	82.08	12.14	0.6162	0.0226	1.3815	0.0222	62.4	3.3	61.0	3.2
	1.13	56.40	20.07	0.6244	0.0216	1.3924	0.0160	62.8	3.0	62.0	3.0
	1.28	49.02	26.12	0.5906	0.0247	1.3820	0.0165	59.0	3.3	58.4	3.3
	1.33	97.11	13.68	0.5967	0.0231	1.4084	0.0147	58.3	3.0	57.0	2.9
	1.17	165.75	7.07	0.5782	0.0235	1.4222	0.0183	55.3	3.0	52.8	2.8
	1.08	244.94	4.41	0.6027	0.0231	1.4243	0.0183	58.2	3.0	54.2	2.8
	1.06	234.13	4.52	0.6153	0.0244	1.4215	0.0222	59.9	3.3	56.0	3.1
	1.05	369.18	2.84	0.6605	0.0223	1.4123	0.0191	66.3	3.2	60.1	2.9
B3	0.69	39.06	17.58	0.3616	0.0214	1.4289	0.0387	31.3	2.3	30.3	2.3
	0.62	49.56	12.57	0.4003	0.0217	1.4359	0.0262	35.0	2.3	33.6	2.2
	0.70	63.00	11.17	0.3987	0.0203	1.4585	0.0216	34.2	2.1	32.7	2.0
	0.70	31.82	21.94	0.4003	0.0253	1.4384	0.0193	35.0	2.6	34.2	2.6
	0.72	37.71	19.20	0.4118	0.0263	1.4322	0.0296	36.3	2.9	35.4	2.8
	0.77	52.05	14.71	0.4385	0.0177	1.4384	0.0217	38.9	2.0	37.7	1.9
	0.85	64.67	13.07	0.5197	0.0232	1.4071	0.0207	49.1	2.9	47.7	2.8
	0.84	47.66	17.57	0.4360	0.0255	1.4153	0.0184	39.4	2.8	38.4	2.7
	0.91	56.09	16.25	0.4385	0.0166	1.4326	0.0215	39.1	1.9	38.0	1.8
	1.11	68.56	16.18	0.4498	0.0194	1.3992	0.0264	41.5	2.4	40.4	2.3
	1.06	80.72	13.17	0.5303	0.0255	1.4029	0.0274	50.5	3.3	49.2	3.2
	1.02	97.01	10.50	0.5210	0.0189	1.3930	0.0176	49.9	2.4	48.2	2.3
	0.94	79.30	11.81	0.4799	0.0171	1.4384	0.0163	43.3	2.0	41.8	1.9
	0.94	71.88	13.05	0.4491	0.0241	1.4309	0.0202	40.3	2.7	38.9	2.6
	1.05	66.60	15.74	0.5028	0.0193	1.4325	0.0228	46.0	2.3	44.9	2.3

A

B

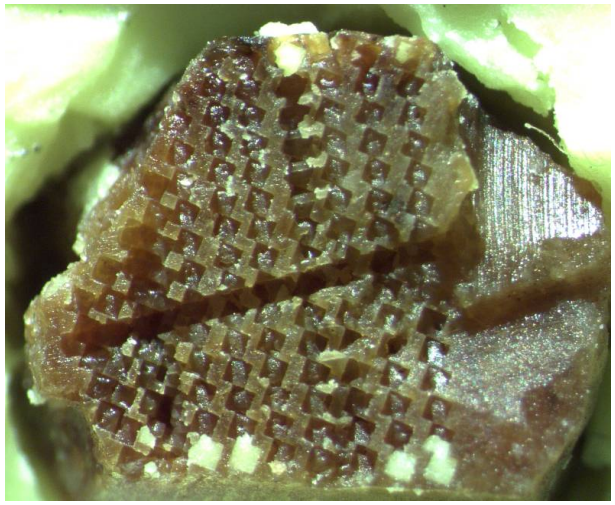

C

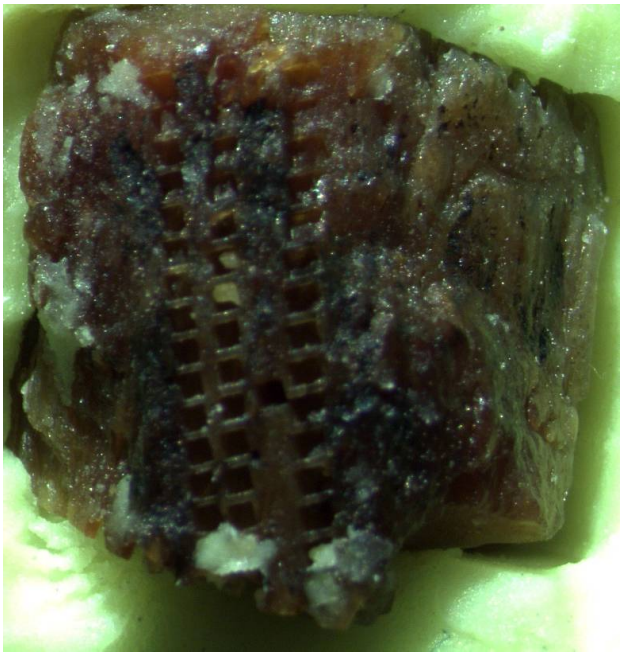

Figure S19. Position of laser spots. A: Cross section 1 (CC1), B: Cross section 2 (CC2), C: Bone surface. Scale, A = 6 mm in width, C = 6 mm in width.

A

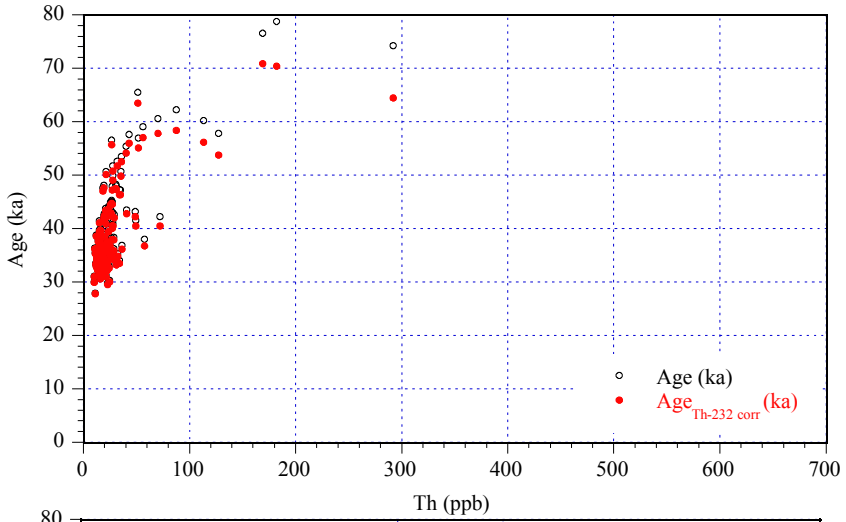

B

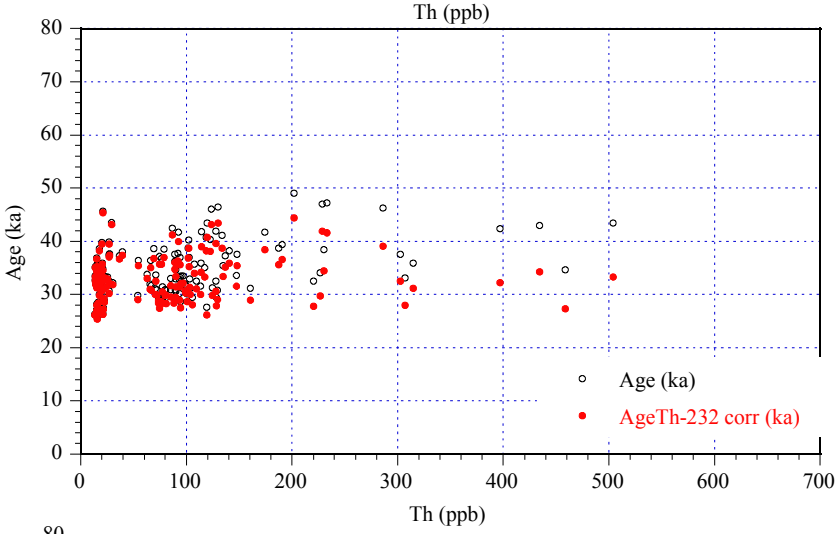

C

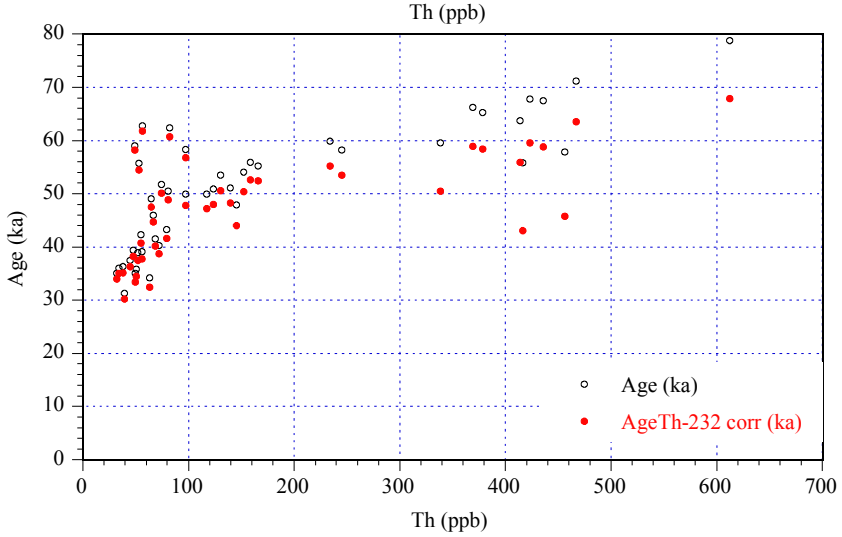

Figure S20. Age and Th corrected age vs Th concentration for CC1 (A), CC1 (B) and the surface tracks (C).

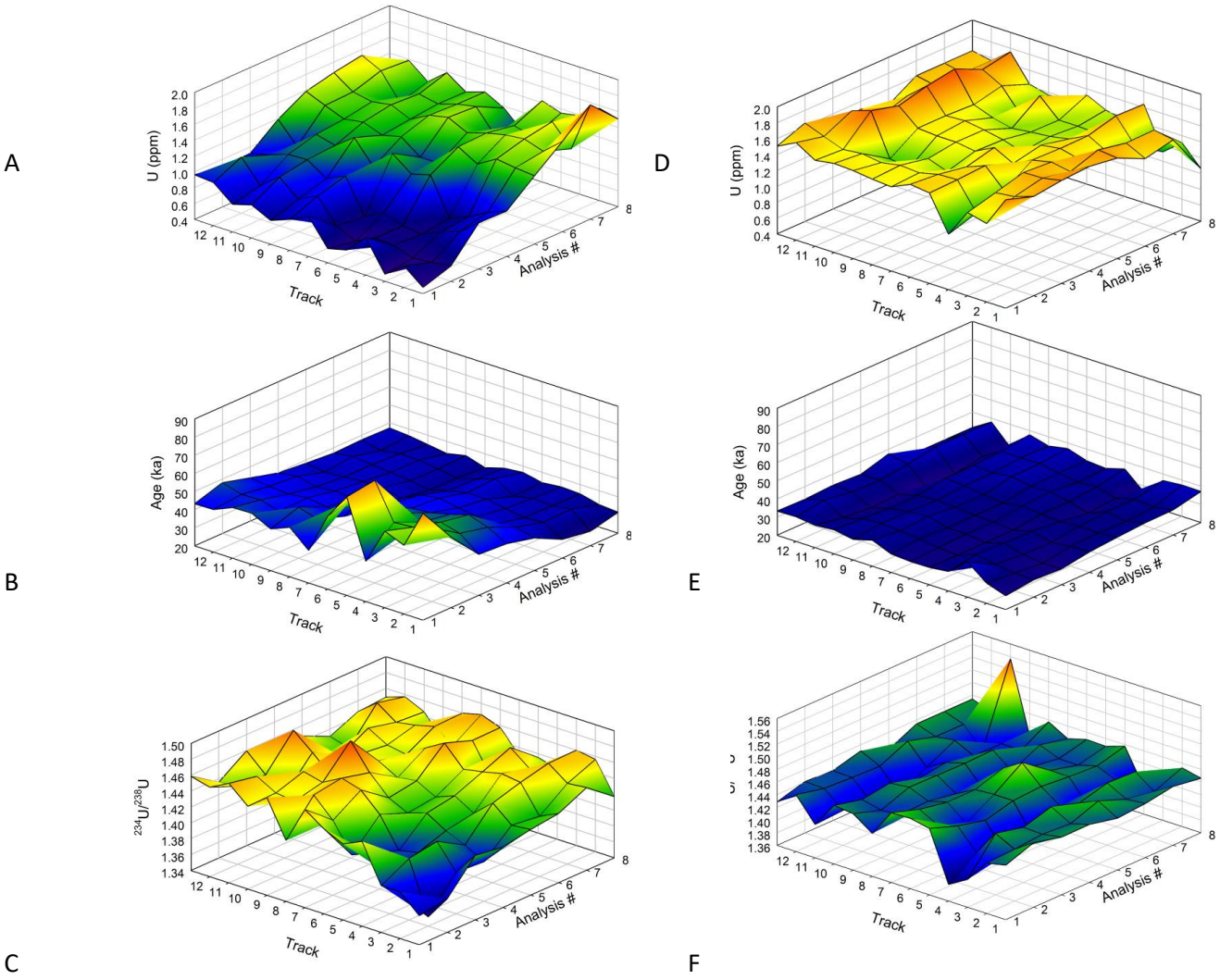

Figure S21. U-concentration (A,D), Age (B,E) and $^{234}U/^{238}U$ (C,F) for CC1 (A-C) and CC2 (D-F).

A

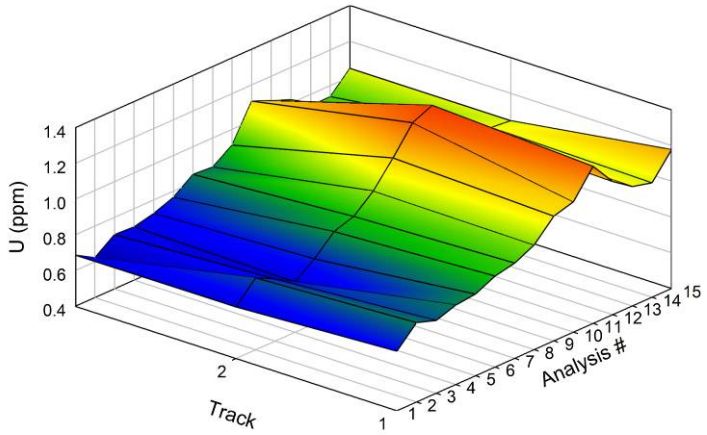

B

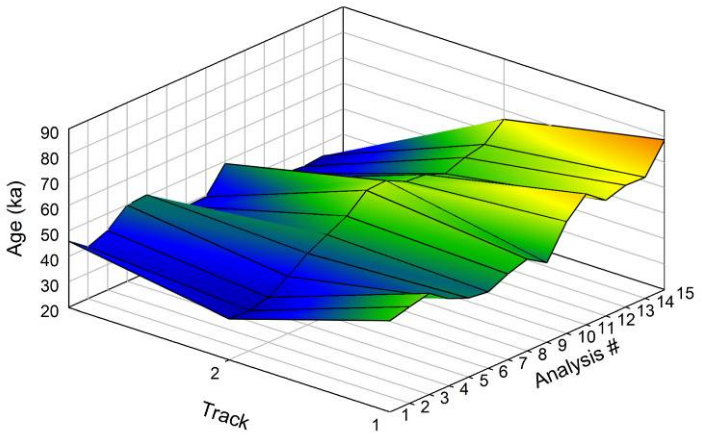

C

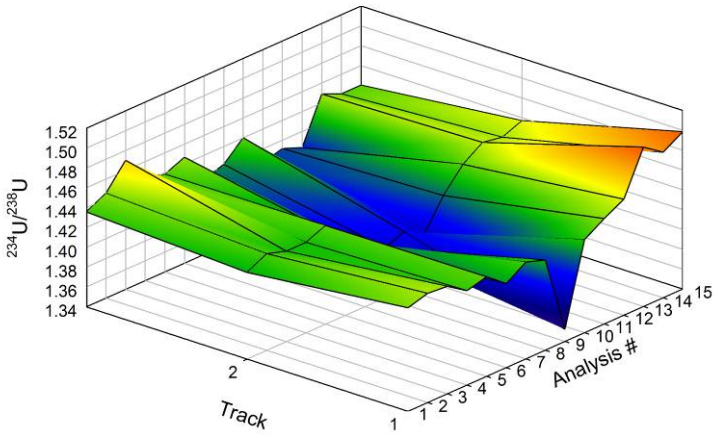

Figure S22. U-concentration (A), Age (B) and $^{234}U/^{238}U$ for the surface analyses.

A

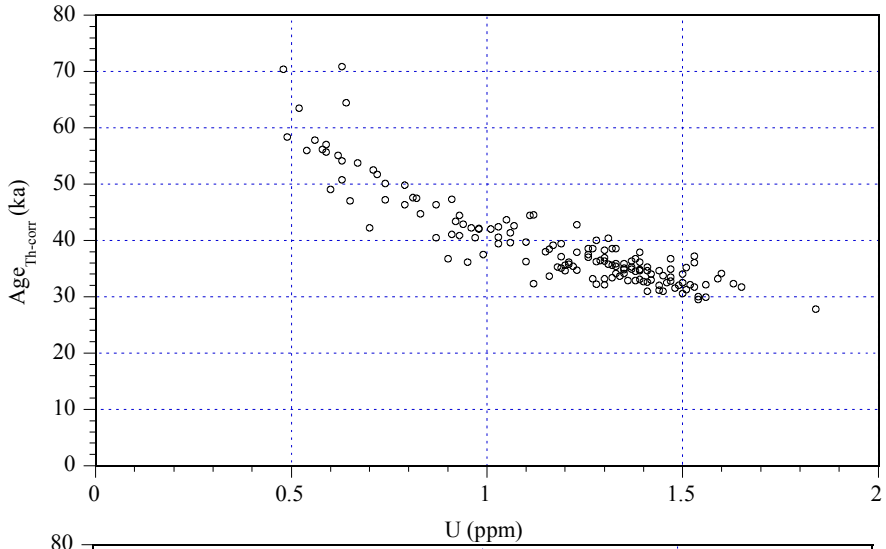

B

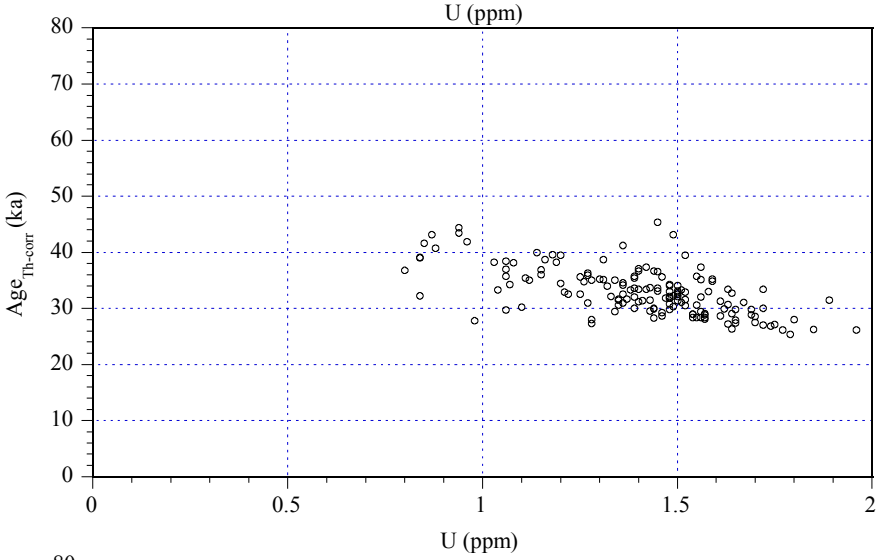

C

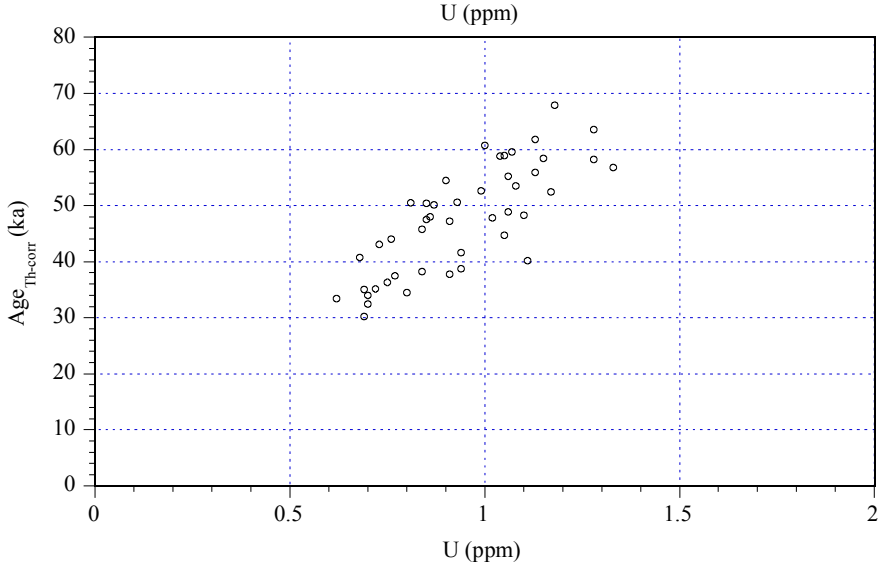

Figure S23. Th-corrected age vs U-concentration for CC1 (A), CC2 (B) and the surface analyses (C).

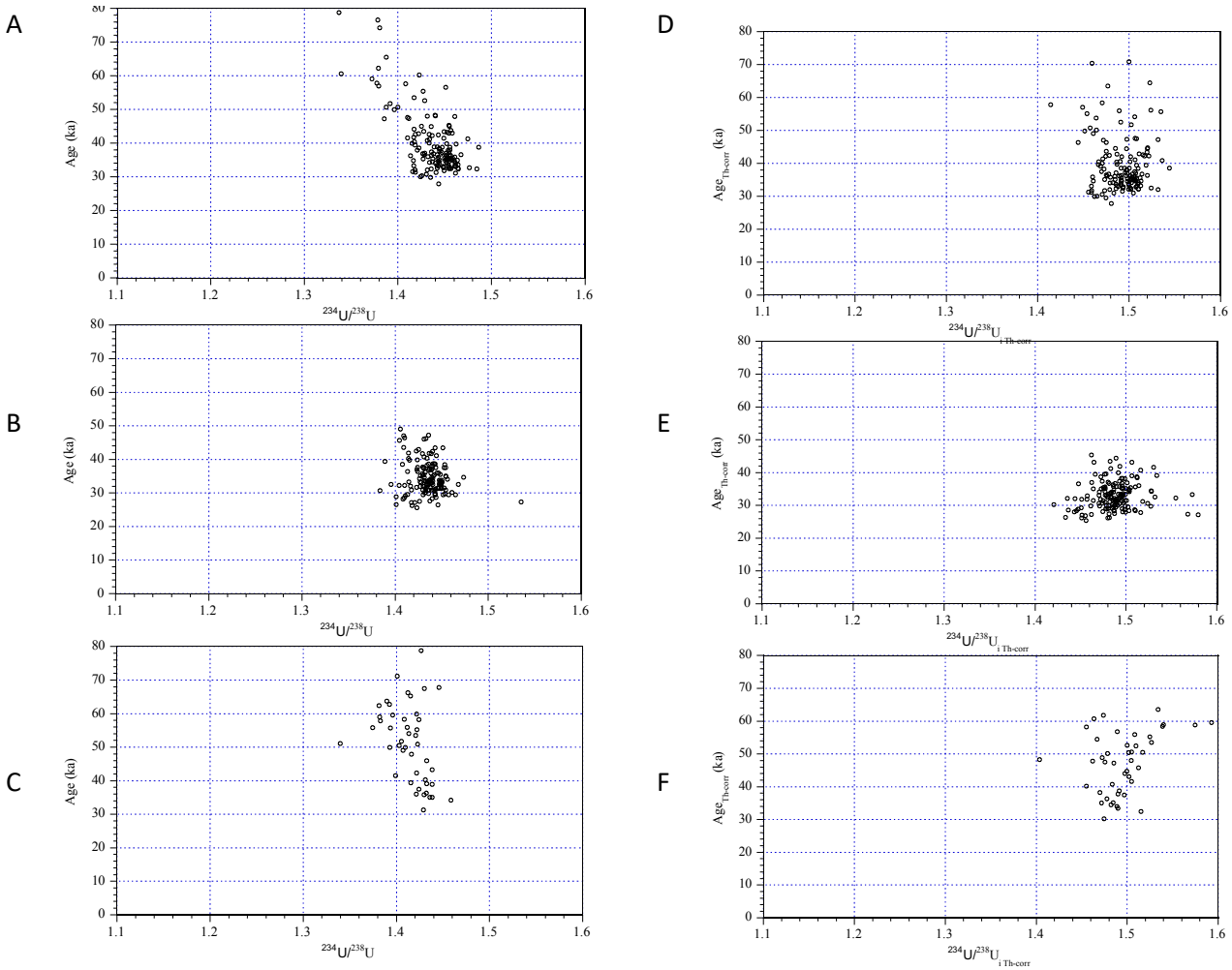

Figure S24. Apparent age vs measured $^{234}U/^{238}U$ ratio (A-C) and Th-corrected age versus initial corrected $^{234}U/^{238}U$ ratio (D-F) for CC1 (A, D), CC2 (B, E) and the surface analyses (C, F).

8. ZOOARCHAEOLOGY BY MASS SPECTROMETRY (ZOOMS)

S. Brown, M. Buckley

Zooarchaeology by Mass Spectrometry (ZooMS) was carried out on bone fragments accessed from the Institute of Archaeology and Ethnography in Novosibirsk. Samples of 2212 bones were analysed from across five layers: layer 9.1 (*n*= 31), layer 9.2 (*n*= 21), layer 9.3 (*n*= 310), layer 11.1 (*n*= 115), layer 11.2 (*n*= 557), layer 11.3 (*n*= 604), and layer 11.4 (*n*= 574). These were excavated during the 2005, 2007, 2009, and 2011 seasons at Denisova Cave. This brings the total to 4527 bones from Denisova Cave analysed using this method.

Samples were in general between 10-50mm in length and had been heavily fragmented, likely the result of taphonomic processes at the site and a high level of carnivore activity. The bone fragments were specifically chosen because they exhibited no diagnostic features which might make identification on the basis of morphology possible. Some however showed evidence of anthropic modification, such as burning and cutmarks.

ZooMS was carried out following the procedures described in Ref. 30 for the discovery of *Denisova 11*[34] (Figure S25a), using facilities at the University of Manchester and the ORAU, University of Oxford. A small fragment, between 20-50mg, was removed from each sample using a diamond disc drill bit. Each bone fragment was demineralised in 0.6M hydrochloric acid (HCl) for 18 hours at -4 ^{o}C. The supernatant was removed into 30 kDa molecular weight cut-off (MWCO) ultrafilters and centrifuged at 3700 rpm for 1 h, fragments were stored as backups at -20 ^{o}C. The remaining residue was then rinsed twice with 500µl of 50 mM ammonium bicarbonate (AmBic), centrifuging at 3700 rpm for 30 mins after each rinse. An additional 200 µL of 50 mM AmBic was allowed to mix with the resulting supernatant, half of which was then stored at -20 ^{o}C as a backup. The remaining 100µl of eluted collagen was treated with 0.2 µg trypsin (sequencing grade; Promega UK) and incubated at 37 ^{o}C for 18 h.

Trypsinised samples were mixed with a matrix solution of 1µl α -cyano-4-hydroxycinnamic acid solution (10 mg/mL in 50% acetonitrile (ACN)/0.1% trifluoroacetic acid (TFA), spotted onto a ground steel target plate (Bruker MTP 384 Target Plate 8280784), and allowed to crystallise. Analysis was performed using a Bruker Ultraflex II (Bruker Daltonics, Bremen) MALDI-Tof/Tof-mass spectrometer. The resulting mass spectra were matched to a reference library of published peptide markers using FlexAnalysis software[111,112,113] resulting in the identification of the three hominin bones *Denisova 14, Denisova 15* and *Denisova 16* (Fig. S13 b,c,d). Additionally, large mammmals such as bovines (*Bos/Bison)*, sheep (*Ovis*), goats (*Capra*), horses (*Equus*), woolly

rhinoceros (*Rhinocerotidae*), mammoths (*Elephantidae*), hyaenas (*Crocuta*), bears (*Ursus*), and a number of small mammals were identified amongst the assemblage.
All radiocarbon dated bones were also analysed using ZooMS to taxonomically identify the bones.

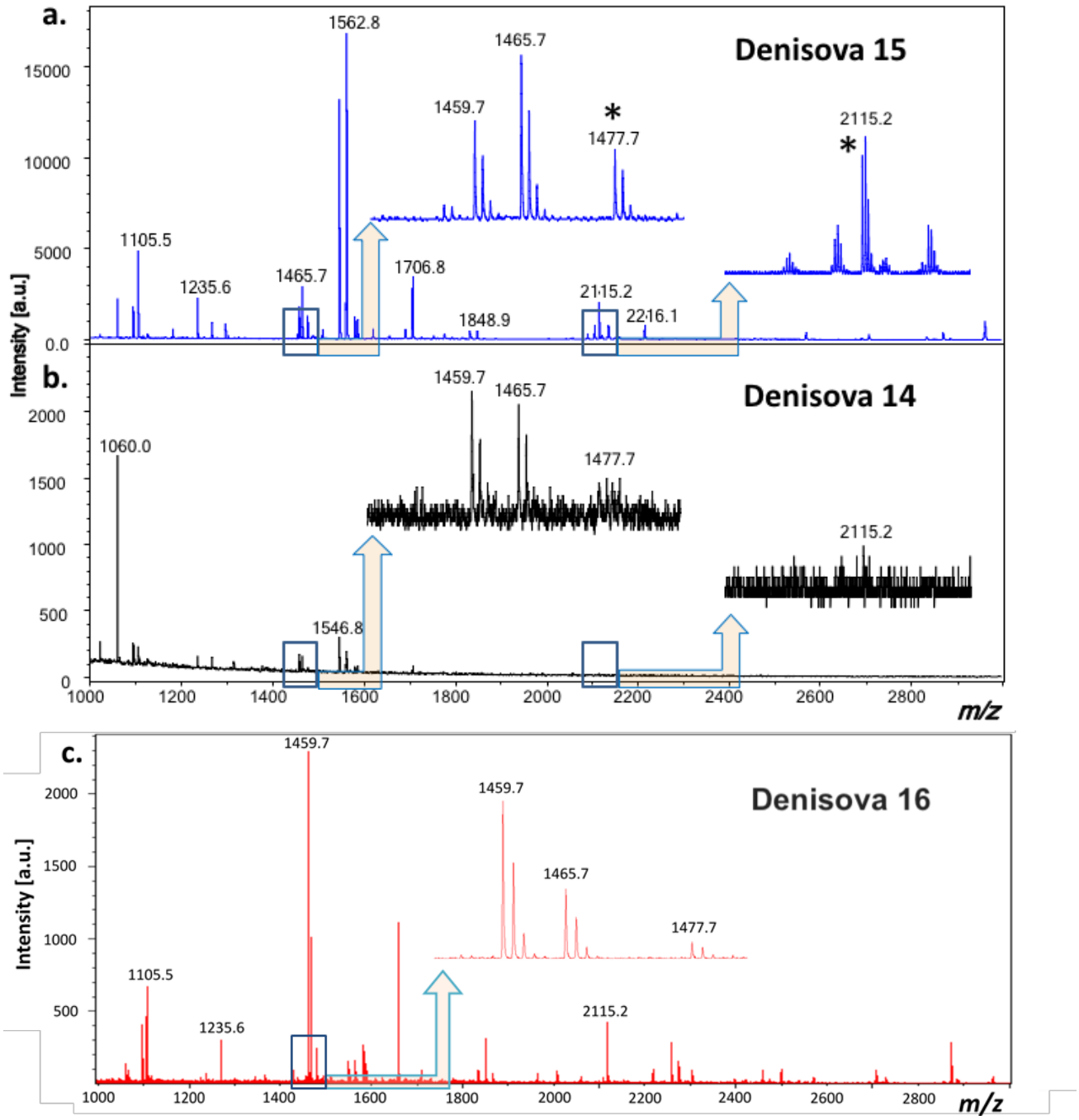

Figure S25. MALDI-ToF mass spectra of digested collagen from (a) *Denisova 15* (DC3753) (b) *Denisova 14* (DC 3758) and (c) *Denisova 16* (DC4114).

9. BAYESIAN AGE MODELLING

C. Bronk Ramsey, K. Douka, T. Higham

We built Bayesian age models to determine the chronometry of the site, and incorporated several different types of information within OxCal 4[18]. These included:

1. Radiocarbon dates calibrated against the IntCal13 calibration curve[19] (Section 2), including one direct radiocarbon age for *Denisova 14*, with the radiocarbon limit given as a *terminus ante quem*;
2. Eleven optical ages (Section 6);
3. Prior information in the form of age-ordering, either from direct stratigraphic constraints within the cave or as inferred from the mtDNA genetic tree;
4. Age differences between hominin remains as inferred from the number of substitutions observed (Section 4). Since this is the only unusual part of the age model, it is covered in more detail below.
5. A radiocarbon dated specimen from the site of Les Cottès (France)[76], dated between 43,740–42,720 cal BP (the actual radiocarbon date remains unpublished), which differs by 25 mutations to *Denisova 11*'s Neanderthal mother's mtDNA sequence.
6. A lower age limit for *Denisova 11* based on direct U-series analyses of the bone in the range of 65 to 70 ka (Section 7). It was inserted using Oxcal's 'Before' command.

We constructed a model for the age-difference between any two hominins based on:

a) The number of substitutions observed between them. The average time between substitutions is assumed to be τ years. The likelihood for the time difference δ between two hominins with k substitutions is assumed to be given by an Erlang distribution. We define x = δ/ τ (normalising to substitution time of 1) and then set:

$$x \sim x^{k-1} e^{-x}/(k-1)!$$

The mean of this distribution is k and so the mean likelihood estimate for δ is τk but with an uncertainty which tends to τ √k for high k values.

b) The mean time τ between each substitution is given a prior:

$$\tau \sim N(2649, 390^2)$$

The number of substitutions data is based on information described previously in Section 4 for the mtDNA mutation rate (the data is contained in Table S7); L to H = 1.76 to 3.23×10^{-8}. Base-

pairs were taken to be: B = 16569. The time for one mutation was then taken to be in the range: 1/(BH) to 1/(BL), assuming a normal distribution for this with a mean: SubstT = (1/(BH) + 1/(BL))/2 and with a standard error of SubstTSigma = (1/(BL) - 1/(BH))/4. The figures give SubstT = 2649 yr and SubstTSigma = 390 yr.

We used these inferred number of substitutions occurring on branches leading to the mtDNA genomes of individuals from Denisova Cave since their split from the common ancestor shared with other archaic individuals to calculate posterior distribution functions (PDFs) in the age model for these nodal positions. Figure S26 shows the position of these nodal positions or split times in the mtDNA trees for Denisovans and Neanderthals.

Note that no nuclear DNA estimates or tip dates were included in any model.

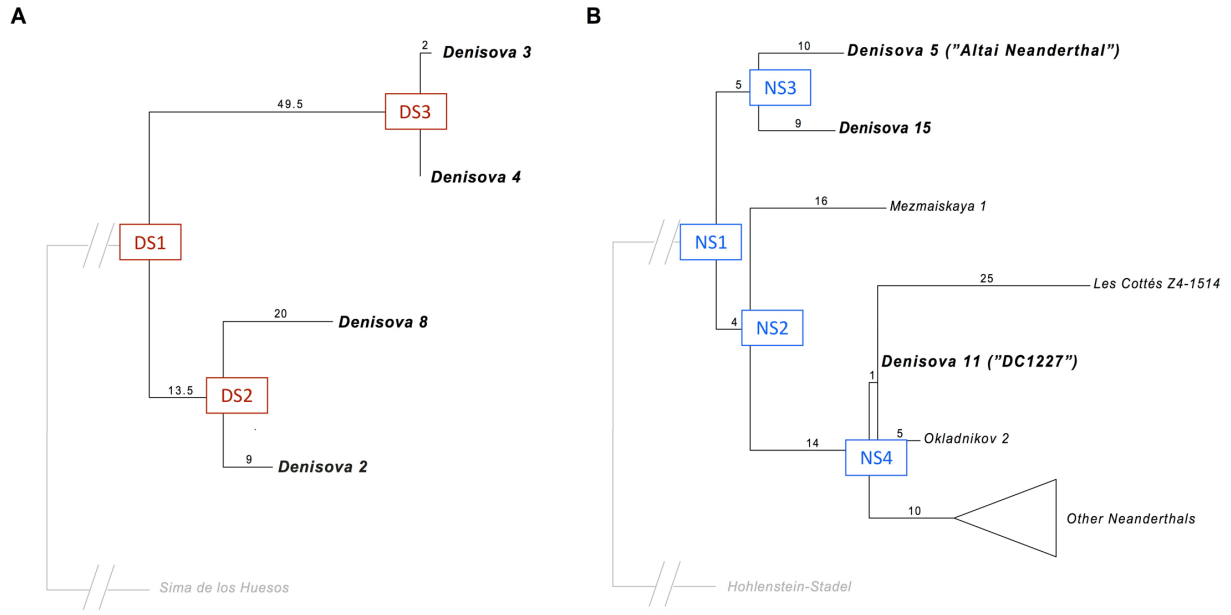

Figure S26. Inferred number of substitutions occurring on branches leading to the mtDNA genomes of individuals from Denisova Cave since their split from the common ancestor shared with other archaic individuals. DS and NS refer to Denisova and Neanderthal split age estimates we used in the Bayesian models to enable us to numerically calculate the split times of the various points on this tree.

In addition, we ran one of the models (Model 1, see below) using a non-informative uniform prior to enable it to find its estimated mutation rate based on the other data in the model (in this case taken over a range of possible values from 2000-10000 years). The result was 3600-8400 yr (at 95.4% probability), compared with the inferred rate of 2649 ± 390 yr.

All models were run with resolution of 250 up to 100k iterations (ie max. 10,000,000 iterations). Model codes are included below as CQL codes designed for OxCal 4.3.

A. Description of each model

Model 1

In this model we tied the age estimate for *Denisova 2* (the oldest Denisovan who lived 50,000–100,000 years before *Denisova 3*) to two optical ages from layer 22.1 (Main Chamber), its original findspot and we included three optical ages in Layer 21 (Main Chamber). We also included three optical ages from layer 12.3 (East Chamber) and three from 11.2.

<u>*Results*</u>: Model agreement for Model 1 was 23.3% (it ought to be >60%). While the Agreement index for *Denisova 2* was acceptable, its range was to the very youngest end of the ages in Layer 22.1, and more similar to those from Layer 21. Optical dating of the sediments from layer 22.1 suggests deposition before 287,000 ± 41,000 years ago[89], which does not fit with the genetic age estimates (*Extended Data Figure 6*). *Denisova 2* fits better if instead it is derived from layer 21 (see Model 2). This model is shown in Figure S27.

Model 2

In this model, the parameters were the same but instead of tying *Denisova 2* to Layer 22.1 we placed it with the optical ages in the overlying Layer 21 (Main Chamber). All other parts of the model were the same. This model is shown in Figure S28.

<u>*Results*</u>: Model agreement was higher at 82.3%, indicating a much better fit between the priors and posterior parts of the model. The age of *Denisova 2* shifted from 189.9-241.7 ka cal BP (Model 1) to 129.5-204.5 ka cal BP. Generally, since Agreement indices are pseudo-Bayes factors, a higher Agreement is significant and suggests this is a more acceptable model than Model 1. The Bayesian model results are more parsimonious with *Denisova 2* being derived from layers overlying the erosional unconformity that separates layers 22.1 and 21.

Model 3

This model is the same as Model 2, the only difference being that *Denisova 11* was moved from Level 12.3 into a post-11.4 level (East Chamber). This was undertaken based on evidence derived from the mtDNA mutation rate estimates which suggests strongly that *Denisova 11* is younger than *Denisova 5*, despite seemingly being excavated from Layer 11.4 just below it. The genetic constraints therefore compel *Denisova 11* to be younger but the stratigraphic sequence priors constrain it to be older. The bone itself was recovered from a bag of small unidentified bones

found in the Layer 12 from the East Chamber, but it may be that it was originally deposited higher up in the stratigraphic sequence. This model is shown in Figure S29.

Results: The model produced an Agreement index of 111.0%; equal highest of all models. All posterior results are similar to Model 2, the only difference being the age for *Denisova 11* which ranges from 115-142 ka BP in Models 1-2 to ~79,200-117,500 cal BP for model 3.

Model 4

This model is the same as Model 3, the only difference being the addition of a U-series date for *Denisova 11* as a minimum age.

Results: The model produced an Agreement index of 111%; equal highest of all models. All posterior results are similar to Model 3, hence the addition of the U-series date does not change the resulting distributions in any significant manner. The age of Denisova 11 under Model 4 is 79,300-118,100 years. This model is shown in Figure S30. This is our favoured model.

The human fossil age estimates calculated for all models are shown in Table S15 for comparison. When we compare the branch shortening age estimates for the nuclear data from *Denisova 3* and *Denisova 5* (Table S5) determined using transversion polymorphisms only and assuming a divergence time to the common ancestor of humans and chimpanzee of 13 million years, with our age estimates (Table S15), we observe that Models 3 and 4 are in closest agreement.

Table S15. Comparisons of age estimates (in thousand years ago) returned for each of the Bayesian models we describe above. The agreement index of each model is shown in the second row. All ranges are at 95.4% probability. The age for Denisova 14 is not modelled, it is the result of the direct AMS date on it.

	Model 1 (ka)	**Model 2 (ka)**	**Model 3 (ka)**	**Model 4 (ka)**
Model agreement index %	*23.3*	*82.3*	*111*	*111*
Denisova 14	45.9–50	45.9–50	45.9–50	45.9–50
Denisova 11	121.8–142.5	115.7–140.9	79.2–117.5	79.3–118.1
Denisova 5	96.4–134.8	92.8–132.0	91.0–129.8	90.9–130.0
Denisova 15	97.9–134.9	94.0–132.1	91.5–130.1	91.4–130.3
Denisova 3	51.7–75.1	51.9–70.3	51.6–76.9	51.6–76.2
Denisova 4	56.2–88.1	55.7–81.2	55.4–84.9	55.2–84.1
Denisova 8	114.5–138.6	107.2–136.4	105.7–136.3	105.6–136.4
Denisova 2	189.9–241.7	129.5–204.5	122.8–194.4	122.7–194.4

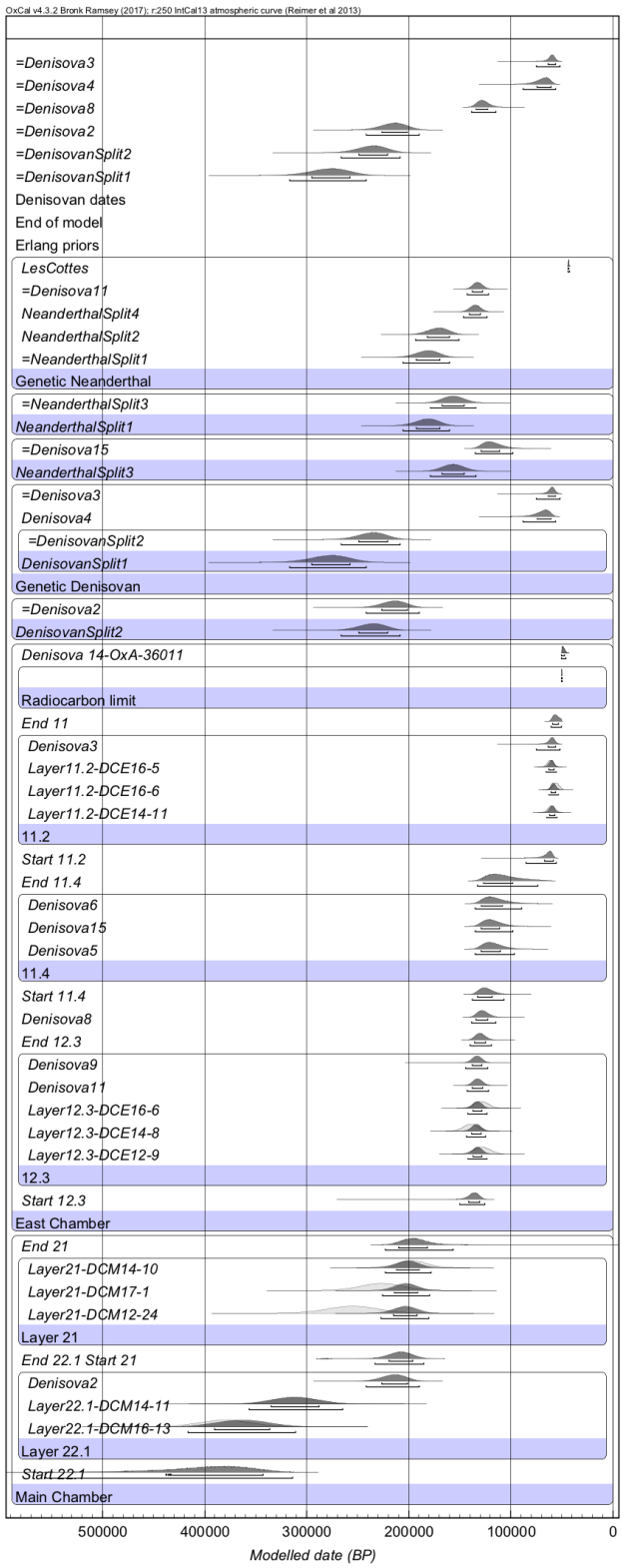

Figure S27. Bayesian age Model 1. Note the young age for *Denisova 2* compared with the optical ages in the same context.

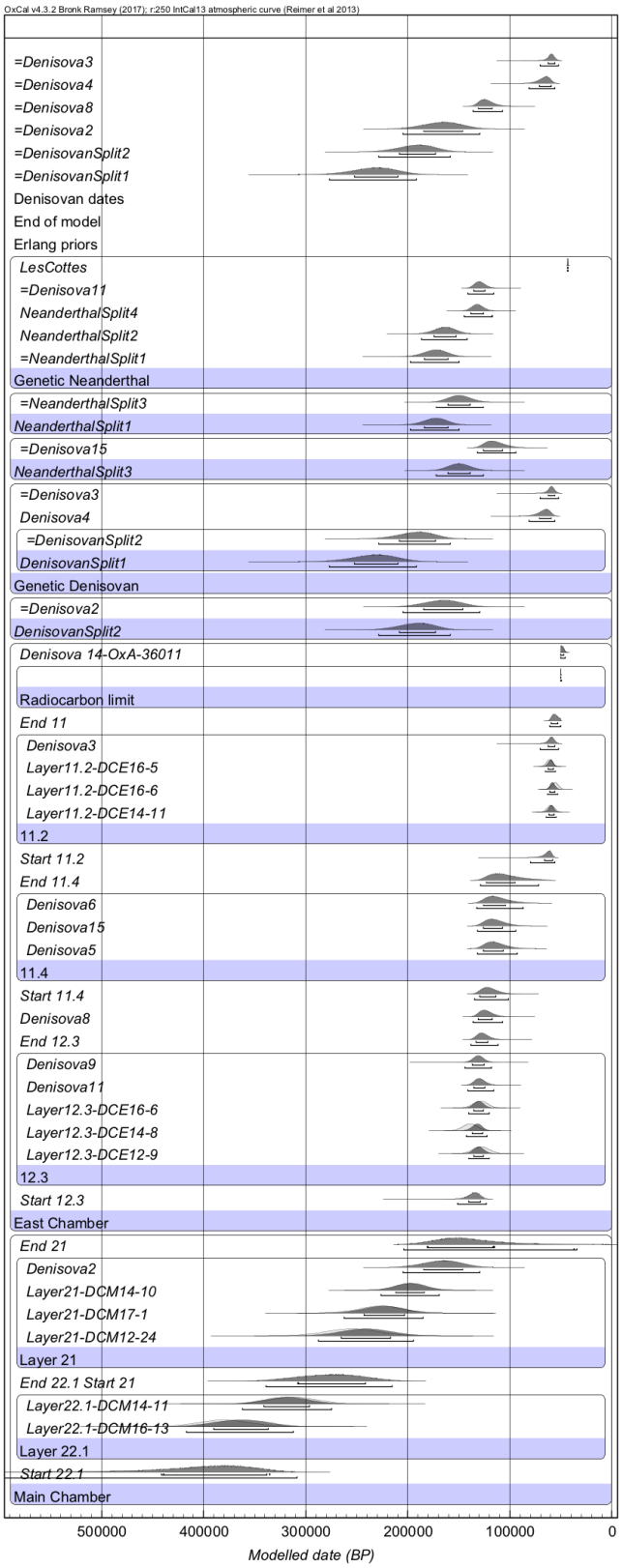

Figure S28. Bayesian age Model 2.

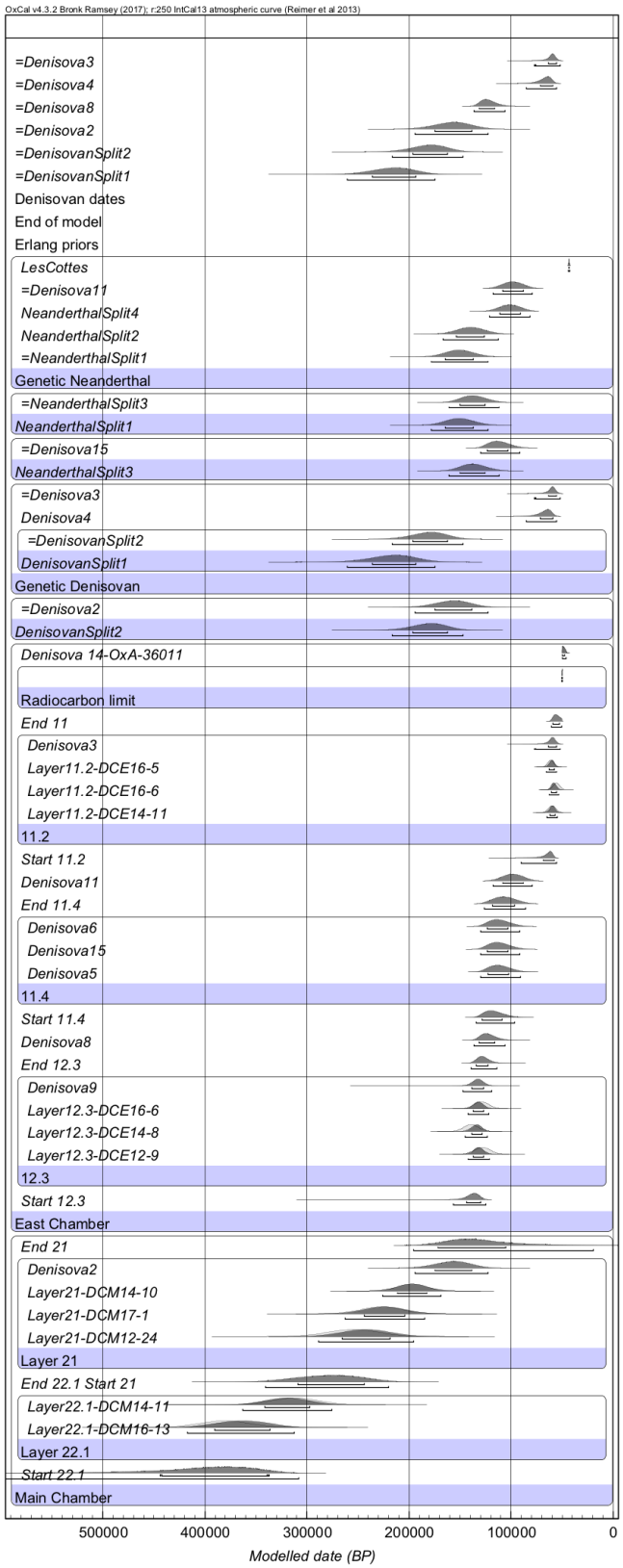

Figure S29. Bayesian age Model 3. In this model *Denisova 11* is moved to be later than the age for *Denisova 6, 15* and *5* in Layer 11.4.

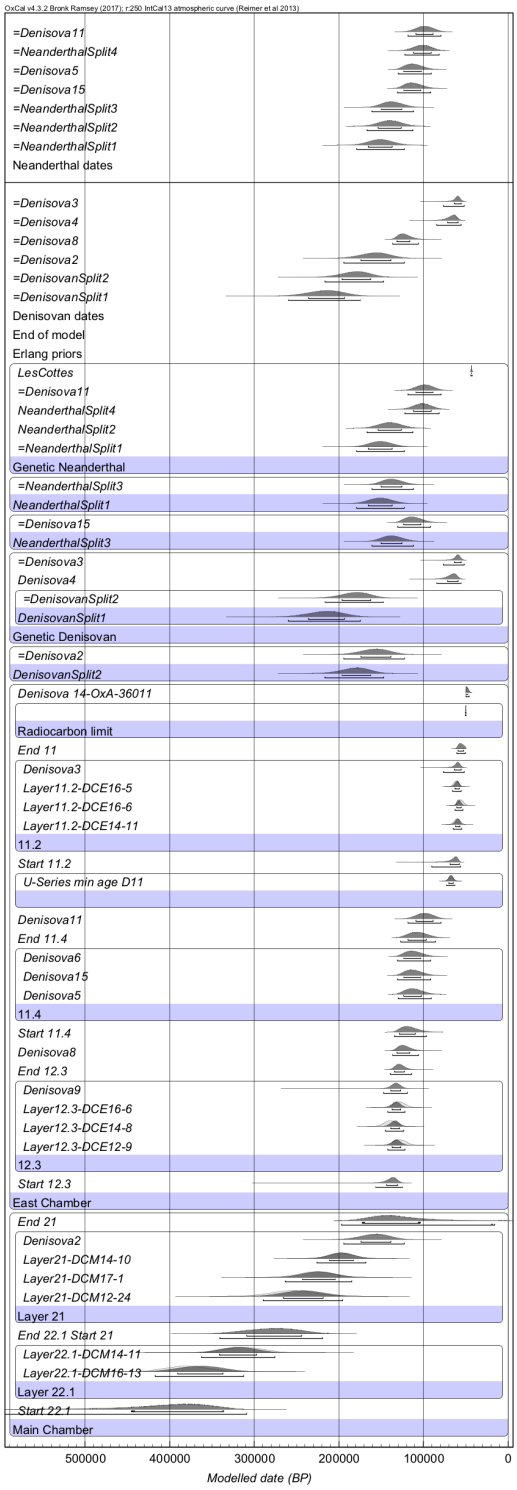

Figure S30. Bayesian age Model 4. In this model we added the Uranium series minimum age to *Denisova 11*.

CQL model code for the Bayesian models described above.

Model 1

```
Options()
 {
  Resolution=250;
  kIterations=100;
 };
/* For mitochondrial mutation rate taken to
be in 95% range:
L to H = 1.76E-08 to 3.23E-08
Basepairs are taked to be:
B = 16569
Time for one mutation is then taken to be in
the range:
1/(BH) to 1/(BL)
We then assume a normal distribution for
this with a mean:
SubstT = (1/(BH) + 1/(BL))/2
and with a standard error of
SubstTSigma = (1/(BL) - 1/(BH))/4
The figures give SubstT = 2649 yr and
Subst_sigma = 390 yr.*/
 Plot()
 {
  // substitution time
  ST=N(2649, 390);
  // site sequences
  Sequence("Main Chamber")
  {
   Boundary("Start 22.1");
   Phase("Layer 22.1")
   {
    Date("Layer22.1-DCM16-
13",N(calBP(380300),25500));
    Date("Layer22.1-DCM14-
11",N(calBP(312000),23500));
    Date("Denisova2");
   };
   Boundary("End 22.1 Start 21");
   Phase("Layer 21")
   {
    Date("Layer21-DCM12-
24",N(calBP(254600),25200));
    Date("Layer21-DCM17-
1",N(calBP(226600),20500));
    Date("Layer21-DCM14-
10",N(calBP(196900),14600));
   };
   Boundary("End 21");
  };
  // site sequences
  Sequence("East Chamber")
  {
   Boundary("Start 12.3");
   Phase("12.3")
   {
    Date("Layer12.3-DCE12-
9",N(calBP(128200),7600));
    Date("Layer12.3-DCE14-
8",N(calBP(139000),7300));
    Date("Layer12.3-DCE16-
6",N(calBP(129000),7100));
    Date("Denisova11");
    Date("Denisova9");
   };
   Boundary("End 12.3");
   Date("Denisova8")
   {
   };
   Boundary("Start 11.4");
   Phase("11.4")
   {
```

```
   Date("Denisova5");
   Date("Denisova15");
   Date("Denisova6");
  };
  Boundary("End 11.4");
  Boundary("Start 11.2");
  Phase("11.2")
  {
   Date("Layer11.2-DCE14-
11",N(calBP(59900),3400));
   Date("Layer11.2-DCE16-
6",N(calBP(55700),3100));
   Date("Layer11.2-DCE16-
5",N(calBP(61100),2900));
   Date("Denisova3");
  };
  Boundary("End 11");
  Before("Radiocarbon limit")
  {
   Date(N(calBP(50000),100,10));
  };
  R_F14C("Denisova 14-OxA-36011",
0.00313, 0.00101);
 };
 // genetic tree for Denisovans
 Date("DenisovanSplit2",Denisova2-
ST*Prior("Erl9"));
 Sequence("Genetic Denisovan")
 {
  Date("DenisovanSplit1",DenisovanSplit2-
ST*Prior("Erl13_5"));
  Interval("DS1_to_4");
  Date("Denisova4");
  Interval("DS4_to_3");
  Date("=Denisova3");
 };

Difference("DS2_to_8","Denisova8","Denis
ovanSplit2");
 // genetic tree for Neanderthals
 Date("NeanderthalSplit3",Denisova15-
ST*Prior("Erl9"));

Date("NeanderthalSplit1",NeanderthalSplit
3-ST*Prior("Erl5"));
 Sequence("Genetic Neanderthal")
 {
  Date("=NeanderthalSplit1");
  Interval("NS1_to_NS2");
  Date("NeanderthalSplit2");
  Interval("NS2_to_NS4");
  Date("NeanderthalSplit4");
  Interval("NS4_to_11");
  Date("=Denisova11");
  Interval("NS11_to_LesC");
  Date("LesCottes",N(calBP(43230),255));
 };

Difference("NS3_to_5","Denisova5","Neand
erthalSplit3");
 Label("Erlang priors");
 s1=DS1_to_4/ST;
 Prior("=s1","Erl49_5");
 s2= DS4_to_3/ST;
 Prior("=s2","Erl2");
 s3= DS2_to_8/ST;
 Prior("=s3","Erl20");
 s4= NS1_to_NS2/ST;
 Prior("=s4","Erl4");
 s5= NS2_to_NS4/ST;
 Prior("=s5","Erl14");
 s6= NS4_to_11/ST;
 Prior("=s6","Erl1");
 s7= NS3_to_5/ST;
 Prior("=s7","Erl10");
 s8= NS11_to_LesC/ST;
 Prior("=s8","Erl25");
 Label("End of model");
```

```
 Page();
 Label("Denisovan dates");
 Plot()
 {
  Date("=DenisovanSplit1");
  Date("=DenisovanSplit2");
  Date("=Denisova2");
  Date("=Denisova8");
  Date("=Denisova4");
  Date("=Denisova3");
 };
 Line();
 Label("Neanderthal dates");
 Plot()
 {
  Date("=NeanderthalSplit1");
  Date("=NeanderthalSplit2");
  Date("=NeanderthalSplit3");
  Date("=Denisova15");
  Date("=Denisova5");
  Date("=NeanderthalSplit4");
  Date("=Denisova11");
 };
};
```

Model 2

```
Options()
 {
  Resolution=250;
  kIterations=100;
 };
/* For mitochondrial mutation rate taken to be in 95% range:
L to H = 1.76E-08 to 3.23E-08
Basepairs are taked to be:
B = 16569
Time for one mutation is then taken to be in the range:
1/(BH) to 1/(BL)
We then assume a normal distribution for this with a mean:
SubstT = (1/(BH) + 1/(BL))/2
and with a standard error of
SubstTSigma = (1/(BL) - 1/(BH))/4
The figures give SubstT = 2649 yr and Subst_sigma = 390 yr.*/
 Plot()
 {
  // substitution time
  ST=N(2649, 390);
  Sequence("Main Chamber")
  {
   Boundary("Start 22.1");
   Phase("Layer 22.1")
   {
    Date("Layer22.1-DCM16-13",N(calBP(380300),25500));
    Date("Layer22.1-DCM14-11",N(calBP(312000),23500));
    //   Date("Denisova2");
   };
   Boundary("End 22.1 Start 21");
   Phase("Layer 21")
   {
    Date("Layer21-DCM12-24",N(calBP(254600),25200));
    Date("Layer21-DCM17-1",N(calBP(226600),20500));
    Date("Layer21-DCM14-10",N(calBP(196900),14600));
    Date("Denisova2");
   };
```

```
  Boundary("End 21");
 };
 // site sequences
 Sequence("East Chamber")
 {
  Boundary("Start 12.3");
  Phase("12.3")
  {
   Date("Layer12.3-DCE12-
9",N(calBP(128200),7600));
   Date("Layer12.3-DCE14-
8",N(calBP(139000),7300));
   Date("Layer12.3-DCE16-
6",N(calBP(129000),7100));
   Date("Denisova11");
   Date("Denisova9");
  };
  Boundary("End 12.3");
  Date("Denisova8")
  {
  };
  Boundary("Start 11.4");
  Phase("11.4")
  {
   Date("Denisova5");
   Date("Denisova15");
   Date("Denisova6");
  };
  //Replaced Nuclear age estimate for D 3
with the meaned OSL date from layer 11.2
  Boundary("End 11.4");
  Boundary("Start 11.2");
  Phase("11.2")
  {
   Date("Layer11.2-DCE14-
11",N(calBP(59900),3400));
   Date("Layer11.2-DCE16-
6",N(calBP(55700),3100));
   Date("Layer11.2-DCE16-
5",N(calBP(61100),2900));
   Date("Denisova3");
  };
  Boundary("End 11");
  Before("Radiocarbon limit")
  {
   Date(N(calBP(50000),100,10));
  };
  R_F14C("Denisova14-OxA-36011",
0.00313, 0.00101);
 };
 // genetic tree for Denisovans
 Date("DenisovanSplit2",Denisova2-
ST*Prior("Erl9"));
 Sequence("Genetic Denisovan")
 {
  Date("DenisovanSplit1",DenisovanSplit2-
ST*Prior("Erl13_5"));
  Interval("DS1_to_4");
  Date("Denisova4");
  Interval("DS4_to_3");
  Date("=Denisova3");
 };

Difference("DS2_to_8","Denisova8","Denis
ovanSplit2");
 // genetic tree for Neanderthals
 Date("NeanderthalSplit3",Denisova15-
ST*Prior("Erl9"));

Date("NeanderthalSplit1",NeanderthalSplit
3-ST*Prior("Erl5"));
 Sequence("Genetic Neanderthal")
 {
  Date("=NeanderthalSplit1");
  Interval("NS1_to_NS2");
  Date("NeanderthalSplit2");
  Interval("NS2_to_NS4");
```

```
  Date("NeanderthalSplit4");
  Interval("NS4_to_11");
  Date("=Denisova11");
  Interval("NS11_to_LesC");
  Date("LesCottes",N(calBP(43230),255));
 };

Difference("NS3_to_5","Denisova5","Neand
erthalSplit3");
 Label("Erlang priors");
 s1=DS1_to_4/ST;
 Prior("=s1","Erl49_5");
 s2= DS4_to_3/ST;
 Prior("=s2","Erl2");
 s3= DS2_to_8/ST;
 Prior("=s3","Erl20");
 s4= NS1_to_NS2/ST;
 Prior("=s4","Erl4");
 s5= NS2_to_NS4/ST;
 Prior("=s5","Erl14");
 s6= NS4_to_11/ST;
 Prior("=s6","Erl1");
 s7= NS3_to_5/ST;
 Prior("=s7","Erl10");
 s8= NS11_to_LesC/ST;
 Prior("=s8","Erl25");
 Label("End of model");
 Page();
 Label("Denisovan dates");
 Plot()
 {
  Date("=DenisovanSplit1");
  Date("=DenisovanSplit2");
  Date("=Denisova2");
  Date("=Denisova8");
  Date("=Denisova4");
  Date("=Denisova3");
 };
 Line();
 Label("Neanderthal dates");
 Plot()
 {
  Date("=NeanderthalSplit1");
  Date("=NeanderthalSplit2");
  Date("=NeanderthalSplit3");
  Date("=Denisova15");
  Date("=Denisova5");
  Date("=NeanderthalSplit4");
  Date("=Denisova11");
 };
};
```

Model 3

```
Options()
 {
  Resolution=250;
  kIterations=100;
 };
/* For mitochondrial mutation rate taken to
        be in 95% range:
L to H = 1.76E-08 to 3.23E-08
Basepairs are taked to be:
B = 16569
Time for one mutation is then taken to be in
        the range:
1/(BH) to 1/(BL)
We then assume a normal distribution for
        this with a mean:
SubstT = (1/(BH) + 1/(BL))/2
and with a standard error of
SubstTSigma = (1/(BL) - 1/(BH))/4
```

```
The figures give SubstT = 2649 yr and
        Subst_sigma = 390 yr.*/
 Plot()
 {
  // substitution time
  ST=N(2649, 390);
  // site sequences
  Sequence("Main Chamber")
  {
   Boundary("Start 22.1");
   Phase("Layer 22.1")
   {
    Date("Layer22.1-DCM16-
        13",N(calBP(380300),25500));
    Date("Layer22.1-DCM14-
        11",N(calBP(312000),23500));
   };
   Boundary("End 22.1 Start 21");
   Phase("Layer 21")
   {
    Date("Layer21-DCM12-
        24",N(calBP(254600),25200));
    Date("Layer21-DCM17-
        1",N(calBP(226600),20500));
    Date("Layer21-DCM14-
        10",N(calBP(196900),14600));
    Date("Denisova2");
   };
   Boundary("End 21");
  };
  Sequence("East Chamber")
  {
   Boundary("Start 12.3");
   Phase("12.3")
   {
    Date("Layer12.3-DCE12-
        9",N(calBP(128200),7600));
    Date("Layer12.3-DCE14-
        8",N(calBP(139000),7300));
    Date("Layer12.3-DCE16-
        6",N(calBP(129000),7100));
    Date("Denisova9");
   };
   Boundary("End 12.3");
   Date("Denisova8")
   {
   };
   Boundary("Start 11.4");
   Phase("11.4")
   {
    Date("Denisova5");
    Date("Denisova15");
    Date("Denisova6");
   };
   Boundary("End 11.4");
   Date("Denisova11");
   Boundary("Start 11.2");
   Phase("11.2")
   {
    Date("Layer11.2-DCE14-
        11",N(calBP(59900),3400));
    Date("Layer11.2-DCE16-
        6",N(calBP(55700),3100));
    Date("Layer11.2-DCE16-
        5",N(calBP(61100),2900));
    Date("Denisova3");
   };
   Boundary("End 11");
   Before("Radiocarbon limit")
   {
    Date(N(calBP(50000),100,10));
   };
   R_F14C("Denisova          14-OxA-36011",
        0.00313, 0.00101);
  };
  // genetic tree for Denisovans
  Date("DenisovanSplit2",Denisova2-
        ST*Prior("Erl9"));
```

```
Sequence("Genetic Denisovan")
{
 Date("DenisovanSplit1",DenisovanSplit2-
        ST*Prior("Erl13_5"));
 Interval("DS1_to_4");
 Date("Denisova4");
 Interval("DS4_to_3");
 Date("=Denisova3");
};

        Difference("DS2_to_8","Denisova8",
        "DenisovanSplit2");
// genetic tree for Neanderthals
Date("NeanderthalSplit3",Denisova15-
        ST*Prior("Erl9"));

        Date("NeanderthalSplit1",Neandert
        halSplit3-ST*Prior("Erl5"));
Sequence("Genetic Neanderthal")
{
 Date("=NeanderthalSplit1");
 Interval("NS1_to_NS2");
 Date("NeanderthalSplit2");
 Interval("NS2_to_NS4");
 Date("NeanderthalSplit4");
 Interval("NS4_to_11");
 Date("=Denisova11");
 Interval("NS11_to_LesC");
 Date("LesCottes",N(calBP(43230),255));
};

        Difference("NS3_to_5","Denisova5",
        "NeanderthalSplit3");
Label("Erlang priors");
s1=DS1_to_4/ST;
Prior("=s1","Erl49_5");
s2= DS4_to_3/ST;
Prior("=s2","Erl2");
s3= DS2_to_8/ST;
Prior("=s3","Erl20");
s4= NS1_to_NS2/ST;
Prior("=s4","Erl4");
s5= NS2_to_NS4/ST;
Prior("=s5","Erl14");
s6= NS4_to_11/ST;
Prior("=s6","Erl1");
s7= NS3_to_5/ST;
Prior("=s7","Erl10");
s8= NS11_to_LesC/ST;
Prior("=s8","Erl25");
Label("End of model");
Page();
Label("Denisovan dates");
Plot()
{
 Date("=DenisovanSplit1");
 Date("=DenisovanSplit2");
 Date("=Denisova2");
 Date("=Denisova8");
 Date("=Denisova4");
 Date("=Denisova3");
};
Line();
Label("Neanderthal dates");
Plot()
{
 Date("=NeanderthalSplit1");
 Date("=NeanderthalSplit2");
 Date("=NeanderthalSplit3");
 Date("=Denisova15");
 Date("=Denisova5");
 Date("=NeanderthalSplit4");
 Date("=Denisova11");
};
};
```

Model 4

```
Options()
 {
  Resolution=250;
  kIterations=100;
 };
/* For mitochondrial mutation rate taken to be in 95% range:
L to H = 1.76E-08 to 3.23E-08
Basepairs are taked to be:
B = 16569
Time for one mutation is then taken to be in the range:
1/(BH) to 1/(BL)
We then assume a normal distribution for this with a mean:
SubstT = (1/(BH) + 1/(BL))/2
and with a standard error of
SubstTSigma = (1/(BL) - 1/(BH))/4
The figures give SubstT = 2649 yr and Subst_sigma = 390 yr.*/
 Plot()
 {
  // substitution time
  ST=N(2649, 390);
  // site sequences
  Sequence("Main Chamber")
  {
   Boundary("Start 22.1");
   Phase("Layer 22.1")
   {
    Date("Layer22.1-DCM16-13",N(calBP(380300),25500));
    Date("Layer22.1-DCM14-11",N(calBP(312000),23500));
    //   Date("Denisova2");
   };
   Boundary("End 22.1 Start 21");
   Phase("Layer 21")
   {
    Date("Layer21-DCM12-24",N(calBP(254600),25200));
    Date("Layer21-DCM17-1",N(calBP(226600),20500));
    Date("Layer21-DCM14-10",N(calBP(196900),14600));
    Date("Denisova2");
   };
   Boundary("End 21");
  };
  Sequence("East Chamber")
  {
   Boundary("Start 12.3");
   Phase("12.3")
   {
    Date("Layer12.3-DCE12-9",N(calBP(128200),7600));
    Date("Layer12.3-DCE14-8",N(calBP(139000),7300));
    Date("Layer12.3-DCE16-6",N(calBP(129000),7100));
    Date("Denisova9");
   };
   Boundary("End 12.3");
   Date("Denisova8")
   {
   };
   Boundary("Start 11.4");
   Phase("11.4")
   {
    Date("Denisova5");
    Date("Denisova15");
    Date("Denisova6");
   };
```

```
  Boundary("End 11.4");
  Date("Denisova11");
  Before()
  {
   Date("U-Series min age
D11",N(calBP(67500),2500));
  };
  Boundary("Start 11.2");
  Phase("11.2")
  {
   Date("Layer11.2-DCE14-
11",N(calBP(59900),3400));
   Date("Layer11.2-DCE16-
6",N(calBP(55700),3100));
   Date("Layer11.2-DCE16-
5",N(calBP(61100),2900));
   Date("Denisova3");
  };
  Boundary("End 11");
  Before("Radiocarbon limit")
  {
   Date(N(calBP(50000),100,10));
  };
  R_F14C("Denisova 14-OxA-36011",
0.00313, 0.00101);
 };
 // genetic tree for Denisovans
 Date("DenisovanSplit2",Denisova2-
ST*Prior("Erl9"));
 Sequence("Genetic Denisovan")
 {
  Date("DenisovanSplit1",DenisovanSplit2-
ST*Prior("Erl13_5"));
  Interval("DS1_to_4");
  Date("Denisova4");
  Interval("DS4_to_3");
  Date("=Denisova3");
 };

Difference("DS2_to_8","Denisova8","Denis
ovanSplit2");
 // genetic tree for Neanderthals
 Date("NeanderthalSplit3",Denisova15-
ST*Prior("Erl9"));

Date("NeanderthalSplit1",NeanderthalSplit
3-ST*Prior("Erl5"));
 Sequence("Genetic Neanderthal")
 {
  Date("=NeanderthalSplit1");
  Interval("NS1_to_NS2");
  Date("NeanderthalSplit2");
  Interval("NS2_to_NS4");
  Date("NeanderthalSplit4");
  Interval("NS4_to_11");
  Date("=Denisova11");
  Interval("NS11_to_LesC");
  Date("LesCottes",N(calBP(43230),255));
 };

Difference("NS3_to_5","Denisova5","Neand
erthalSplit3");
 Label("Erlang priors");
 s1=DS1_to_4/ST;
 Prior("=s1","Erl49_5");
 s2= DS4_to_3/ST;
 Prior("=s2","Erl2");
 s3= DS2_to_8/ST;
 Prior("=s3","Erl20");
 s4= NS1_to_NS2/ST;
 Prior("=s4","Erl4");
 s5= NS2_to_NS4/ST;
 Prior("=s5","Erl14");
 s6= NS4_to_11/ST;
 Prior("=s6","Erl1");
 s7= NS3_to_5/ST;
 Prior("=s7","Erl10");
 s8= NS11_to_LesC/ST;
```

```
 Prior("=s8","Erl25");
 Label("End of model");
 Page();
 Label("Denisovan dates");
 Plot()
 {
  Date("=DenisovanSplit1");
  Date("=DenisovanSplit2");
  Date("=Denisova2");
  Date("=Denisova8");
  Date("=Denisova4");
  Date("=Denisova3");
 };
 Line();
 Label("Neanderthal dates");
 Plot()
 {
  Date("=NeanderthalSplit1");
  Date("=NeanderthalSplit2");
  Date("=NeanderthalSplit3");
  Date("=Denisova15");
  Date("=Denisova5");
  Date("=NeanderthalSplit4");
  Date("=Denisova11");
 };
};
```

Erlang model

```
Plot()
 {
  P(Erl49_5, 0.1, 200, exp(48.5*ln(Erl49_5)-Erl49_5), 0.1);
  P(Erl25, 0.1, 200, exp(24*ln(Erl25)-Erl25), 0.1);
  P(Erl20, 0.1, 200, exp(19*ln(Erl20)-Erl20), 0.1);
  P(Erl14, 0.1, 200, exp(13*ln(Erl14)-Erl14), 0.1);
  P(Erl13_5, 0.1, 200, exp(12.5*ln(Erl13_5)-Erl13_5), 0.1);
  P(Erl10, 0.1, 200, exp(9*ln(Erl10)-Erl10), 0.1);
  P(Erl9, 0.1, 200, exp(8*ln(Erl9)-Erl9), 0.1);
  P(Erl5, 0.1, 200, exp(4*ln(Erl5)-Erl5), 0.1);
  P(Erl4, 0.1, 200, exp(3*ln(Erl4)-Erl4), 0.1);
  P(Erl2, 0.1, 200, exp(1*ln(Erl2)-Erl2), 0.1);
  P(Erl1, 0, 20, exp(-Erl1), 0.01);
 };
```

SUPPLEMENTARY REFERENCES

1 Derevianko, A. P., Shunkov, M. V., Agadzhanyan, A. K., Baryshnikov, G. F., Malaeva, E. M., Ulianov, V. A., Kulik, N. A., Postnov, A. V., Anoikin, A. A. *Prirodnaya sreda i chelovek v paleolite Gornogo Altaya*. Novosibirsk: IAET SB RAS. 448 p. (in Russian) (2003).

2 Okladnikov, A. P. & Ovodov, N. D. Paleoliticheskaya stoyanka v Denisovoi peshchere na Altae. *Archaeological discoveries 1977*. Moskow: Nauka Publ., pp. 266–268. (in Russian) (1978).

3 Derevianko, A. P. & Molodin, V. I. *Denisova peshchera*. Novosibirsk: Nauka Publ. Part 1. 262 p. (in Russian) (1994).

4 Ulianov, V. A., Kozlikin, M. B., Belousova, N. E., Shunkov, M. V. Stroenie pleistotsenovykh otlozhenii v tsentral'nom zale Denisovoi peshchery. *Problems of Archaeology, Ethnography, Anthropology of Siberia and Neighboring Territories*. Novosibirsk: IAET SB RAS. pp. 169–172. (in Russian) (2016).

5 Ulianov, V. A. & Shunkov, M. V. Nekotorye osobennosti sedimentogeneza v vostochnoi galeree Denisovoi peshchery. *Problems of Archaeology, Ethnography, Anthropology of Siberia and Neighboring Territories*. Novosibirsk: IAET SB RAS. pp. 159–162. (in Russian) (2013).

6 Ulianov, V. A., Kozlikin, M. B., Shunkov, M. V. Stroenie razreza pleistotsenovykh otlozhenii v vostochnoi galeree Denisovoi peshchery (po dannym raskopok 2015 goda). *Problems of Archaeology, Ethnography, Anthropology of Siberia and Neighboring Territories*. Novosibirsk: IAET SB RAS. pp. 157–160. (in Russian) (2015).

7 Derevianko, A. P. & Shunkov, M. V. Middle Palaeolithic industries with foliate bifaces in Altai Mountains. *Archaeology, Ethnology and Anthropology of Eurasia* **1**, 16–42 (2002).

8 Derevianko, A. P. & Shunkov, M. V. Formation of the Upper Palaeolithic Traditions in the Altai. *Archaeol. Ethnol. Anthropol. Eurasia* **3**, 12–40 (2004).

9 Reich, D., et al. Genetic history of an archaic hominin group from Denisova Cave in Siberia. *Nature* **468**(7327), 1053–1960 (2010).

10 Viola, B. T, Markin, S. V., Buzhilova, A. P., Mednikova, M. B., Dobrovolskaya, M. V., Le Cabec, A., Shunkov, M. V., Derevianko, A. P., Hublin, J.-J. New Neanderthal remains from Chagyrskaya Cave (Altai Mountains, Russian Federation). *American Journal of Physical Anthropology* **147**(Suppl. 54), 293–294 (2012).

11 Derevianko, A. P., Shunkov, M. V. & Markin S. V. *The dynamics of the Palaeolithic industries in Africa and Eurasia in the Late Pleistocene and the issue of the* Homo sapiens *origin*. Novosibirsk: IAET SB RAS. 228 p. (2014).

12 Slon, V., et al. A fourth Denisovan individual. *Sci. Advances* **3**(7), p. e1700186 (2017).

13 Slon, V. et al. Neandertal and Denisovan DNA from Pleistocene sediments. *Science* **356**, 605–608 (2017).

14 Fu, Q., et al. Genome sequence of a 45,000-year-old modern human from western Siberia. *Nature* **514** (7523), 445–449 (2014).

15 Brock, F., Higham, T. F. G, Ditchfield, P., Ramsey, C. B. Current Pretreatment Methods for AMS Radiocarbon Dating at the Oxford Radiocarbon Accelerator Unit (ORAU). *Radiocarbon* **52**, 103–112 (2010).

16 Devièse, T., Comeskey, D., McCullagh, J., Ramsey,. C B., Higham, T. New protocol for compound specific radiocarbon analysis of archaeological bones. *Rapid Communications in Mass Spectrometry* **32**, 373-379 (2018).

17 Bird, M. I. *et al.* Radiocarbon Dating of 'Old' Charcoal Using a Wet Oxidation, Stepped-Combustion Procedure. *Radiocarbon* **41**, 127–140 (1999).
18 Ramsey, C. OxCal 4.2 Web Interface Build(78) (2013).
19 Reimer, P. J. *et al.* IntCal13 and Marine13 Radiocarbon Age Calibration Curves 0–50,000 Years cal BP. *Radiocarbon* **55**, 1869–1887 (2013).
20 Turner, C. G. in *Chronostratigraphy of the Palaeolithic in North, Central, East Asia and America*, A. P. Derevianko, Eds. (Novosibirsk: Institute of History, Philology and Philosophy, Siberian Branch of the USSR Academy of Sciences), pp. 239-243 (1990).
21 Shpakova, E. G. & Derevianko, A. P. The interpretation of odontological features of Pleistocene human remains from the Altai. *Archaeol. Ethnol. Anthropol. Eurasia* **1**, 125–138 (2000).
22 Shpakova, E. G. Paleolithic human dental remains from Siberia. *Archaeol. Ethnol. Anthropol. Eurasia* **4** (8), 64–76 (2001).
23 Bailey, S. Beyond shovel-shaped incisors: Neandertal morphology in a comparative context. *Periodicum Biologorum* **108** (3), 253–267 (2006).
24 Krause, J., et al. The complete mitochondrial DNA genome of an unknown hominin from southern Siberia*. Nature* **464**(7290), 894–897 (2010).
25 Meyer, M., et al. A high-coverage genome sequence from an archaic Denisovan individual. *Science* **338**(6104), 222–226 (2012).
26 Sawyer, S., et al. Nuclear and mitochondrial DNA sequences from two Denisovan individuals. *Proc. Natl. Acad. Sci. USA* **112**(51), 15696–15700 (2015).
27 Mednikova, M. B. A. Proximal pedal phalanx of a Paleolithic hominin from Denisova Cave, Altai. *Archaeol. Ethnol. Anthropol. Eurasia* **39**, 129–138 (2011).
28 Prüfer, K., et al. The complete genome sequence of a Neanderthal from the Altai Mountains. *Nature* **505**(7481), 43–49 (2014).
29 Mednikova, M. Distal Phalanx of the Hand of Homo from Denisova Cave Stratum 12: A Tentative Description. *Archaeol. Ethnol. Anthropol. Eurasia* **41**, 146–155 (2013).
30 Brown, S. et al. Identification of a new hominin bone from Denisova Cave, Siberia using collagen fingerprinting and mitochondrial DNA analysis. *Scientific Reports* **6**, doi:10.1038/srep23559 (2016).
31 Prüfer, K., et al. A high-coverage Neandertal genome from Vindija Cave in Croatia*. Science* **358**(6363), 655–658 (2017).
32 Narasimhan, V.M, et al. Estimating the human mutation rate from autozygous segments reveals population differences in human mutational processes. *Nature Communications* **8** (1), 303 (2017).
33 Scally, A. & Durbin, R. Revising the human mutation rate: implications for understanding human evolution. *Nature Reviews Genetics* **13**, 745–753 (2012).
34 Slon, V., et al. The genome of the offspring of a Neandertal mother and a Denisovan father. *Nature* **561**, 113–116 (2018).
35 Dabney, J., et al. Complete mitochondrial genome sequence of a Middle Pleistocene cave bear reconstructed from ultrashort DNA fragments. *Proc Natl Acad Sci USA* **110**(39), 15758–15763 (2013).
36 Korlević, P., et al. Reducing microbial and human contamination in DNA extractions from ancient bones and teeth*. Biotechniques* **59**(2), 87–93 (2015).

37 Gansauge, M.T., et al. Single-stranded DNA library preparation from highly degraded DNA using T4 DNA ligase. *Nucleic Acids Res.* **45**(10): e79 (2017).
38 Kircher, M., S. Sawyer, and M. Meyer. Double indexing overcomes inaccuracies in multiplex sequencing on the Illumina platform. *Nucleic Acids Res.* 40(1): e3 (2012).
39 Fu, Q., et al., DNA analysis of an early modern human from Tianyuan Cave, China. *Proc Natl Acad Sci USA* **110**(6), 2223–2227 (2013).
40 Renaud, G., Stenzel, U. & Kelso, J. leeHom: adaptor trimming and merging for Illumina sequencing reads. *Nucleic Acids Res*. **42**(18), 141 (2014).
41 Li, H. & Durbin, R. Fast and accurate long-read alignment with Burrows-Wheeler transform. *Bioinformatics* **26**(5), 589–595 (2010).
42 Briggs, A.W., et al. Patterns of damage in genomic DNA sequences from a Neandertal. *Proc Natl Acad Sci USA* **104**(37), 14616–14621 (2007).
43 Huson, D. H., et al. MEGAN analysis of metagenomic data. *Genome Res*. **17**(3), 377–386 (2007).
44 Slon, V., et al. Mammalian mitochondrial capture, a tool for rapid screening of DNA preservation in faunal and undiagnostic remains, and its application to Middle Pleistocene specimens from Qesem Cave (Israel). *Quaternary International* **398**, 210–218 (2016).
45 Prüfer, K. & Meyer, M. Comment on "Late Pleistocene human skeleton and mtDNA link Paleoamericans and modern Native Americans". *Science* **347**(6224), 835 (2015).
46 Meyer, M., et al. A mitochondrial genome sequence of a hominin from Sima de los Huesos. *Nature* **505**(7483), 403-406 (2014).
47 Green, R. E., et al. A complete Neandertal mitochondrial genome sequence determined by high-throughput sequencing. *Cell* **134**(3), 416–426 (2008).
48 Li, H., et al. The Sequence Alignment/Map format and SAMtools. *Bioinformatics* 25(16), 2078–2079 (2009).
49 Li, M. K., et al. Detecting Heteroplasmy from high-throughput sequencing of complete human mitochondrial DNA genomes. *American Journal of Human Genetics* **87**(2), 237–249 (2010).
50 Tamura, K., et al. MEGA6: Molecular Evolutionary Genetics Analysis version 6.0. *Mol Biol Evol*. 30(12), 2725–2729 (2013).
51 Katoh, K. & Standley, D. M. MAFFT multiple sequence alignment software version 7: improvements in performance and usability. *Mol Biol Evol* **30**(4), 772–780 (2013).
52 Schliep, K.P. phangorn: phylogenetic analysis in R. *Bioinformatics* **27**(4), 592–593 (2011).
53 Posth, C., et al. Deeply divergent archaic mitochondrial genome provides lower time boundary for African gene flow into Neanderthals. *Nature Communications* **8**, 16046 (2017).
54 Drummond, A. J. et al. Bayesian Phylogenetics with BEAUti and the BEAST 1.7. *Molecular Biology and Evolution* **29**(8), 1969–1973 (2012).
55 Fu, Q., et al. A revised timescale for human evolution based on ancient mitochondrial genomes. *Curr Biol* **23**(7), 553–559 (2013).
56 Tamura, K. & Nei, M. Estimation of the number of nucleotide substitutions in the control region of mitochondrial DNA in humans and chimpanzees. *Mol Biol Evol* **10**(3), 512–526 (1993).
57 Darriba, D., et al. jModelTest 2: more models, new heuristics and parallel computing. *Nat Methods* **9**(8), 772 (2012).

58 Kass, R. E. & Raftery, A. E. Bayes Factors. *Journal of the American Statistical Association* **90**(430), 773–795 (1995).
59 Bronk Ramsey, C. Methods for Summarizing Radiocarbon Datasets. *Radiocarbon* **59**(6), 1809–1833 (2017).
60 Ermini, L., et al., Complete mitochondrial genome sequence of the Tyrolean Iceman. Curr Biol, 18(21): p. 1687–1693 (2008).
61 Hedges, R.E.M., et al. Radiocarbon-Dates from the Oxford AMS System. Archaeometry Datelist 15. *Archaeometry* **34**, 337–357 (1992).
62 Krause, J., et al., A Complete mtDNA Genome of an Early Modern Human from Kostenki, Russia. *Current Biology* **20**(3): 231–236 (2010).
63 Marom, A., et al., Single amino acid radiocarbon dating of Upper Paleolithic modern humans. *Proceedings of the National Academy of Sciences of the United States of America* **109**(18): 6878–6881 (2012).
64 Delsate, D., Guinet, J. M. & Saverwyns, S. De l'ocre sur le crâne mésolithique (haplogroupe U5a) de Reuland-Loschbour (Grand-Duché de Luxembourg)? *Bull. Soc. Préhist. Luxembourgeoise* **31**, 7–30 (2009).
65 Gilbert, M. T., et al., Paleo-Eskimo mtDNA genome reveals matrilineal discontinuity in Greenland. *Science* **320**(5884), 178–179 (2008).
66 Rasmussen, M., et al., Ancient human genome sequence of an extinct Palaeo-Eskimo. Nature **463**(7282), 757–762 (2010).
67 Shang, H., et al. An early modern human from Tianyuan cave, Zhoukoudian, China. *Proceedings of the National Academy of Sciences of the USA* **104**(16), 6573–6578 (2007).
68 Briggs, A.W., et al. Targeted retrieval and analysis of five Neandertal mtDNA genomes. *Science* **325**(5938), 318–321 (2009).
69 Schmitz, R.W., et al. The Neandertal type site revisited: Interdisciplinary investigations of skeletal remains from the Neander Valley, Germany. *Proceedings of the National Academy of Sciences of the United States of America* **99**(20), 13342–13347 (2002).
70 Ingman, M., et al. Mitochondrial genome variation and the origin of modern humans. *Nature* **408**(6813), 708–713 (2000).
71 Rougier, H., et al., Neandertal cannibalism and Neandertal bones used as tools in Northern Europe. *Scientific Reports* **6** (2016).
72 Ingman, M. & Gyllensten, U. Mitochondrial genome variation and evolutionary history of Australian and New Guinean aborigines. *Genome Res* **13**(7), 1600–1606 (2003).
73 Mishmar, D., et al. Natural selection shaped regional mtDNA variation in humans. *Proc Natl Acad Sci USA* **100**(1), 171–176 (2003).
74 Maca-Meyer, N., et al. Major genomic mitochondrial lineages delineate early human expansions. *BMC Genet* **2**, 13 (2001).
75 Achilli, A., et al. Saami and Berbers-an unexpected mitochondrial DNA link. *Am J Hum Genet* **76**(5), 883–886 (2005).
76 Hajdinjak, M., et al. Reconstructing the Genetic History of Late Neandertals. *Nature* **555**, 652–656 (2018).
77 Pinhasi, R., et al. Revised age of late Neanderthal occupation and the end of the Middle Paleolithic in the northern Caucasus. *Proceedings of the National Academy of Sciences of the USA* **108**(21), 8611-8616 (2011).

78 Skoglund, P., et al. Separating endogenous ancient DNA from modern day contamination in a Siberian Neandertal. *Proc Natl Acad Sci USA* 111(6), 2229–2234 (2014).
79 Semal, P. et al. New Data on the Late Neandertals: Direct Dating of the Belgian Spy Fossils. *American Journal of Physical Anthropology* 138(4), 421–428 (2009).
80 Serre, D. et al. No evidence of Neandertal mtDNA contribution to early modern humans. *Plos Biology* 2(3), 313–317 (2014).
81 Gansauge, M. T. & Meyer, M. Selective enrichment of damaged DNA molecules for ancient genome sequencing. *Genome Res*. **24**(9):1543–1549 (2014).
82 Horai, S., et al. Recent African origin of modern humans revealed by complete sequences of hominoid mitochondrial DNAs. *Proc Natl Acad Sci USA* **92**(2), 532–536 (1995).
83 Huntley, D. J., Godfrey-Smith, D. I. & Thewalt, M. L. W. Optical dating of sediments. *Nature* **313**, 105–107 (1985).
84 Hütt, G., Jaek, I. & Tchonka, J. Optical dating: K-feldspars optical response stimulation spectra. *Quat. Sci. Rev.* **7**, 381–385 (1988).
85 Aitken, M. J. *An Introduction to Optical Dating: the dating of Quaternary sediments by the use of photon-stimulated luminescence* (Oxford Univ. Press, Oxford, 1998).
86 Jacobs, Z. & Roberts, R. G. Advances in optically stimulated luminescence dating of individual grains of quartz from archeological deposits. *Evol. Anthropol.* **16**, 210–223 (2007).
87 Wintle, A. G. in *Treatise on Geochemistry*, 2nd ed. (eds Holland, H. D. & Turekian, K. K.), **14**, 17–35 (Elsevier, Oxford, 2014).
88 Roberts, R. G. *et al.* Optical dating in archaeology: thirty years in retrospect and grand challenges for the future. *J. Archaeol. Sci.* **56**, 41–60 (2015).
89 Jacobs, Z. *et al*. Timing of archaic hominin occupation of Denisova Cave in southern Siberia. *Nature* (in press 2018).
90 Bøtter-Jensen, L. & Mejdahl, V. Assessment of beta dose-rate using a GM multicounter system. *Nucl. Tracks Radiat. Meas.* **14**, 187–191 (1988).
91 Jacobs, Z. & Roberts, R. G. An improved single grain OSL chronology for the sedimentary deposits from Diepkloof Rockshelter, Western Cape, South Africa. *J. Archaeol. Sci.* **63**, 175–192 (2015).
92 Mercier, N. & Falguères, C. Field gamma dose-rate measurement with a NaI(Tl) detector: re-evaluation of the "threshold" technique. *Anc. TL* **25**, 1–4 (2007).
93 Rhodes, E. J. & Schwenninger, J. L. Dose rates and radioisotopes in the concrete calibration blocks at Oxford. *Anc. TL* **25**, 5–8 (2007).
94 Prescott, J. R. & Hutton, J. T. Cosmic ray contributions to dose rates for luminescence and ESR dating: large depths and long-term time variations. *Radiat. Meas.* **23**, 497–500 (1994).
95 Huntley, D. J. & Hancock, R. G. V. The Rb contents of the K-feldspars being measured in optical dating. *Anc. TL* **19**, 43–46 (2001).
96 Duller, G. A. T. Single-grain optical dating of Quaternary sediments: why aliquot size matters in luminescence dating. *Boreas* **37**, 589–612 (2008).
97 Bøtter-Jensen, L., Andersen, C. E., Duller, G. A. T. & Murray, A. S. Developments in radiation, stimulation and observation facilities in luminescence measurements. *Radiat. Meas.* **37**, 535–541 (2003).

98 Galbraith, R. F., Roberts, R. G., Laslett, G. M., Yoshida, H. & Olley, J. M. Optical dating of single and multiple grains of quartz from Jinmium rock shelter, northern Australia: Part I, experimental design and statistical models. *Archaeometry* **41**, 339–364 (1999).
99 Murray, A. S. & Wintle, A. G. Luminescence dating of quartz using an improved single-aliquot regenerative-dose protocol. *Radiat. Meas.* **32**, 57–73 (2000).
100 Thomsen, K. J., Murray, A. S., Jain, M. & Bøtter-Jensen, L. Laboratory fading rates of various luminescence signals from feldspar-rich sediment extracts. *Radiat. Meas.* **43**, 1474–1486 (2008).
101 Li, B., Jacobs, Z., Roberts, R. G. & Li, S. H. Review and assessment of the potential of post-IR IRSL dating methods to circumvent the problem of anomalous fading in feldspar luminescence. *Geochronometria* **41**, 178–201 (2014).
102 Blegen, N. *et al*. Distal tephras of the eastern Lake Victoria basin, equatorial East Africa: correlations, chronology and a context for early modern humans. *Quat. Sci. Rev.* **122**, 89–111 (2015).
103 Li, B., Roberts, R. G., Jacobs, Z. & Li, S. H. Single-grain dating of potassium-rich feldspar grains: towards a global standardised growth curve for the post-IR IRSL signal. *Quat. Geochronol.* **45**, 23–36 (2018).
104 Li, B., Jacobs, Z. & Roberts, R. G. An improved multiple-aliquot regenerative-dose (MAR) procedure for post-IR IRSL dating of K-feldspar. *Anc. TL* **35**, 1–10 (2017).
105 Galbraith, R.F. & Roberts, R. G. Statistical aspects of equivalent dose and error calculation and display in OSL dating: an overview and some recommendations. *Quat. Geochronol.* **11**, 1–27 (2012).
106 Roberts, R. G., Galbraith, R. F., Yoshida, H., Laslett, G. M. & Olley, J. M. Distinguishing dose populations in sediment mixtures: a test of single-grain optical dating procedures using mixtures of laboratory-dosed quartz. *Radiat. Meas.* **32**, 459–465 (2000).
107 Powell, R., Hergt, J. & Woodhead, J. Improving isochron calculations with robust statistics and the bootstrap. *Chem. Geol.* **185**, 191–204 (2002).
108 Rousseeuw, P. J., Debruyne, M., Engelen, S. & Hubert, M. Robustness and outlier detection in chemometrics. *Crit. Rev. Anal. Chem.* **36**, 221–242 (2006).
109 Grün, R., Eggins, S., Kinsley, L., Mosely, H., Sambridge, M. Laser ablation U-series analysis of fossil bones and teeth. Palaeogeography, Palaeoclimatology, Palaeoecology **416**, 150-167 (2014).
110 Paul, D., White, W.M., & Turcotte, D.L. Constraints on the $^{232}Th/^{238}U$ ratio (k) of the continental crust. Geochem. Geophys. Geosyst., **4**(12), 1102, 1-17 (2003).
111 Buckley, M., Collins, M., Thomas-Oates, J., Wilson, J.C. Species Identification by Analysis of Bone Collagen Using Matrix-Assisted Laser Desorption/ionisation Time-of-Flight Mass Spectrometry. *Rapid Communications in Mass Spectrometry*: RCM **23** (23), 3843–54 (2009).
112 Buckley, M., & Kansa Whitcher, S. Collagen Fingerprinting of Archaeological Bone and Teeth Remains from Domuztepe, South Eastern Turkey. *Archaeological and Anthropological Sciences* **3** (3), 271–280 (2011).
113 Kirby, D. P., Buckley, M., Promise, E., Trauger, S.A., Holdcraft, T.R. Identification of Collagen-Based Materials in Cultural Heritage. *The Analyst* **138** (17), 4849–58 (2013).